Investigation of the Treatment of Epilepsy with Cannabinoids

by

Roshni S. Kollipara, B.Sc. (Hons.), M.Sc.

A thesis submitted to the

School of Graduate Studies

in partial fulfilment of the requirements

for the degree of

Master of Science in Medicine

Faculty of Medicine

Division of Biomedical Sciences

Memorial University of Newfoundland

May 2023
St. John's, Newfoundland and Labrador, Canada

Abstract

Cannabis has been consumed by humans for millennia, and is currently used in Canada for the treatment of a variety of medical conditions including anxiety, PTSD, and chronic pain. The medical community is hesitant to accept the use of *Cannabis* and cannabinoids to treat epilepsy due to inadequate information on mechanism of action and long-term effects. Cannabidiol (CBD) is approved to treat pediatric patients with severe epilepsies such as Dravet Syndrome and Lennox-Gastaut Syndrome in the US and some European countries, but there are many individuals with less severe epilepsies whose quality of life is affected by negative side-effects from current anti-epileptic drugs. This research aims to globally evaluate which of the 6 most prevalent cannabinoids show seizure reduction and to investigate the mechanism of action of cannabinoids in an epilepsy model. Using a chemical model of epilepsy, zebrafish larvae were treated with phytocannabinoids, and their seizures measured through an optimized behaviour tracking method. Unique to this study, cannabinoid uptake was measured in larvae with a novel HPLC method developed in this project. This accomplishment is superior to previous attempts to quantify cannabinoid uptake by measuring losses in the water used to deliver cannabinoid to fish, which assumes that all losses are due to uptake and metabolism by the study organisms. CBD induced seizure reduction is partially mediated by the G-protein coupled receptor GPR55 and potentially through CB1R. Treatment with cannabinol (CBN) and cannabichromene (CBC) decreased seizure intensity at lower concentrations than CBD. Δ^9-tetrahydrocannabinol (Δ^9-THC), Δ^8-tetrahydrocannabinol (Δ^8-THC), and cannabigerol (CBG) only showed antiepileptic effects at a high

concentration, but when concentrationd in combination with CBD reduced seizures more than either treatment alone. RT-qPCR showed changes in expression of endocannabinoid system (*napepld, gde1, faah, ptgs1, ptgs2a*) and neural (*fosab, pyya*) genes in response to phytocannabinoid treatment. The data reported in this thesis supports the hypothesis that phytocannabinoids are promising anti-epileptics and could be used in combination therapies for more effective seizure relief.

General Summary

The medical community is hesitant to accept the use of cannabis to treat epilepsy due to inadequate information on mechanism of action and long-term effects. Cannabidiol (CBD) is approved to treat patients with severe epilepsy, but there are many individuals with less severe epilepsies whose quality of life is negatively affected by side-effects from current antiepileptic drugs (AEDs). This research aims to determine which cannabinoids have antiepileptic activity and to evaluate which treatments are most effective. Zebrafish larvae were treated with phytocannabinoids and exposed to a convulsant. Seizures were measured to determine anti-epileptic effects, and cannabinoid uptake was measured with a novel measurement method. Treatment with cannabinol (CBN) and cannabichromene (CBC) decreased seizure intensity at lower concentrations than CBD. Δ^9-tetrahydrocannabinol (Δ^9-THC), Δ^8-tetrahydrocannabinol (Δ^8-THC), and cannabigerol (CBG) showed antiepileptic effects at a high concentration. Treatments of combined cannabinoids show CBD has synergistic effects with Δ^9-THC, Δ^8-THC, and CBG. RT-qPCR showed changes in expression of endaocannabinoid and neural genes in response to phytocannabinoid treatment. The data shown in this thesis supports the hypothesis that phytocannabinoids are promising antiepileptics and could be used in combination therapies for more effective treatment.

Co-Authorship Statements

I am the sole author of all components of the main body of the thesis. I conducted all experiments and data analysis for the behavioural tracking and qPCR troubleshooting and results. The sample processing and HPLC method for quantification of cannabinoids in zebrafish tissues was created by Dr. Evan Langille as a collaborator. I conducted sample processing and Dr. Langille operated the HPLC. We conducted data analysis together, with Dr. Langille leading interpretation of the chromatograms. Undergraduate student Cameron Tobin assisted in zebrafish husbandry and behaviour experiments, with me leading the lab work and guiding him. Dr. French was the Principal Investigator of this project, obtained funding, and contributed to study design. The contents of the main body of this thesis will be adapted for a manuscript to be submitted to a peer-reviewed journal during review of this thesis.

Appendix C is a published paper in which I am co-author for the contribution of cartilage and bone staining experiments. This paper is published in Genes (MDPI) and is features as a main chapter in PhD candidate Alexia Hawkey-Noble's thesis. I optimized, performed and imaged the alcian blue/alizarin red double staining of all mutant and wildtype larvae ages 4-10 dpf. I interpreted the results with the assistance of Alexia Hawkey-Noble and Dr. French. All other data in the paper were collected and analysed by the respective co-authors.

Acknowledgements

I wouldn't have made it this far if it were not for the efforts of my mentors at every step of my scientific journey. I thank my high school science teachers for indulging my overly enthusiastic teenage self, and my alma mater Acadia University for providing the best foundation I could hope for. Most of all, I want to thank my mentors whose answer was never "no", but always "let's try it and find out", namely Dr. Russell Easy and Dr. Jon Geske. This attitude is something I hope to keep with me for the rest of my life. I fondly remember my times in the labs of Dr. Kirk Hillier, Dr. Alison Walker, and the Research & Development lab at BioMedica Diagnostics Inc. Erin Falkenham, who taught me much about lab and life at BioMedica, has remained a dear friend and a guiding light.

I am so grateful for Dr. Andrew Lang, who supervised my first MSc, and the Lang Lab, who unexpectedly became my rock on The Rock. Both current members and alumni were always willing to be a sounding board and a supportive community. I am also grateful for the community of kindred spirits I found in the Discipline of Biomedical Sciences. I hope the Bestie Gals group chats live on, and we all continue learning from each other.

I thank Dr. Curtis French for his supervision and guidance during this project. My first foray into the world of zebrafish happened before I was finished high school, and my time in the French Lab has reconfirmed that the Twitter handle "Zebrafish Rock" is in fact true. I am grateful for the conference and publication opportunities he facilitated that helped me develop my network and career. I thank my committee members Dr. Matt

Parsons and Dr. John Weber for their guidance and advice during my program, and for their feedback on my thesis. Dr. Ann Dorward helped me tremendously throughout my program, in a way that I cannot put into words. I value her mentorship and support and could not have made it through without her. The Faculty of Medicine's Office of Research and Graduate Studies is staffed by some of the people who make the world go around. I thank them for helping me navigate the quagmire of paperwork that happens during a graduate program, and for generally providing a helping hand whenever needed.

I offer my sincerest thanks to the many organizations who financially supported this project and my program stipend: Mitacs, Epilepsy NL, CEPG Design and Consulting Inc., the School of Graduate Studies at Memorial University of Newfoundland, Research and Graduate Studies in the Faculty of Medicine at Memorial University of Newfoundland, and the Women's Association of Memorial University of Newfoundland. This study would not have been possible without their generous support.

I want to thank my friends and family for their support during this degree program. The jokes, laughs, and love were a necessary break from the struggle of graduate school. I particularly want to thank my best friend and husband, Evan Langille. After going through grad school together (and a total of 5 university degrees), I know that we can face anything. You have always been my biggest fan and my home. Of course, I must give an honourable mention to my dog Jake, the rescue who rescued me, for his never-ending emotional support.

Table of Contents

List of Tables

List of Figures

Figure A13. Comparison of LOWESS smoothing bin averaging sizes combined with MDM filtering on distance travelled after PTZ treatment.

List of Appendices

List of Abbreviations

Δ^8-THC	Δ^8-tetrahydrocannabinol
Δ^9-THC	Δ^9-tetrahydrocannabinol
2-AG	2-arachidonyl glycerol
5-HTR	5-hydroxytryptamine receptor
AEA	anandamide
AED	anti-epileptic drug
ANOVA	analysis of variance
BM	baseline movement
CB1R	cannabinoid receptor 1
CB2R	cannabinoid receptor 2
CBC	cannabichromene
CBD	cannabidiol
CBG	cannabigerol
CBN	cannabinol
CHO	Chinese hampster ovary
CNS	central nervous system
COX-1	cyclooxygenase 1
COX-2	cyclooxygenase 2
Cys-LT1R	cysteinyl leukotriene receptor 1
Cys-LT2R	cysteinyl leukotriene receptor 2
DMSO	dimethyl sulfoxide

DNA	deoxyribonucleic acid
dpf	days post fertilization
ECS	endocannabinoid system
EM	embryo media
EMA	European medicines agency
FAAH	fatty acid amide hydrolase
FDA	federal drug administration
GDE1	glycerophosphodiester phosphodiesterase 1
GPR	G-protein coupled receptor
GPR55	G-protein coupled receptor 55
HEK	human embryonic kidney
HPLC	high performance liquid chromatography
ILAE	International League Against Epilepsy
IR	infrared
LOWESS	locally weighted scatterplot smoothing
MDM	minimum distance moved
MeOH	methanol
MP	megapixels
mRNA	messenger ribonucleic acid
NAPE-PLD	N-acyl phosphatidylethanolamine phospholipase D
NPY	neuropeptide Y
PPARγ	peroxisome proliferator-activated receptor γ

PTSD	post-traumatic stress disorder
PTZ	pentylenetetrazole
pyya	peptide YY a
RNA	ribonucleic acid
RT-qPCR	reverse transcriptase quantitative polymerase chain reaction
TRPA1	transient receptor potential cation channel subfamily A member 1
TRPM8	transient receptor potential cation channel subfamily M member 8
TRPV1	transient receptor potential vanilloid 1
TRPV2	transient receptor potential vanilloid 2
VC	vehicle control
Y	tyrosine

Introduction

Epilepsy & Seizures

Epilepsy is a complex disorder characterized by repeated seizures, which are rapid discharges of action potential in the brain that can result in uncontrolled movement and periods of lack of awareness. Having an epilepsy disorder can greatly impact a person's life, as a lack of clinical seizure control can impede their day-to-day independence and frequent seizures have been associated with neuroinflammation and reduced cognitive function[1]. Epilepsy is a disorder that is disproportionately diagnosed in children and elderly people,[2] two vulnerable populations that are especially affected by cognitive decline and dependence on others. Clinical seizure control can be difficult to achieve because approximately one third of epilepsies do not have a known cause, and greater than 30% of patients with epilepsy do not respond to currently available treatments (refractory epilepsy)[2,3]. Those who do respond to currently available anti-epileptic drugs (AEDs) often will not get optimal seizure control from the first drug or concentration they try[2], and even then they may not be able to tolerate the adverse effects[4]. Some adverse effects to current AEDs are drowsiness, double vision, depression, hepatotoxic effects, aseptic meningitis, and birth defects in offspring[4]. Epilepsy has diverse etiologies, confounded by several types of seizures and six categories of epilepsy, as per the ILAE guidelines[5]. Further complicating our understanding of epilepsies, the wide variability and scope of epilepsy leads to both a challenge and an opportunity for researchers studying this disorder.

The Pentylenetetrazole Epilepsy Model

Animal models of epilepsy are necessary tools to investigate the efficacy of AEDs and the mechanism of action of both AEDs and epilepsy disorders. Some of the original AEDs were discovered after studies on animal models, as discussed by Perucca, 2019[6]. The most common methods to model epilepsy in animals is exposure to a convulsant, thermal induction of seizures, physical trauma, or creation of genetic mutations causing epileptic disorders[7,8]. Pentylenetetrazole (PTZ) is a non-competitive $GABA_A$ receptor antagonist and causes depolarization and thus excitation[9,10]. PTZ exposure models spontaneous epilepsy, and invokes concentration-dependent seizure behaviours[11,12]. The PTZ model of epilepsy has been used in animal models to describe the efficacy of synthetic and naturally derived potential AEDs[7,13–16], with rodent models being the most commonly used after the 1980s[8]. Zebrafish models are prominent in drug-discovery studies due to their high fecundity, low cost to maintain, and optical clarity, which all begets a high-throughput workflow to evaluate anti-epileptic efficacy[7]. Zebrafish PTZ models have been shown to respond to current AEDs[11,17], synthetic AED candidates[18,19], and naturally derived AED candidates[13,18,19].

The PTZ model of epilepsy, specifically in larval zebrafish, has been well characterized by Baraban and colleagues[11] who categorized behaviours into three stages. Stage I is a dramatic increase in swimming behaviour, Stage II is defined by rapid circling in a "whirlpool" pattern, and Stage III involves clonus-like convulsions ultimately leading to periods of inactivity and a loss of posture. It has been observed that due to the concentration-dependent response to PTZ, higher concentrations shorten the exposure

time needed to reach Stage III behaviour. The PTZ model of epilepsy in adult zebrafish has been well characterized by Mussulini and colleagues[12], who created a 6 score behaviour phenotype system. A score of 0 indicated no seizure behaviour, wherein the fish had short swimming activity at the bottom of the tank. A score of 1 was associated with increased swimming activity and frequent movement of the operculum. A score of 2 was given for burst swimming and erratic movements, and a score of 3 was given for rapid circular movements. Clonic-like behaviour such as abnormal whole-body contractions lead to a score of 4. Tonic-like behaviour such as sinking and a loss of posture lead to a score of 5, and finally death was given a score of 6. The behavioural characterizations of PTZ induced seizures are consistent between the two research groups and indicate that stage of development (larval vs adult) does not affect PTZ activity.

The gene *fosab* encodes the protein Fos that is produced in firing neurons[20,21]. The gene in zebrafish is *fosab*, in rodents it is c-*fos*, in humans it is FOS. c-*fos* expression has been used as a metabolic seizure marker in rodents[11,12,20–22], however it more accurately depicts neuronal changes rather than seizure intensity[20]. Early characterization of PTZ models of epilepsy in zebrafish observed an increase in c-*fos* expression in spatially distinct brain structures and the embryonic trunk muscle after seizures caused by PTZ exposure[11,18]. c-*fos* is defined as a protooncogene and is involved in neurodevelopment[23], growth[24], response to stimuli[25], stress[26], and is an AP-1 transcription factor when in complex with c-Jun[27].

Endocannabinoid System

Phytocannabinoids act on our endocannabinoid system (ECS). The ECS is an endogenous system that maintains homeostasis and plays a role in the regulation of many body systems. There is much research ongoing to further elucidate the specifics of the ECS, and it has been established to be involved in immune response, CNS development, appetite, pain, inflammation, mood, and memory, among many other functions. The ECS is mostly comprised of G-protein coupled receptors. Lipid-derived endocannabinoids, the most ubiquitous and studied are anandamide (AEA) and 2-archidonyl glycerol (2-AG), which act through retrograde synaptic signalling to modulate synaptic transmission[28]. A visual summary of the ECS as pertinent to this thesis is provided in Figure 1.

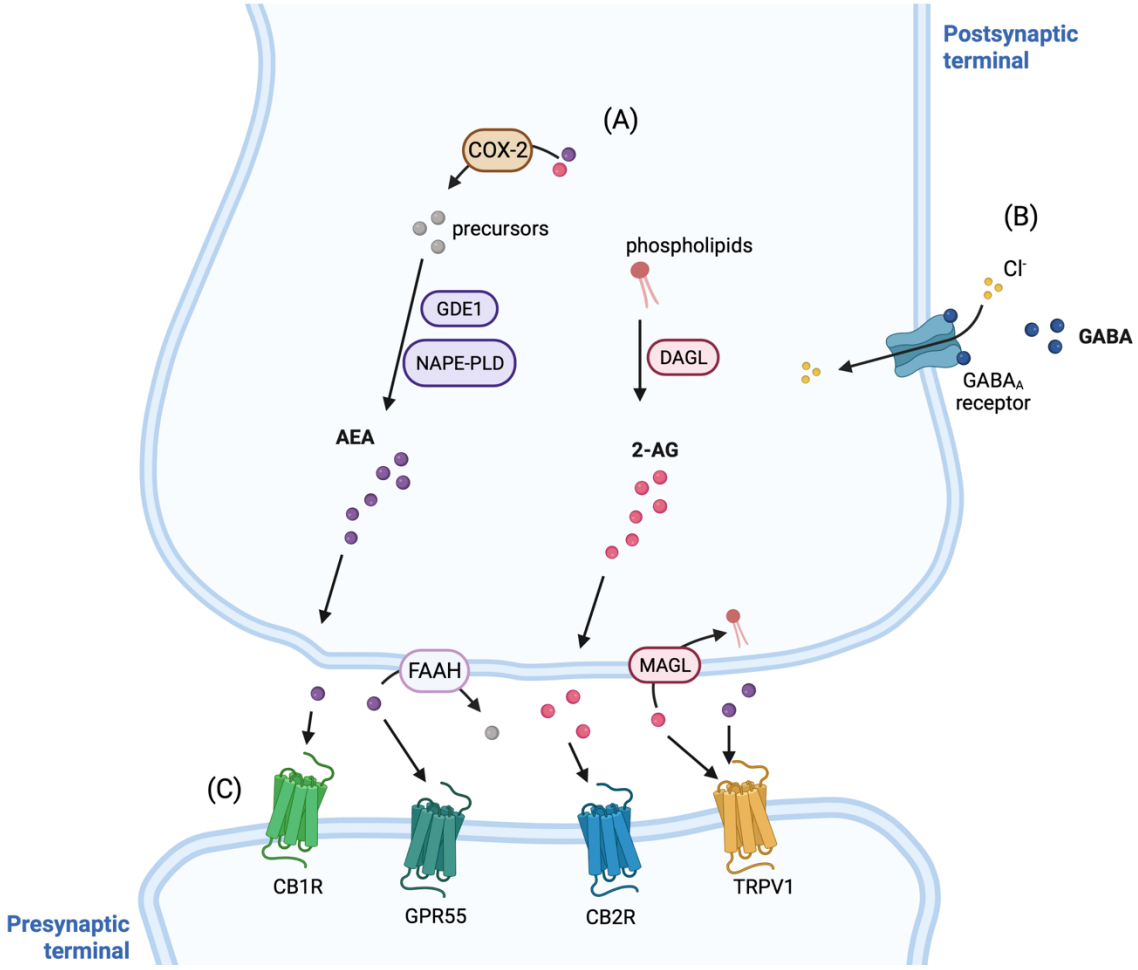

Figure 1. Diagram of the endocannabinoid system and GABA signalling as pertinent to this thesis. (A) Synthesis and degradation of the endocannabinoids AEA and 2-AG; enzymes are represented as rounded rectangles. (B) Function of the $GABA_A$ receptor. (C) Receptors upon which AEA and 2-AG act. Figure created using Biorender.com.

It is established that endocannabinoids are rapidly produced as needed and rapidly degraded[29,30]. AEA is responsible for synaptic strengthening and 2-AG is associated with many processes and is hypothesized to exist in a storage pool within cells in addition to being created on demand[30]. Preventing AEA degradation reduces pain perception,

inflammation, and depression, while blocking 2-AG degradation causes hypothermia, analgesia, and reduced mobility[30]. It has been reported that preventing degradation of both AEA and 2-AG at the same time mimics the effects of Δ^9-THC[30,31].

There are three established ECS receptors: cannabinoid receptor 1 (CB1R), cannabinoid receptor 2 (CB2R), and recently G-protein coupled receptor 55 (GPR55)[32,33] (Fig. 1C). These three receptors can be found around the body, but CB1R is mainly expressed in the CNS[33], CB2R is mostly expressed in immune tissues[33], and GPR55 is found in adipose tissue, immune tissues, the brain, and on large-diameter dorsal root ganglion cells, which are associated with nociception[33,34]. CB1R and CB2R commonly form heteromers that are expressed in pallidal neurons and activated microglia[35]. AEA has been shown to act on CB1R and 2-AG has been shown to act on CB2R[36]. AEA has also been shown to activate transient receptor potential cation channel subfamily V member 1 (TRPV1) (Fig. 1C), which is currently believed to be a non-cannabinoid receptor[37]. Interestingly, CBD has been suggested to desensitize TRPV1, acting in a manner opposite to AEA[37].

GPR55 is transitioning from its designation as an orphan receptor to being an established member of the ECS. GPR55 has been shown to increase intracellular calcium release within neurons after treatment with AEA or Δ^9-THC, thereby increasing neuronal excitability, and has also been shown to inhibit M-type potassium current[32]. The orphan receptor G-protein coupled receptor 18 (GPR18) has also been the focus of recent studies for its involvement in the ECS, where it has been shown to have negative cross-talk and cross-antagonism with CB2R[38]. GPR18 was originally reported to be expressed in the spleen and testis[39] but was more recently found in all lymphoid hematopoietic cell lines,

predominantly in T and B cells[40]. GPR18 causes an increase in intracellular calcium when activated by *N*-arachidonylglycine, an endocannabinoid precursor[40].

The following ECS genes and orthologs are summarized in Table 1. N-acyl phosphatidylethanolamine phospholipase D (NAPE-PLD), encoded by *napepld*, is the main enzyme responsible for the creation of AEA[41] (Fig. 1A), though there is evidence that other pathways exist[29]. NAPE-PLD is membrane bound to the endoplasmic reticulum in neurons[29] but is expressed ubiquitously in the body[42]. As the name suggests, fatty acid amide hydrolase (FAAH), encoded by *faah*, is a catabolic enzyme that degrades AEA[43–45] (Fig. 1A) and is widely expressed in the nervous system[43,46,47]. FAAH has been linked to pain perception, anxiety, and depression, and has a paralog FAAH2 that is conserved between humans and zebrafish but not rodents[46,48]. Cannabinoids have been shown to inhibit FAAH activity in rodent models[49–51], and FAAH inhibition or complete loss leads to an increase in neuroprogenitors[30,52].

Glycerophosphodiester phosphodiesterase 1 (GDE1), encoded by the gene *gde1*, is predicted to be involved in ethanolamine metabolic process (Fig. 1A). Glycerophosphodiester phosphodiesterases were originally discovered in bacterial species, but were found to be evolutionarily conserved in mammals[53]. GDE1 is an enzyme that creates an AEA pre-cursor molecule in the AEA synthesis pathway and is expressed ubiquitously in the body[42,48]. GDE activity is interconnected with GPRs[53], and this combined with involvement in ethanolamine metabolism makes GDE1 a possible important player in the ECS.

The zebrafish orthologs of cyclooxygenase-1 (COX-1) and cyclooxygenase-2 (COX-2) are *ptgs1* and *ptgs2a*, respectively. Both COX-1 and COX-2 use arachidonic

acid as a substrate[50], with COX-2 being shown to breakdown AEA and 2-AG[54] (Fig. 1A). COX-2 can be rapidly expressed in neurons and glia in response to pro-inflammatory compounds[55], whereas COX-1 is ubiquitous in the body[50]. COX-2 has been implicated in epilepsy and neuroinflammation, as brains after seizures and patients with epilepsy have been observed to have increased levels of COX-2[56,57].

Table 1. Summary of ECS genes relevant to this study with human, rodent, and zebrafish orthologs.

Human Gene	Rodent Ortholog	Zebrafish Ortholog	Role/Function
FOS	Fos or cFos	*fosab*	Forms the transcription factor complex AP-1 with JUN proteins, regulates cell proliferation, differentiation, and transformation. Observed the increase in expression in specific brain structures after seizures.
NAPEPLD	Napepld	*napepld*	Involved in biosynthesis of N-acylethanolamide by breaking down N-acyl-phosphatidylethanolamine.
FAAH	Faah	*faah*	Catalyses hydrolysis of primary and secondary fatty acid amines, of note anandamide and oleamide.
FAAH2	Gene not found	*faah2*	Catalyses hydrolysis of N-acylethanolamines, fatty acid primary amides, and N-acyl amino acids, paralog of FAAH/*faah*
GDE1	Gde1	*gde1*	Predicted to be involved in N-acylethanolamine metabolic process, predicted to be located on plasma membrane of cells.
COX-1 or PTGS1	Cox-1 or Ptgs1	*ptgs1*	Catalyses the conversion of arachidonate to prostaglandin, regulates angiogenesis in edothelial cells, functions as a cycloxygenase and a peroxidase.
COX-2 or PTGS2	Cox-2 or Ptgs2	*ptgs2a*	Involved in prostaglandin biosynthesis, suggested to play a role in inflammation, can act as a dioxygenase and a peroxidase.

Cannabis & Cannabinoids

Cannabis is a versatile medicinal plant with several health applications, and has been used to treat convulsions since ancient times[58]. Due to the prohibition of and the social stigma associated with cannabis, information regarding treating medical conditions with cannabis is incomplete. Another challenge that was faced by patients seeking treatment was the availability and quality of cannabis preparations prior to medical cannabis legalization in their respective countries[59]. The term cannabinoid describes a broad class of compounds that generally contain a terpenophenolic backbone. Comprehensive research regarding efficacy, safety, and mode of action needs to be conducted before the medical community can fully accept the use of cannabis or cannabinoid-based therapies[60,61]. There are over 100 phytocannabinoids (cannabinoids of plant origin) found naturally in *Cannabis sativa* and *Cannabis indica*[62,63]. In this thesis I focus on 6 of the most prevalent: cannabidiol (CBD), Δ^9-tetrahydrocannabinol (Δ^9-THC), Δ^8-tetrahydrocannabinol (Δ^8-THC), cannabinol (CBN), cannabichromene (CBC), and cannabigerol (CBG). A summary of what is known this far about receptor activity of these six cannabinoids is shown in Table 2.

Table 2. Summary of receptor interactions that have been discovered thus far for the six phytocannabinoids in this thesis.

Gene Name (human, zebrafish)	**CBD**	**CBN**	**Δ^9THC**	**Δ^8THC**	**CBG**	**CBC**
CB1R, *cnr1*	Antagonist[50,64]	Very Low affinity[65]	Agonist[36,50,66]	Low affinity agonist[67–69]	Low affinity antagonist[70,71]	Partial agonist[72]
CB2R, *cn2r*	Antagonist[50,64]	Acts on[65]	Agonist[36,50,66]	Low affinity agonist[69]	Partial agonist[70,73]	Partial agonist[72,74]
GPR55, *gpr55a*	Antagonist[50,75–77]	No interaction[77]	Agonist[36,50,66]	*No data*	Possible antagonist[78]	*No data*
TRPV1, *trpv1*	Agonist[37,50,79,80]	Very low affinity[79]	No interaction[79]	*No data*	Agonist[73,79,81]	Very low affinity[79]
TRPV2, *trpv2*	Agonist[50,79,80]	Agonist[79]	Agonist[79]	*No data*	Agonist[73,79,81]	No interaction[79]
5-HTRs, *htrs*	Acts on[82,83]	*No data*	Agonist[36,50,66]	*No data*	Antagonist[70]	*No data*
TRPA1, *trpa1a*	Possible agonist/ desensitizes[79]	Agonist/ desensitizes[51,79]	Moderately modulates[79]	*No data*	Agonist/ desensitizes[73,79,84]	Agonist/ desensitizes[51,79]
TRPM8, gene not found	Acts on[79]	Antagonist[51,79]	Weak antagonist[79]	*No data*	Antagonist[73,79,81]	No interaction[79]
PPARγ, *pparg*	Agonist[85,86]	*No data*	Agonist[86]	*No data*	Antagonist or agonist[73,73,86]	Agonist[86]

CB1R: Cannabinoid receptor 1; CB2R: Cannabinoid receptor 2; GPR55: G-protein coupled receptor 55; TRPV1: Transient receptor potential cation channel subfamily V member 1; TRPV2: Transient receptor potential cation channel subfamily V member 2; 5-HTR: 5-hydroxytryptamine receptor; TRPA1: Transient receptor potential cation channel subfamily A member 1; TRPM8: Transient receptor potential cation channel subfamily M member 8; PPARγ: Peroxisome proliferator-activated receptor γ.

CBD is the active component in a treatment that overcame the many challenges related to the medical use of cannabinoids, Epidiolex® in the United States and EPIDYOLEX in the European Union[87–90]. The FDA and EMA approved Epidiolex for treating patients 2 years and older with Dravet Syndrome and Lennox-Gastaut Syndrome[91,92]. Epidiolex still has not received Health Canada approval, likely due to insufficient long-term data and the commercial availability of CBD oil in the country. While approval to treat patients with Dravet Syndrome and Lennox-Gastaut Syndrome is a significant step, this still disqualifies many patients from treatment who have less severe epilepsies. CBD has also been shown to have analgesic and anxiolytic effects and is used in palliative care[93].

CBD is considered an antagonist of CB1R based on studies on mice[64], CB2R based on studies on human CB2R expressed in Chinese hamster ovary cells (CHO)[64], and GPR55 based on studies on mouse neuron cell culture and a mouse model of Dravet Syndrome[75–77], as it is a negative allosteric modulator of these receptors[50]. It has also been shown to act on human 5-hydroxytryptamine receptors (5-HTR) expressed in CHO[82] and in a rat model[83], TRPV1 and transient receptor potential cation channel subfamily V member 2 (TRPV2) based on studies of cultured mouse microglia[50,79,80], and transient receptor potential cation channel subfamily M member 8 (TRPM8) based on studies of HEK-293 cells[84]. CBD is also an agonist of peroxisome proliferator-activated receptor γ (PPARγ) based on studies on rat models[85,86], and is suspected to be an agonist of transient receptor potential cation channel subfamily A member 1 (TRPA1) based on studies of HEK-293 cells[79,84]. CBD is of particular interest given its broad range of reported

interactions involving many body systems including pain, anxiety and neuronal excitability.

CBN has been reported to display anti-epileptic effects greater than CBD in an zebrafish model of Dravet syndrome[94] and has also reported to have anti-cancer effects on human Lewis lung adenocarcinoma xenografted into mice and in preclinical studies[95,96]. CBN inhibits cellular uptake of AEA and is an agonist of and desensitizes TRPA1, and acts as an antagonist of TRPM8, as determined by studies on HEK-293 cell culture[51]. CBN has also been reported to reduce food intake in rats, as summarized by Hill, 2012[97]. CBN is an agonist of TRPV2 but has very low affinity to TRPV1, based on studies of HEK-293 cells[51,79]. Similarly, CBN has recently been reported to act on CB2R but has very low affinity to CB1R based on studies in a zebrafish model[65], and has no interaction with GPR55 based on study of HEK-293 cells[77].

CBC is one of the most abundant cannabinoids in *Cannabis* but has not been well studied[36,98]. There is evidence that CBC when used in combination with CBD or Δ^9-THC can help alleviate symptoms of insomnia and depression in humans and rats[99,100]. As a sole treatment, CBC exhibits neuroprotective effects based on studies of cultured mouse neural cells[101,102]. CBC is a partial agonist of both CB1R and CB2R, as shown in CHO cells, AtT20 cells, and a mouse model[72,74]. CBC is an agonist of and desensitizes TRPA1 channels[51] and is an agonist of PPARγ[86] , as determined by studies on HEK-293 cell culture. CBC has very low affinity or no interaction with TRPV1, TRPV2, and TRPM8[79].

CBG does not currently have established clinical relevance, but was determined to be non-psychotropic based on treatment of mixed breed dogs, Rhesus monkeys, mice,

wild gerbil, and albino rats[103,104] and is of interest commercially as it is abundant in some commonly used hemp plants. CBG has a higher affinity to CB2R and is a partial agonist[70,73], but also has been shown to bind CB1R[70,71], as evidenced in studies on human CB1R and CB2R expressed in CHO cells and Sf9 cells. It is speculated that CBG is an antagonist of GPR55, based on studies on HEP-293 cells[78]. Based on a study utilizing mouse brain membranes, CBG is an antagonist of 5-HTR[70]. CBG has a unique and broad range of binding affinities, with evidence that in a micromolar dosage range it may modulate TRPA1 through agonism or desensitization in HEK293 cells and human CB1R and CB2R expressed in CHO cells[73,84]. In a 10 μM dosage range, CBG antagonizes GPRs and in a nanomolar dosage range CBG is an agonist for α_2-adrenoceptor, shown in a study using mouse brain membranes[70]. CBG has also been shown to be an agonist of TRPV1 and TRPV2, an antagonist of TRPM8 channels, and an agonist of the nuclear receptor PPARγ at very high micromolar dosage in human CB1R and CB2R expressed in CHO cells and HEK-293T cell culture[73,81]. *In vivo* studies of CBG have suggested possibility of treating inflammatory bowel disease in a mouse model by preventing nitrite release from macrophages and reducing oxidative stress[105]. The use of CBG in this work was investigative, to determine if there are any individual or synergistic effects of its use in epilepsy models.

Δ^9-THC is the most psychoactive compound found in cannabis and is the compound regulated for recreational use in countries where cannabis is legal. Δ^9-THC is an agonist of CB1R, CB2R, GPR55, and 5-HTR, as evidenced by studies on cloned rat receptors into mammalian cell culture or *Xenopus* oocytes[36,50,66]. Δ^9-THC has no

interaction with TRPV1 but is an agonist of TRPV2, based on studies on HEK-293 cells, which also suggest that Δ^9-THC is a weak antagonist of TRPM8 and moderately modulates TRPA1[79]. Δ^9-THC is also an agonist of PPARγ[86]. Treatment with Δ^9-THC in combination with CBD has been the main focus of recent studies, and has been associated with improved symptoms of Alzheimer's disease, neuroinflammation as it relates to Parkinson's disease, multiple sclerosis, and Huntington's disease, pain perception, depression, and sleep disorders as reviewed by Zhang and colleagues in 2022[36]. A combination of Δ^9-THC and CBD has also been shown to be anti-epileptic in a mouse model of Dravet Syndrome and a zebrafish model of neuro-hyperactivity[14,36,106]. Sole treatment with Δ^9-THC is generally reserved for extreme medical cases because of the psychoactive effects, and can be used to treat anorexia[107] and severe emesis[108,109] as shown in pilot clinical studies. Reports of Δ^9-THC treatment of glaucoma in a cat model administered by eye drops are conflicted as a significant reduction in intraocular pressure is often paired with ocular toxicity[98,110]. There is also evidence that Δ^9-THC treatment inhibits fear learning in a zebrafish model[111] and is being investigated for treatment of psychological illnesses such as post-traumatic stress disorder (PTSD) in humans[112].

Δ^8-THC is a less psychoactive analog of Δ^9-THC, described as having mildly euphoric effects with less paranoia. A self-reporting study on the effects of Δ^8-THC indicated more tolerable negative side-effects while maintaining pain relief and relaxation as compared to Δ^9-THC[113]. The altered structure of Δ^8-THC leads to a lower affinity for CB1R and CB2R, shown in human tissue and in HEK-293 cells[67–69]. The current hypothesis in the field is that Δ^8-THC has similar receptor binding interactions as Δ^9-THC

just with lower affinities, but this has not yet been thoroughly investigated. An ongoing interventional clinical trial in the United States aims to compare the pharmacokinetic and pharmacodynamic effects of Δ^8-THC to Δ^9-THC and placebo controls using healthy human subjects[114]. A previous clinical trial that was terminated in 2009 aimed to use Δ^8-THC as an antiemetic treatment after chemotherapy[115]. There is significant value in understanding the effects of phytocannabinoids and their interactions with each other, particularly in the case of epilepsy it has been observed in patients as well as in zebrafish and mouse models that *Cannabis* extracts have different anti-epileptic efficacy[116,117] even when normalized for concentration of CBD[62].

A common side-effect of consuming *Cannabis* is a dysregulation of appetite, medically termed polyphagia, and indeed this dysregulation is supported in the literature even after treatment with purified cannabinoids[93,107–109,115]. The neuropeptide Y (NPY) system is a highly interlinked system of peptide ligands and receptors that are involved in appetite regulation, endocrine regulation, and cardiovascular regulation[118–120]. Peptide YY, coded by *pyya*, is heavily implicated in the negative regulation of appetite and speed of digestion[118,120,121]. Though expression of peptide YY is primarily in the digestive system, it has also been shown to bind to some NPY receptors in the central nervous system (CNS), and therefore may share some effects with NPY[118,120,122]. NPY has been heavily investigated for seizure rescue, with expression increasing in models of epilepsy and injection of NPY reducing seizures in epilepsy models[123]. Some studies have associated peptide YY with the inhibition of seizures, neuroprotection from stress, and anxiolysis[119,120]. *pyya* was reported to increase in expression, particularly in the posterior hindbrain, after PTZ exposure in zebrafish embryos[18] and in a genetic model of

Angelman syndrome caused by the loss of function mutation *mib*^{hi904} [124]. Peptide YY has not been thoroughly investigated in the context of treating epilepsy with cannabinoids and may provide insight into the potential side-effects of cannabinoid treatment. This is particularly important to investigate when considering that many patients medicating their epilepsy disorder with cannabinoids or *Cannabis* preparations are pediatric, and so dysregulation of appetite and hunger could have lasting effects into adulthood.

Aims

Zebrafish are an attractive model for drug research due to ease of treatment by addition of drugs to their water and the availability of robust behavioral, genetic, and biochemical assays to gauge phenotypic effects[125,126]. In this thesis, I model spontaneous epilepsy with the convulsant PTZ, which acts by binding the $GABA_A$ receptor and preventing Cl^- ions from entering the cell (Fig. 1B), leading to depolarization and thus excitation. Seizures caused by PTZ are visually dramatic movements and are measured, alongside the effects of cannabinoids on overall seizure intensity, using behaviour tracking through activity analysis.

Measurement of drug absorption into any treated biological system provides a lens into the pharmacological processes and mechanism of action. By correlating the concentration of cannabinoid, amount absorbed into tissue, and the reduction in seizures, it may be possible to determine a more potent cannabinoid treatment for epilepsy. Previously reported methods quantified cannabinoids in fish water and tissues, but was limited to the analysis of Δ^9-THC and CBD and involved complicated and lossy organic extraction steps[127,128]. In this thesis a novel, simple, method for the direct quantification of

six common cannabinoids in pooled zebrafish larvae is presented. Cannabinoids are quantified in larvae after treatment using a novel HPLC method.

The effects of cannabinoids on body systems are still largely unknown but can be elucidated by studying changes in expression after cannabinoid treatment. Using RT-qPCR, this study will monitor a seizure marker (*fosab*), ECS genes (*napepld, faah, gde1, ptgs1,* and *ptgs2a*), and a potential biomarker for cannabinoid side-effects (*pyya*), yielding global understanding of the impact of cannabinoids.

The research question being investigated in this thesis, using a global study approach, is how effective the six most abundant cannabinoids are for the treatment of epilepsy, in individual and combined dosing regimens. This thesis is one of the most thorough studies on the effects of cannabinoids, with the most cannabinoids directly tested, to date and will make a significant contribution to the field.

Methods

Zebrafish Husbandry

Wild-type zebrafish (strain AB) were reared and staged under standard conditions as previously described[129]. All experiments were completed in accordance with Memorial University of Newfoundland's Animal Care Committee and the Canadian Council on Animal Care. Zebrafish larvae were reared in embryo media, consisting of 14.97 mM NaCl, 0.50 mM KCl, 0.99 mM $CaCl_2 \cdot 2H_2O$, 0.15 mM KH_2PO_4, 0.05 mM Na_2HPO_4, 0.99 mM $MgSO_4 \cdot 7H_2O$, and 0.71 mM $NaHCO_3$.

Cannabinoid Dosing and Seizure Tracking

All phytocannabinoids were purchased from Sigma Aldrich (Ontario, Canada). AEA and 2-AG were purchased from Cayman Chemicals (Michigan, USA). Larvae were collected and reared according to breeding pairs. One larva was added per well in a 96-well plate, and 180 µL of cannabinoid treated embryo media added. The plate was incubated at 29°C for 30 minutes, and then recorded in a tracking apparatus for 30 minutes with a 5-minute acclimation. In the dark, PTZ (prepared just before the assay in embryo media 1% DMSO) was added to a concentration of 2.75 mM and the plate was recorded for 30 additional minutes with a 5-minute acclimation. Activity, measured as percent pixel change, was measured for 30 minutes using Noldus EthoVision.

Cannabinoid Extraction

Visual description of protocol can be found in Figure 2. Larvae were pooled in groups of 12 according to treatment received, rinsed twice in ice cold embryo media, and euthanized by incubation on ice. Excess embryo media was removed, and samples stored at -80°C until extraction. All steps of extraction were completed at 4-8°C. 200 µL of extraction solvent (methanol with 0.1% formic acid) was added to the larvae, which were then bead beaten for 3 minutes in an equal volume of 1 mm glass beads. Homogenate was then centrifuged for 30 minutes at 18,000 x G and the supernatant 0.2 µm filtered prior to HPLC analysis.

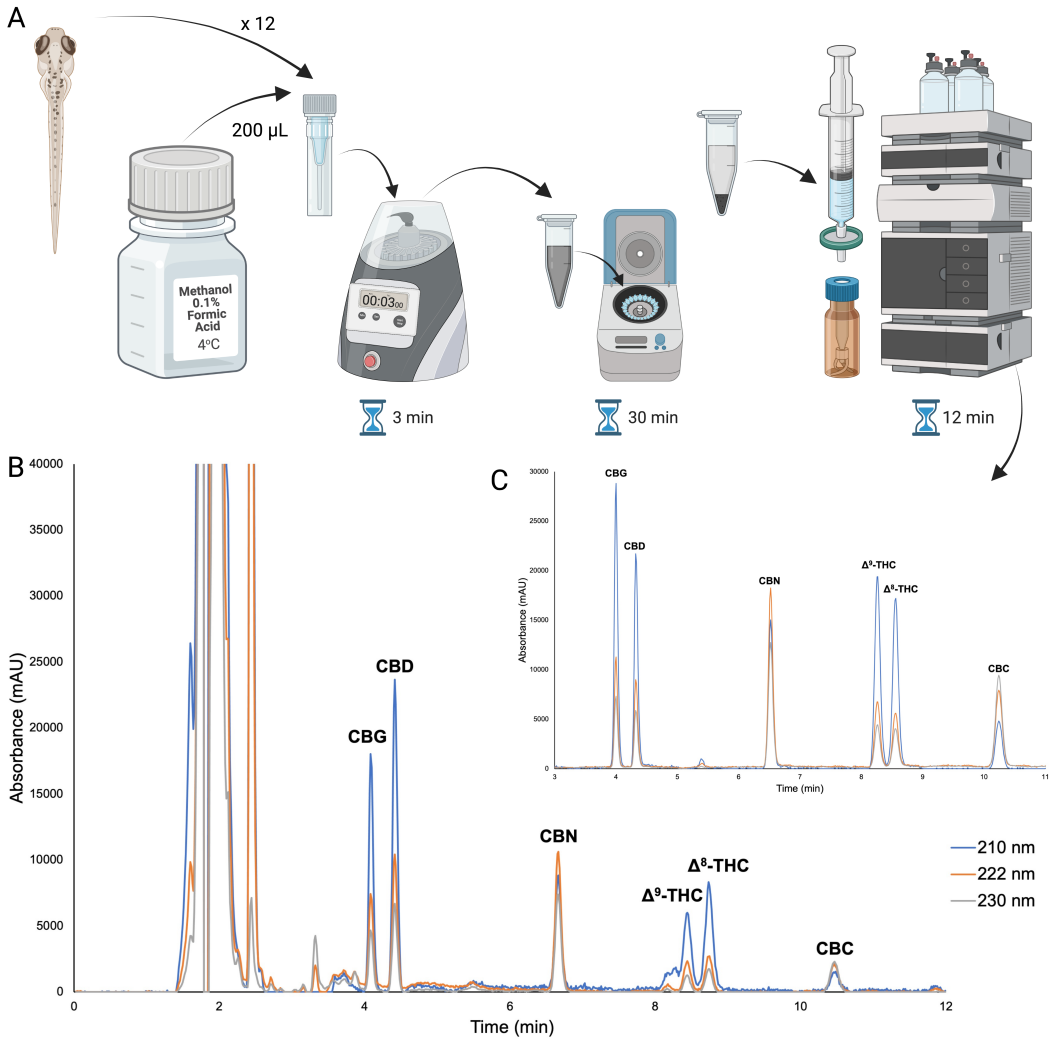

Figure 2. Overview of the cannabinoid extraction and HPLC method presented. A) Graphical summary of cannabinoid extraction protocol from zebrafish. B) Representative chromatogram of extraction of 12 pooled larvae treated with 6 cannabinoids at 4 µM. C) Representative chromatogram of 2.5 $\mu g \cdot mL^{-1}$ mixed standard of cannabinoids in extraction solvent. The three traces depict absorption at different wavelengths as stated in the figure. The wavelength with the highest relative absorbance was used for quantification of standards and samples. Peaks are labelled with corresponding compound abbreviations.

HPLC Analysis of Cannabinoids

Analytical HPLC was carried out on an HP 1050 system equipped with two HALO 2.7 µm C18 100 x 4.6 mm columns (200 mm total length). A diode array detector monitored 200-400 nm. Extracted wavelength chromatograms at 210 nm for CBG, CBD, Δ^9-THC, and Δ^8-THC, 222nm for CBN and 230 nm for CBC were used for quantification using TargetLynx software (Waters Corp, Mass, USA), spectra can be found in Figure 2. Mobile phase consisted of an isocratic mixture of 17.5:82.5 water 0.1% formic acid: acetonitrile 0.1% formic acid, v/v at a flow rate of 1 mL·min^{-1} resulting in a system backpressure of approximately 20 MPa. Triplicate 20 µL injections were performed per sample. External standards of the cannabinoids in extraction solvent were used to generate calibration curves (0, 0.1, 0.25, 0.5, 1, 2.5, 5 and 10 µg·mL^{-1}).

RT-qPCR

Larvae (6 dpf) were treated using the same method described for seizure tracking and pooled in groups of 12 for RNA isolation. RNA was isolated using the PureLink™ RNA Mini Kit (Invitrogen) with on-column DNAase treatment using the PureLink™ DNase Set (Invitrogen) and cDNA synthesized using the High-Capacity cDNA Reverse Transcription Kit (ThermoFisher). qPCR was performed with Taqman Gene Expression Master Mix and Taqman assays (FAM) for *fosab* (Dr03100809_g1), *pyya* (Dr03138152_m1), *gde1* (Dr03434842_m1), *napepld* (Dr03117925_m1), *faah* (Dr03093136_m1), *ptgs2a* (Dr03080325_m1), and *ptgs1* (Dr03087197_m1) using a ViiA 7 qPCR machine. Wells were duplexed with the endogenous control, TATA-box binding protein (*tbp*) (VIC). Data were analyzed using the ΔΔCt method and presented as means

± standard error of the mean. Two biological replicates of 12 pooled larvae, with three technical replicates for each sample, were analysed.

Statistics

Significance was determined by one-way ANOVAs and post-hoc Tukey HSD using astatsa.com (copyright Navendu Vasavada), assuming normal distribution. Significance is displayed in the figures with lettered data labels. Bars labelled with different letters are statistically significant. For example, if there are three bars labelled "a", "b", and "ab", the first two bars are statistically different, but the third bar is statistically insignificant from the first two. Simple statistical calculations such as mean, standard deviation, and standard error of the mean were completed on Microsoft Excel.

Results

Optimization of Seizure Tracking

Behaviour, and specifically epileptic behaviour, tracking of zebrafish was a new technique at Memorial University of Newfoundland. To adapt published methods to in-house capabilities, several optimization experiments were conducted (Appendix B; Fig A1-A13). Published methods were inconsistent on several important details such as age of the subjects, concentration of convulsant, length of time in which data was recorded, data filtering and recording settings, and parameter reported[11,15,17,106,116,130–141]. This inconsistent precedent was further complicated by the equipment available to me, which was a prototype of what would become the commercial DanioVision system. The prototype allowed for manual configuration, with adjustable camera height and angle, and non-centralized controls. The manual nature of the prototype lead to issues when used by an inexperienced user, such as myself when I started my program. The camera height and angle had to be adjusted for the micro-plate format used in this study, which could only happen once I determined that this was the cause of the problems I was experiencing. While early studies that used seizure measurement likely utilized similar apparatus or home-made apparatus, modern equipment is available, such as DanioVision and ZebraBox systems, wherein the camera is non-adjustable, the configuration is already optimized for use with a well-plate, and the filming environment is temperature and light controlled.

The Noldus EthoVision XT software is a powerful tracking tool and has several outputs that can measure movement. I began by attempting to replicate PTZ

concentration-responses reported in the literature and found that the intensity of seizures expected with higher concentrations of PTZ was unable to be measured. Additionally, visual inspection of the larval behaviour indicated that intense seizure behaviours were occurring but were not reflected in the quantitation. The apparatus was investigated for misalignment causing parallax error and several data filtering steps were thoroughly investigated. Data filtering is generally not reported in the literature, and it is likely that more sensitive tracking equipment leads to data that does not need to be filtered too heavily. This led us to the conclusion that replacing the camera used to record tracking videos with a much more sensitive model, the details of which are outlined in Table 3, was the best path forward.

Table 3. Specifications of original TrackSys IR video camera (Sony XC-EI50) compared to upgraded IR video camera (FLIR Blackfly S).

	Sony XC-EI50	**FLIR Blackfly S**
Resolution (H x V, MP)	768 x 494, 0.38 MP	2048 x 1536, 3.2 MP
Frame rate (Hz)	30	60
Wavelength range (nm)	400-870	300-1000
Communication protocol	NTSC (analog coaxial)	USB 3.1, GenICam (digital lossless)

This major upgrade provided an opportunity for a more sensitive measure of movement, termed “activity analysis” by Noldus Ethovision. Frames of the video are compared to each other, and the number of pixels that have a change in colour (the result of a change in the image, such as an animal moving) are represented as a percentage of pixels changed, or percent activity (Fig 3).

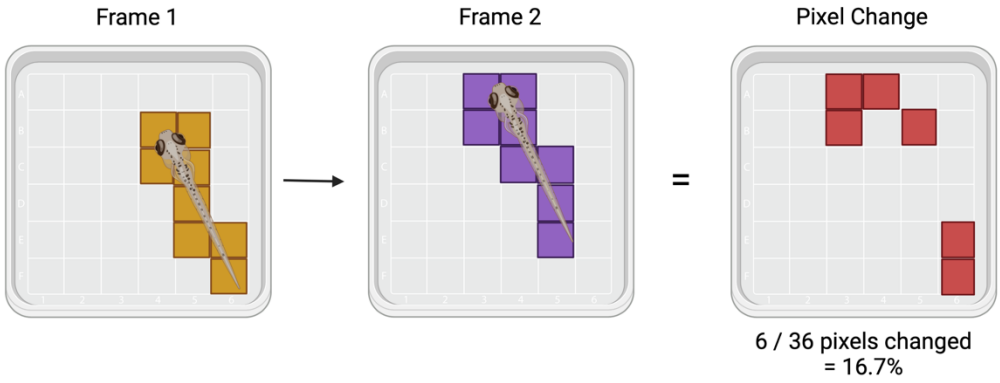

Figure 3. Diagram describing the process of percent activity calculation. Each pixel in a frame is compared to the subsequent frame, to produce a matrix of colour changes per pixel for that frame. The number of pixels that change between each frame are summed to produce a percentage of pixel change between the frames. Created on Biorender.com.

In a given assay time, the percentages are summed to give total pixel change, or total percent activity. Activity was determined to be the most sensitive measure of seizure activity as this measured overall movement of the larvae, not just 2D translational distance. Seizure phenotypes with minimal movement, such as tail flicks, and phenotypes with large movement, such as rapid circling in a plane perpendicular to the camera, are included in activity measure. These behaviours were not able to be discerned using the distance moved or velocity tracking as the larva is reduced to a point (approximately mid-

body) and tracked only in the plane parallel to the camera. Activity analysis also requires threshold cut-offs to counter noise in the video. In order to determine the threshold for units of pixel change that would constitute real movement, activity data was plotted as a histogram (Fig 4).

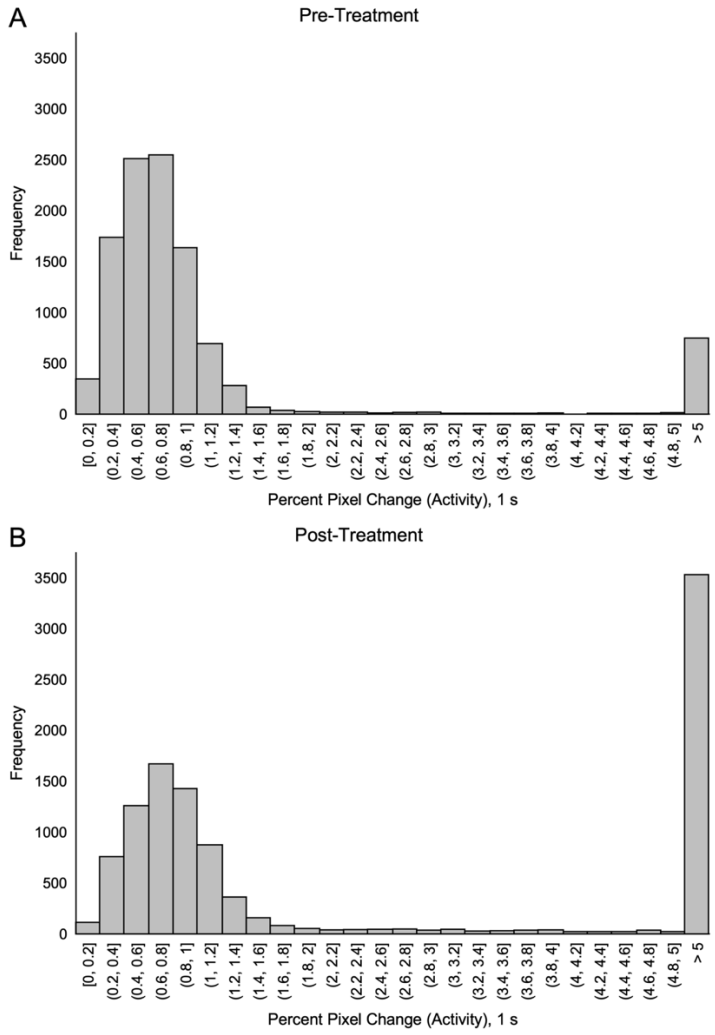

Figure 4. Distribution of percent pixel change as represented by activity per second over a 15 min assay. Percent activity is binned in 0.2% intervals from 0-5%. A: Distribution of activity prior to PTZ treatment. B: Distribution of activity after 25 mM PTZ treatment. n=10,800 samples from 12 individuals per histogram.

The distribution of the data both before (Fig 4A) and after (Fig 4B) PTZ treatment is similar in that there is a Gaussian distribution of points between 0 and 1.8 % pixel change and a peak of data points >5% pixel change. The frequency of points between 0 and 1.8 % are lower after PTZ exposure, whereas the frequency of points >5% pixel change are higher after PTZ exposure. This indicates that the data collected between 0 and 1.8 % pixel change is likely noise and the seizure-related movement data is >5% pixel change. The reason a decrease in this low activity related noise is observed after PTZ treatment is that the larvae remain in a high activity state for a higher proportion of the trial time. This result was used to conduct another data analysis study with various activity thresholds on a PTZ concentration-response experiment (Fig 5).

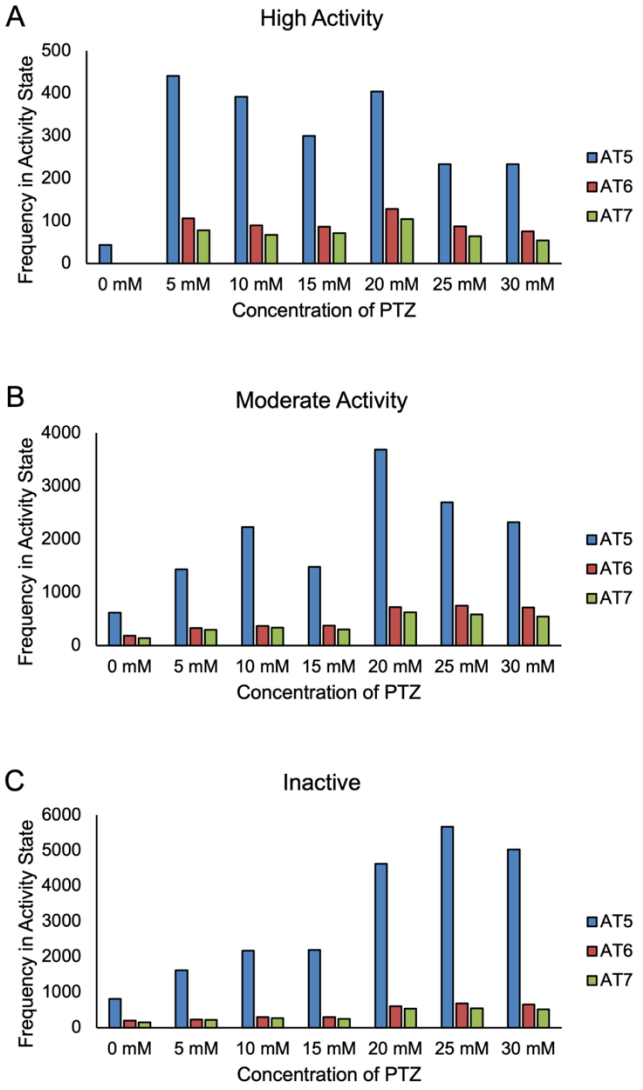

Figure 5. Comparison of frequency entering High Activity state (A), Moderate Activity state (B), and Inactive state (C), based on different Activity Thresholds (AT). Activity states were defined as: High = >2.00%, Moderate = 0.50-2.00%, and Inactive = <0.50%. Legend identifies data smoothed with different AT. n=12 individuals per bar.

Noldus Ethovision has a function to bin activities as high, moderate, or low. This binning analysis was investigated for use in seizure measurement (Fig 5). The activity state study supports earlier data that suggests more movement can be measured with lower concentrations of PTZ. The frequency of high activity is greater in lower PTZ concentrations than in the higher concentrations (Fig 5A), and the frequency of inactivity is greatest in high PTZ concentrations (Fig 5C). A possible bias in this measurement is that the frequency is calculated by a larva entering a certain activity state but does not consider how long the larva stays in that activity state. To answer this potential bias, the cumulative time spent in the activity states was examined (Fig 6).

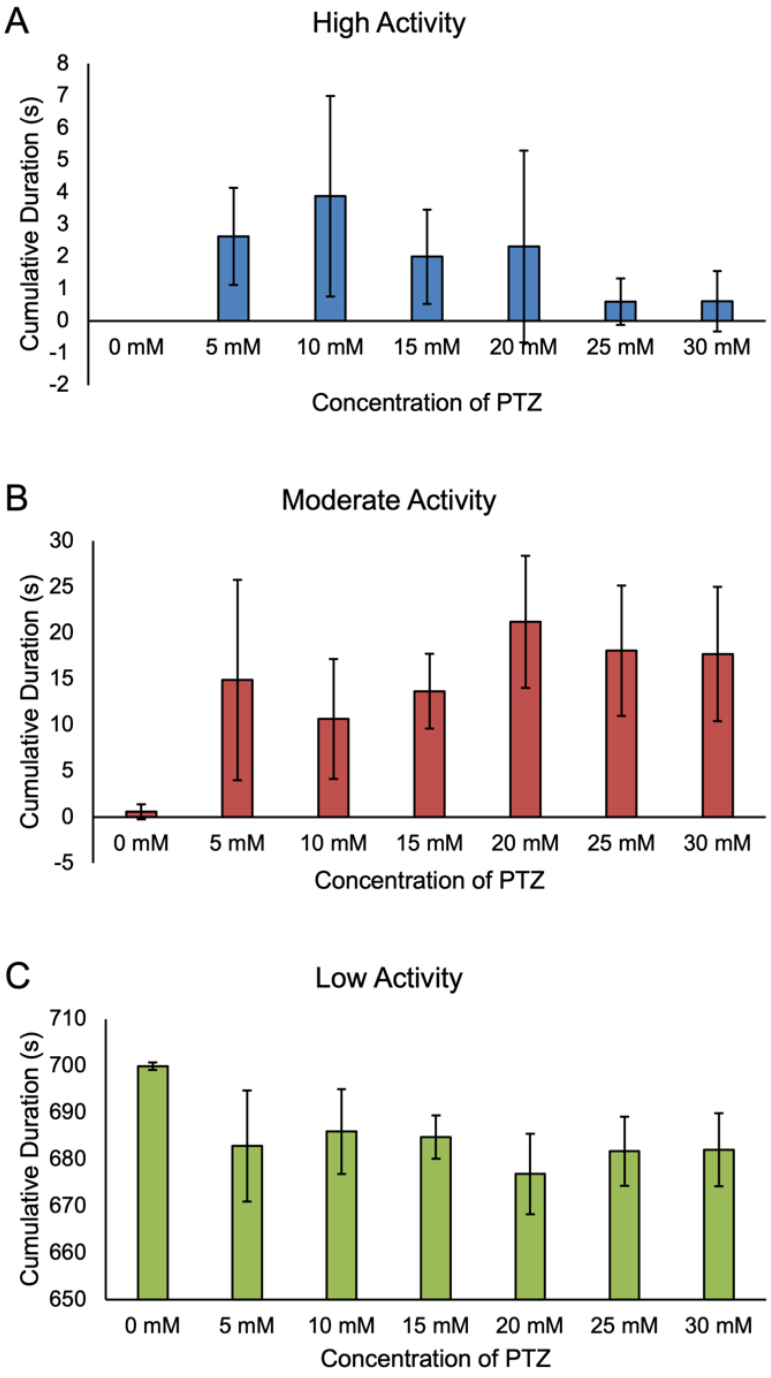

Figure 6. Duration of time in seconds spent in three categories of movement: High (A), Moderate (B), and Low or no activity (C). Error bars are ±SD, n=12 per bar. Trial time was 700 s.

The cumulative time spent in each activity state (Fig 6) correlates with the frequency of entering certain activity states shown in Figure 5. The amount of time that larvae spend in high activity decreases with an increase in PTZ concentration (Fig 6A). However, it seems that time spent in moderate activity increases with PTZ concentration, so the data was summed (Fig 7). The summed data for time spent in a high and moderate activity state still did not support the use of a higher concentration of PTZ, due to the high variability yielding a poor dose-response trend. In fact, the summed data suggests that effective seizure data can be collected at all concentrations of PTZ.

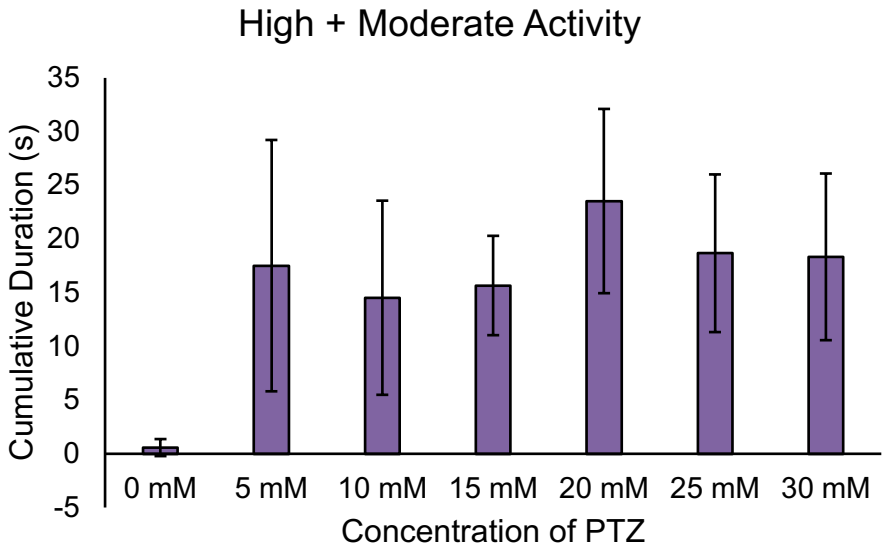

Figure 7. Duration of time in seconds spent in High and Moderate activity combined. Error bars are the sum of SD, n=12 per bar. Trial time was 900 s (15 min).

With sufficient evidence that effective seizure measurements could now be recorded with lower concentrations of PTZ, the effects of dosing with 2.5 mM and 5.0 mM were observed for further work. A variable that had not yet been considered but was

likely contributing greatly to the interindividual variation observed thus far, was the natural variation between offspring from different breeding pairs, or clutches. Larvae were collected from breeding tanks according to breeding pairs and reared separately, they were then exposed to 2.5 mM and 5.0 mM PTZ (Fig 8), on the same day, with the same PTZ stock-solution, and on the same assay plate

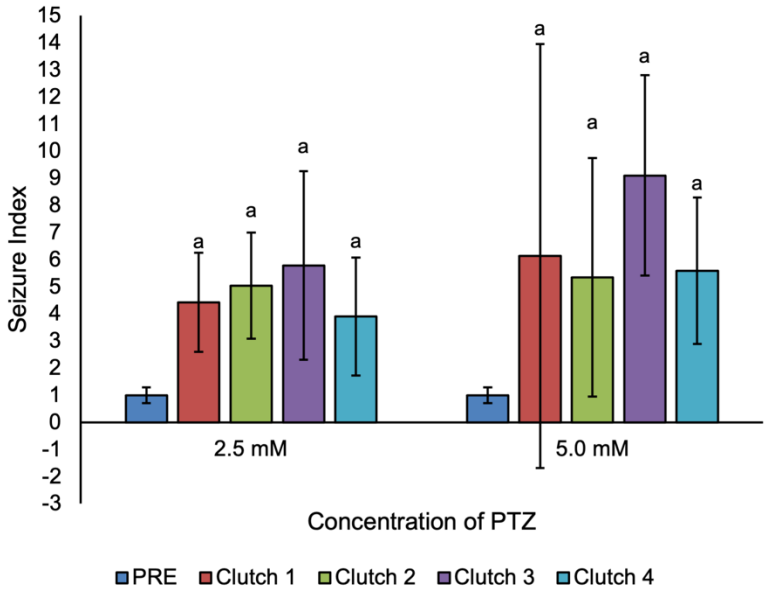

Figure 8. Comparison of response to PTZ, shown as a fold change in activity, normalized to activity before exposure to PTZ. Letters indicate statistical significance by one-way ANOVA. Error bars are ±SD, n_{Clutch}=12, n_{PRE}=96.

Activity data was processed into seizure index, which is a fold change in activity normalized to baseline movement, described in Methods (Fig 8). There were large, but non-significant differences observed in the response to the same treatment of PTZ between clutches. The seizure index was different between clutches and the

interindividual variation varying greatly between clutches. The variation seemed to be less dramatic in the lower concentration of PTZ.

To further investigate the role of clutches and lineage in response to bioactive compounds, a study was conducted to compare the two lineages of wild-type zebrafish possessed by our research group (Fig 9), on the same day, with the same PTZ stock-solution, and on the same assay plate. AB wild-type zebrafish were acquired from the University of Alberta several years prior to the beginning of this study, and AB wild-type zebrafish from Dalhousie University (termed AB(D) in this work) were acquired during this study to maintain variation in the gene pool.

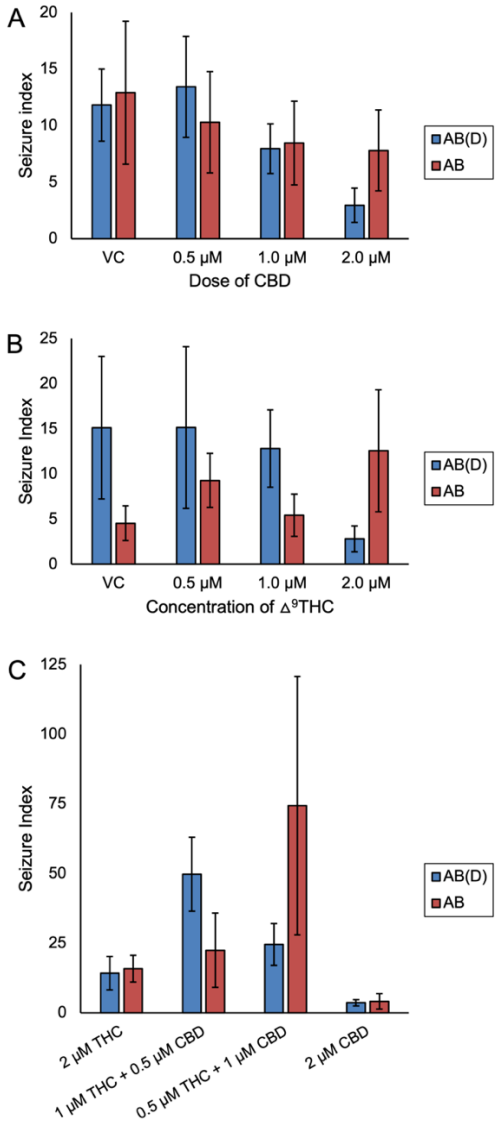

Figure 9. Comparison of response to PTZ and cannabinoids, shown as a fold change in activity (seizure index), normalized to activity before exposure to PTZ. A: Comparing strains AB to AB(D) after treatment with CBD and subsequent exposure to 2.5 mM PTZ. B: Comparing strains AB to AB(D) after treatment with Δ^9-THC and subsequent exposure to 2.5 mM PTZ. C: Comparing strains AB to AB(D) after combined treatment with CBD and Δ^9-THC (THC), with subsequent exposure to 2.5 mM PTZ. Error bars are ±SD, n=12 per bar.

Interestingly, there seemed to be differences observed in the concentration response of each lineage of wild-type zebrafish to cannabinoids. ABs and AB(D)s react similarly to CBD treatment (Fig 9A), but appear to not react similarly to Δ^9-THC treatment, though a two-way ANOVA did not show significant differences between the lineages ($P = 0.9643$) and did not show significant interaction ($P = 0.5409$) (Fig 9B). The response to PTZ was inconsistent between the lineages. Additionally, even the trends in response to combined treatment with CBD and Δ^9-THC did not appear similar between the lineages. To combat the any potential interindividual variation observed, a hybrid cross between AB and AB(D) was the only lineage used for further work, and all larvae were reared separated by clutch.

The described optimization experiments lead to the following parameters for the behaviour monitoring protocol: 6 dpf larvae reared separated by clutch, were treated with potential AEDs or vehicle controls in 180 µL of EM for 30 minutes at 29 °C. Larvae were then tracked for 30 minutes at room temperature, with a 5-minute delay for acclimation. PTZ was then added to a final concentration of 2.75 mM (20 µL of 275 mM) and the larvae were tracked for 30 minutes at room temperature, with a 5-minute delay for acclimation. Larvae were then euthanized and disposed of or stored at -80 °C prior to cannabinoid extraction (described in Methods). Activity analysis was used to quantify movement, with an activity threshold of 2 and a background filtering of 2. It was determined through comparison of analysis methods that seizure index was not a necessary data processing step and so all further data is reported in total activity.

Development of HPLC method

Phytocannabinoids are highly related compounds that have similar chemical properties, therefore optimization steps with analytical standards were necessary prior to processing tissue samples. The optimized method is detailed in Table 4. Calibration curves were created for each of the six cannabinoids in this study using the developed HPLC method (Fig 10).

Table 4. Cannabinoid retention times, quantification wavelengths and analytical figures of merit of the presented method. RT = retention time; Quant. WL = quantification wavelength; LLOD = lower limit of detection; LLOQ = lower limit of quantification; IDV = inter-day variability.

Analyte	**RT (min)**	**Quant. WL (nm)**	**LLOD (µg·mL^{-1} for 20 µL inj.)**	**LLOQ (µg·mL^{-1} for 20 µL inj.)**	**LLOD ng/larva**	**LLOQ ng/larva**	**Linear range and R^2, n=3**	**IDV (%, n=10)**
CBG	4.0	210	0.02	0.07	0.27	1.01	0.1-10 0.9999	5.6
CBD	4.3	210	0.02	0.08	0.28	1.13	0.1-5 0.9997	7.7
CBN	6.6	222	0.01	0.05	0.17	0.66	0.1-10 1.00	3.1
Δ^9-THC	8.3	210	0.01	0.08	0.12	1.04	0.1-5 0.9997	5.9
Δ^8-THC	8.6	210	0.01	0.10	0.17	1.45	0.1-5 0.9994	8.6
CBC	10.3	230	0.03	0.08	0.35	1.11	0.1-10 0.9999	1.3

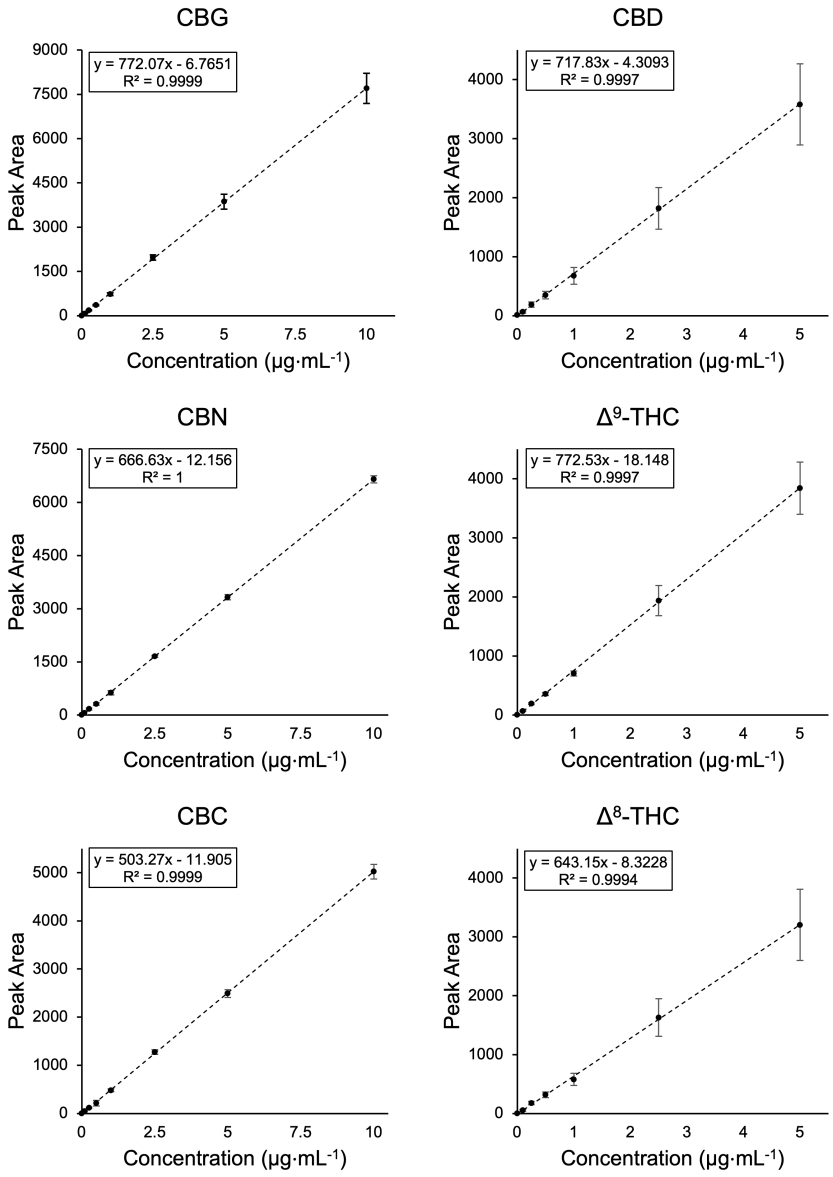

Figure 10. External calibration curves across the linear range of each compound, presented as average of three different days. Error bars represent the standard deviation between the days. Linear regression analysis is plotted as dotted lines with the equation for the line of best fit and the linear correlation coefficient (R^2) in the overlaid boxes.

The procedure for extraction of cannabinoids from zebrafish larvae partitions cannabinoids into the methanol supernatant, leaving insoluble biomatter as a precipitate. To ensure sufficient extraction of cannabinoids, the pellet was extracted two additional times and the extract quantified (Fig 11). The results show that one extraction is sufficient for quantitative measurement of cannabinoids from zebrafish tissue.

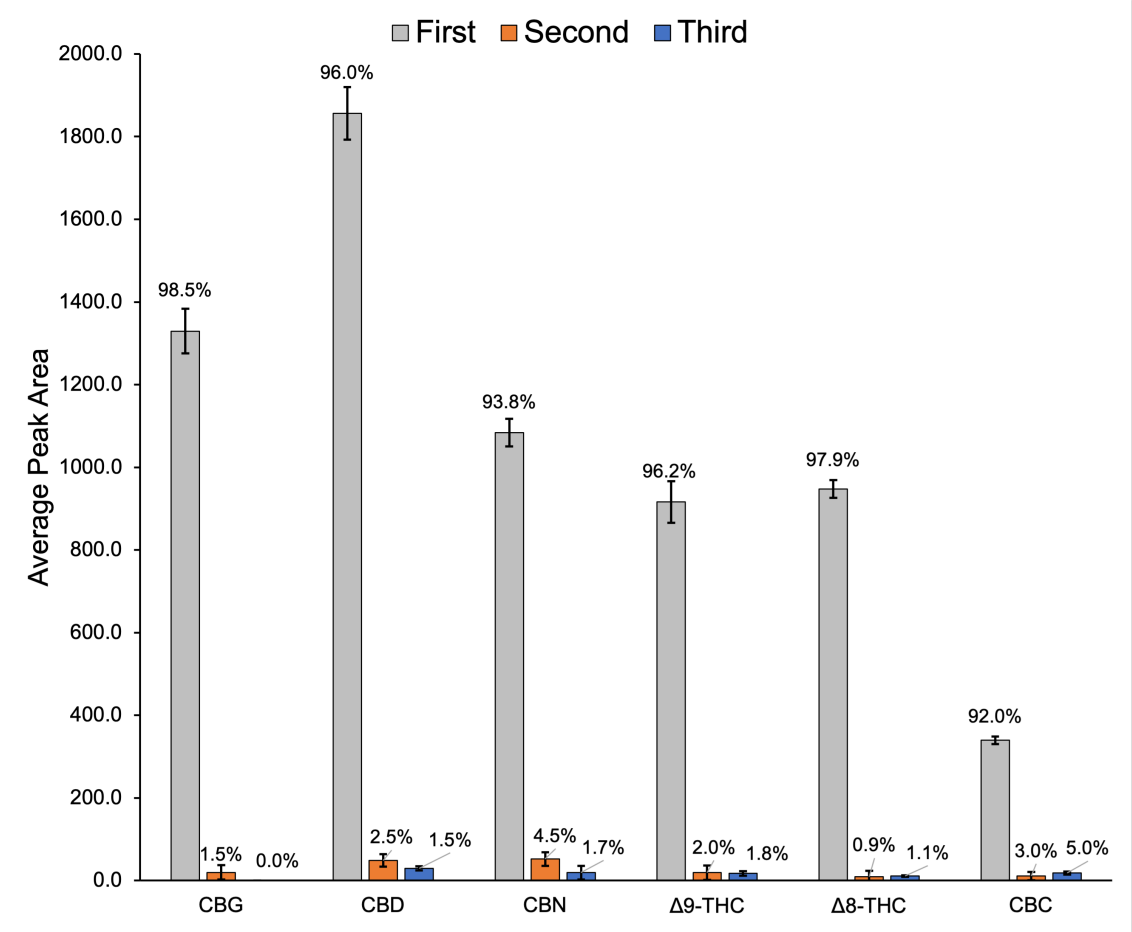

Figure 11. Comparing relative recoveries of three subsequent extractions of 12 pooled larvae treated with 6 cannabinoids at 4 µM. Data labels are relative percent recovery of each extraction. Error bars are SD (n=3).

Individual treatments of cannabinoids

Zebrafish larvae were first given treatment with individual cannabinoids at physiologically relevant concentrations based on literature[106,116], with the intention to compare results to the established anti-epileptic CBD (Fig 12 and 13). Movement after individual treatments of cannabinoid at 1 μM, 2 μM, and 4 μM is shown in Figure 12. Movement is not significantly changed at any concentration of CBD treatment, as compared to vehicle control. However, this is not the case for the remaining five cannabinoid treatments. Treatment with Δ^9-THC, Δ^8-THC, and CBC did not increase movement at 1 μM and 2 μM, but significantly increased movement at 4 μM treatment. Treatment with CBD appeared to decrease movement at 1 μM but increased movement at 4 μM. CBG treatment displays a positive dose-response trend, wherein increasing concentration of treatment increases movement. Upon visual inspection, larvae did not show sedation behaviours within the 30 minute time frame and concentrations of cannabinoids tested. Sedation behaviour can be observed as very minimal movement and delayed or lack of response to stimuli. These individuals were then exposed to PTZ at 2.75 mM concentration in order to model epilepsy, and the seizure movements tracked (Fig 13).

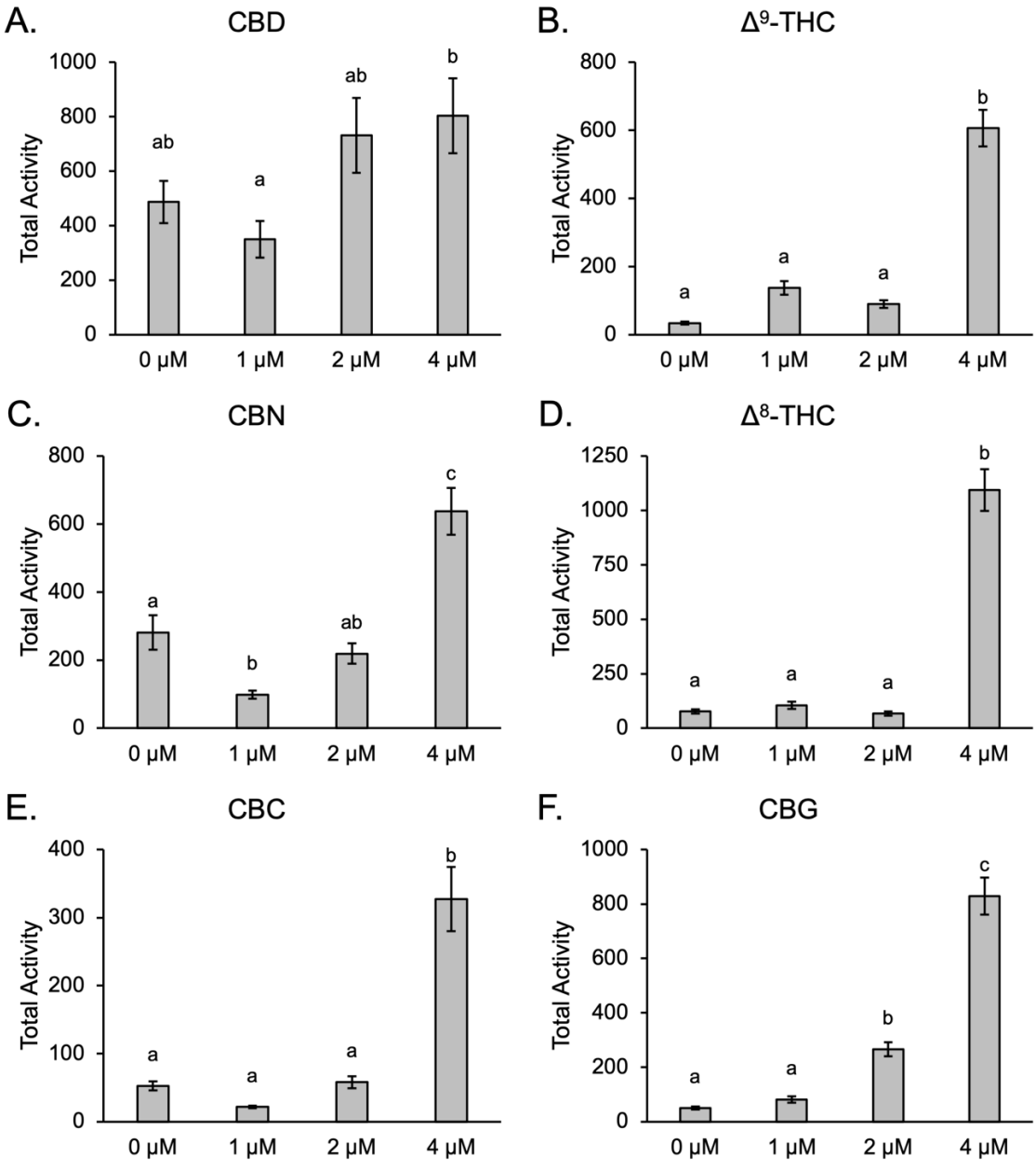

Figure 12. Movement of wildtype zebrafish larvae after cannabinoid treatment, shown as activity. Error bars are SEM, data labels represent significance where different letters are statistically significant (significance calculated by one-way ANOVA, alpha<0.05). A: n=71-72 per treatment, B: n=70-72 per treatment, C: n=69-72 per treatment, D: n=67-72 per treatment, E: n=71-72 per treatment, F: n=70-72 per treatment.

Seizure movements were measured as activity and larvae were then analyzed for cannabinoid tissue accumulation using HPLC. All cannabinoids showed a reduction in seizure activity at a 4 μM cannabinoid treatment, however visual inspection of the larvae suggests that larvae are sedated at this treatment concentration with PTZ As reported previously, CBD showed seizure relief at 2 and 4 μM treatments[116]. This was also observed in individual treatments of CBN and CBC, however there was also a statistically significant reduction in seizures at a 1 μM treatment. Accumulation of CBD, CBN, and CBC in tissue decreased with decreasing concentrations. Interestingly, CBN and CBC provided seizure relief at 1.6 ± 0.1 ng/larva and 1.7 ± 0.3 ng/larva, respectively, the lowest accumulation in tissues in this study.

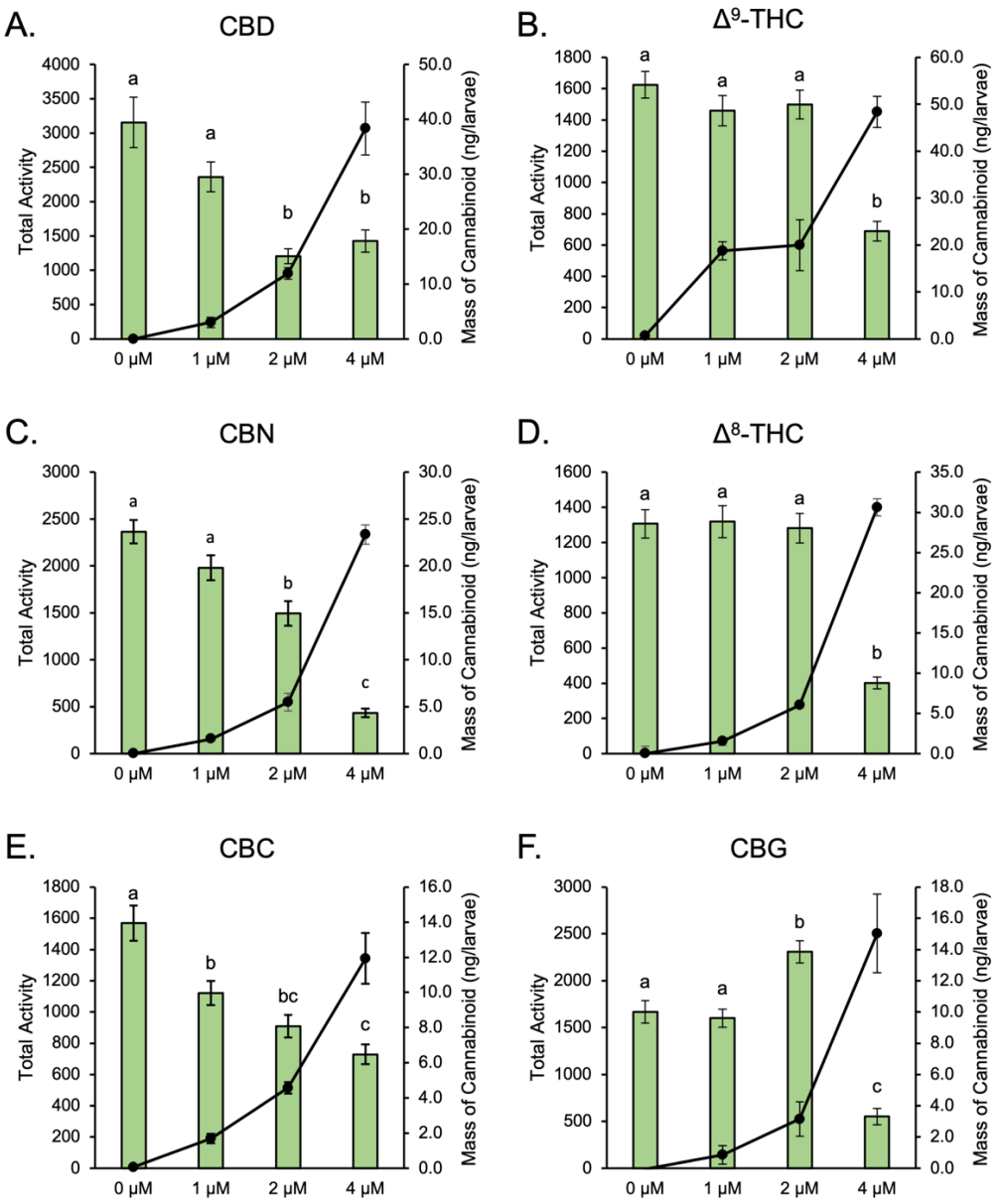

Figure 13. A-F: Seizure reduction and cannabinoid concentration following individual dosing of cannabinoids. Error bars are SEM, significance calculated by one-way ANOVA, alpha<0.05, bars with a different letter data label are significantly different. "0 µM" treatment is the vehicle control. A: n = 71-72, B: n = 71-72, C: n = 68-72, D: n = 71-72, E: n = 71, F: n = 70-72. HPLC quantification of mass of cannabinoid per larva is

shown as connected points (error bars are SD), n=8 samples per data point with triplicate injection.

The accumulation of Δ^8-THC in larval tissue showed an expected concentration-dependent increase. A plateau was observed in Δ^9-THC accumulation, where a difference in accumulation was not seen between 1 and 2 μM treatments (ns, $p< 0.75$, student's t-test) but was observed after 4 μM treatment. A higher mass of Δ^9-THC accumulated in tissue compared to Δ^8-THC. CBG also did not provide seizure relief in treatments below 4 μM, but interestingly there was a repeatable increase in activity observed at a 2 μM treatment.

GPR55 partially mediates CBD seizure relief

CBD treatment was paired with antagonists of receptors that likely mediate seizure relief (Fig 14). CB1R is antagonized by AM-251, GPR55 is antagonized by ML-193, and GPR18 is antagonized by PSB-CB5. The anti-epileptic effect of CBD was not affected by blocking of CB1R or GPR18. Final concentration of concentrations are as follows: 2 μM CBD (based on this work), 1 μM AM-251[85], 2.5 μM ML-193[142], 2.5 μM PSB-CB5[143], 2.75 mM PTZ (based on this work). Seizure relief from CBD treatment was reduced when GPR55 was blocked, however seizures were still reduced as compared to the vehicle control.

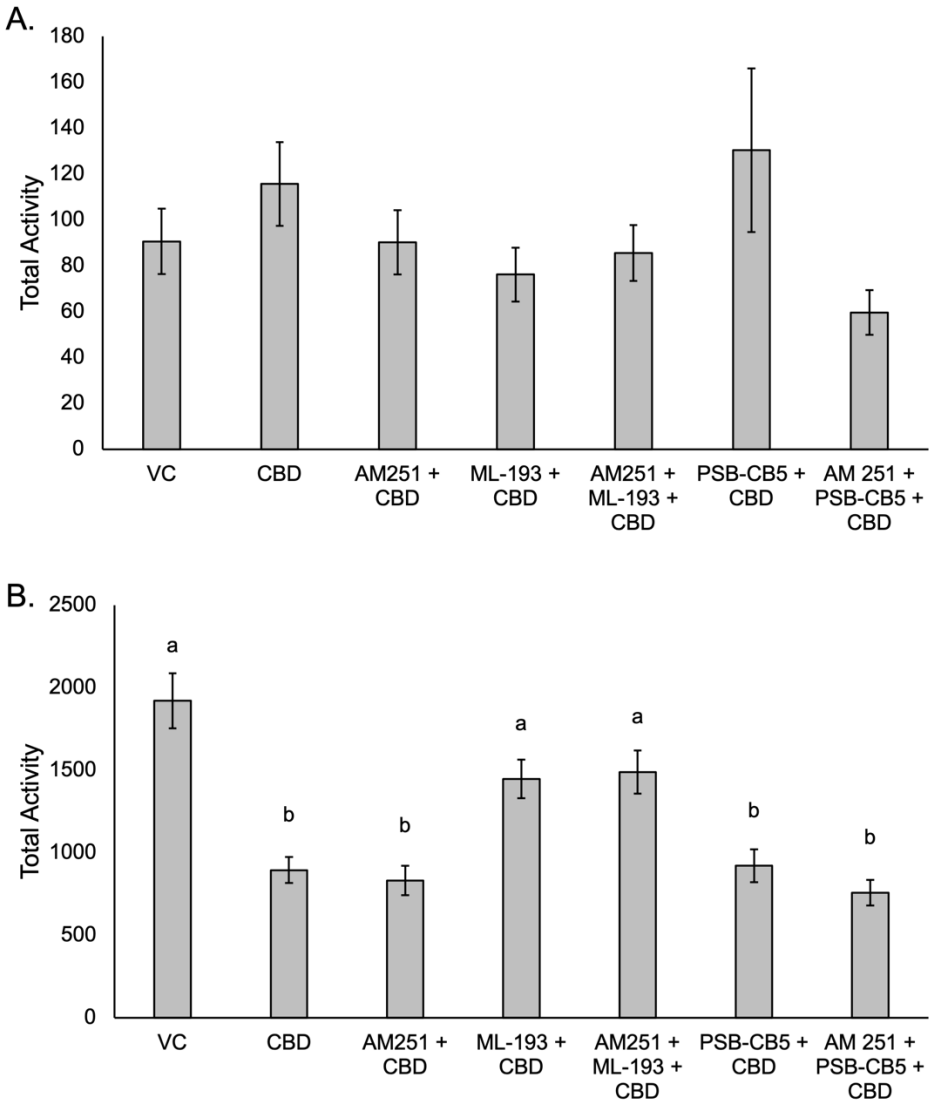

Figure 14. Seizure behaviour after treatment with CBD and receptor antagonists. A: baseline movement before addition of PTZ (n=32-35 per treatment); B: movement after addition of PTZ to final concentration of 2.75 mM (n=34-36 per treatmnet), with x-axis labels corresponding to treatment. VC: vehicle control. Significance is noted by data labels (one-way ANOVA with Tukey HSD, $p<0.05$), data in A is insignificant; bars with a different letter data label are significantly different.

Given the clear involvement of the ECS in CBD induced seizure relief, the potential of treating epilepsy with endocannabinoids was investigated (Fig 15). Larvae were treated using the same protocol as individual cannabinoid treatments, and though some changes in movement were observed in wild-type larvae, there was no seizure relief produced by treatment with 2-AG or AEA in the epilepsy models.

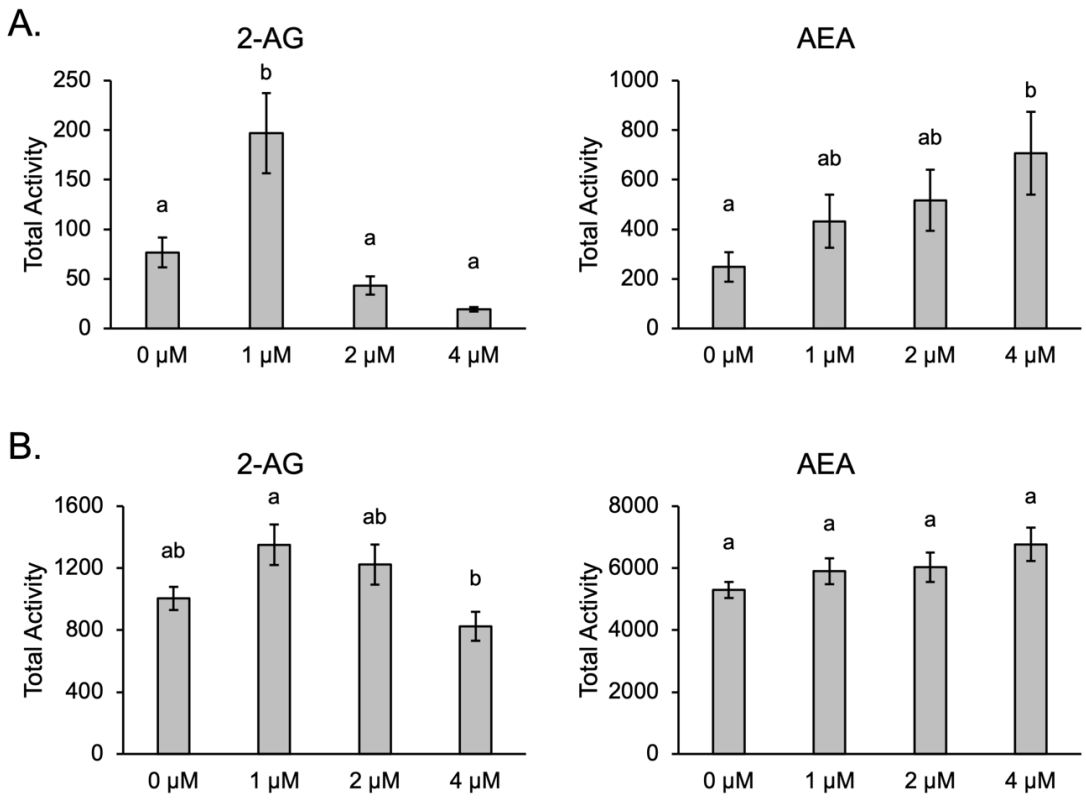

Figure 15. Concentration-response of epilepsy model to endocannabinoid treatment as per the chart titles. A: baseline movement before addition of PTZ. B: movement after addition of PTZ to final concentration of 2.75 mM, with x-axis labels corresponding to concentration of endocannabinoids. "0 µM" treatment is the vehicle control. Error bars are SEM, significance calculated by one-way ANOVA, alpha<0.05. 2-AG: n=44-48 per treatment. AEA: n=35-40 per treatment.

Cannabinoid induced changes in expression

Based on observed anti-epileptic properties, changes in expression of neural and ECS genes were evaluated in our epilepsy model after treatment with CBD, CBN, and Δ^9-THC (Figure 15). Using qPCR on whole body RNA, seven gene targets were investigated: *fosab, pyya, napepld, faah, gde1, ptgs2a*, and *ptgs1*.

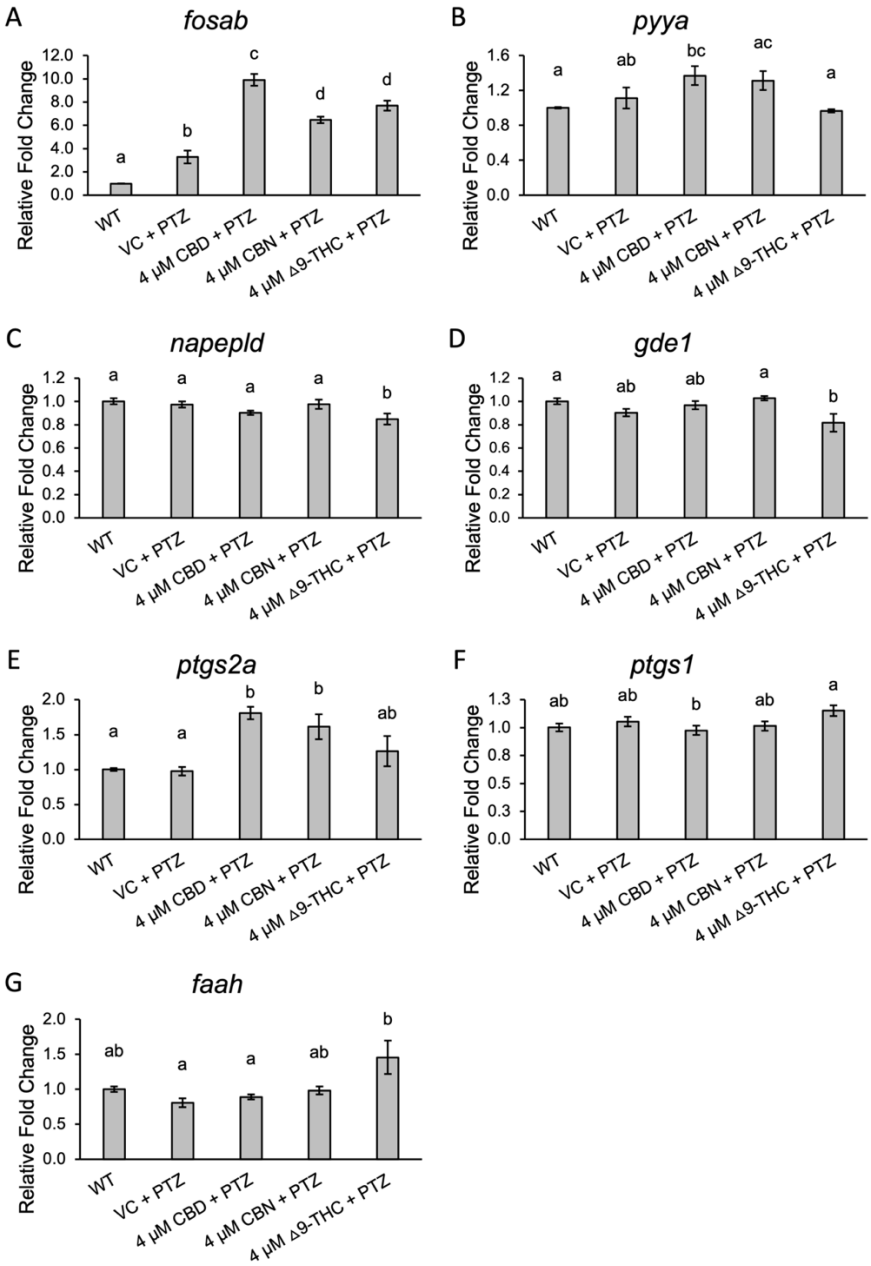

Figure 16. qPCR expression analysis of seizure markers and endocannabinoid system genes. Methanol (0.12%) was used as the vehicle control, with 4 μM cannabinoid concentrations. Significance is noted by data labels (one-way ANOVA with Tukey HSD, $p<0.05$); bars with a different letter data label are significantly different. Error bars are SEM.

Expression of *fosab* was increased in all treatments compared to wildtype but was most increased in the CBD treatment. Treatment with CBN and Δ^9-THC had increased expression of *fosab* compared to PTZ alone, was not as high as the CBD treatment. Expression of *pyya* was significantly increased in CBD treatment and visually increased in CBN treatment but was not statically different from wildtype expression after treatment with PTZ alone or PTZ with subsequent Δ^9-THC treatment. Expression of *napepld* was unchanged in all treatments compared to the wildtype, except the Δ^9-THC treatment where expression was significantly decreased. Similarly, Δ^9-THC was the only treatment to significantly decrease expression of *gde1*, but slight decreases in expression were observed after treatment with PTZ alone or PTZ with subsequent CBD treatment. Expression of *ptgs2a* was unchanged after treatment with PTZ alone but increased with all cannabinoid treatments. CBD and CBN treatment caused significant increase in expression of *ptgs2a*. Expression of *ptgs1* not significantly different in any treatment as compared to wildtype expression, however expression was relatively decreased after CBD treatment and relatively increased after Δ^9-THC treatment.

Expression of *faah* was not as easily understood in our experimental set-up. All treatments were relatively consistent between biological replicates except the larvae treated with Δ^9-THC. In the first biological replicate, Δ^9-THC treatment appeared to increase *faah* expression. This was not the case in the second biological replicate, where *faah* expression decreased. RNA from a third biological replicate of the wild-type control and Δ^9-THC treatment was extracted and analysed, in which *faah* expression was slightly increased but not significantly. To determine if it was experimental error, qPCR was repeated on RNA from the first biological replicate on the same plate as the third. The

result from the first biological replicate was repeated, but the third biological replicate agreed with the second replicate. The replicate data were combined and analysed together (Fig 16G).

Mixed treatments of cannabinoids

The anti-epileptic properties of CBD have been well documented, with some reports of an enhancement of these properties after a combined treatment with other cannabinoids[62,106]. CBD was paired with each of the five remaining cannabinoids in this study, with the results compared to individual treatments (Fig 17). Synergistic anti-epileptic effects were observed in treatments where CBD was paired with CBG, Δ^9-THC, and Δ^8-THC, wherein the activity of the paired treatment was significantly lower than the corresponding individual treatments. Paired treatments of CBD & CBN, and CBD & CBC, did not induce synergistic anti-epileptic effects. Surprisingly, individual treatments of CBD and CBN were statistically different, and the paired treatment showed a medial response.

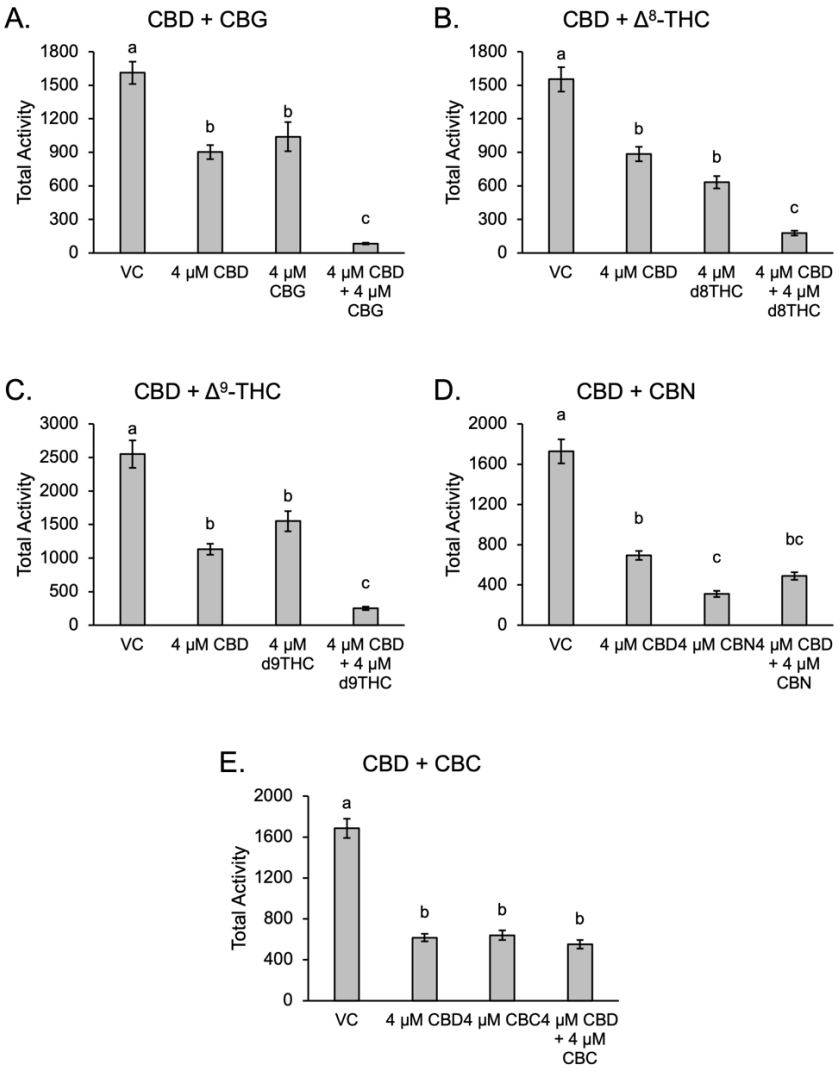

Figure 17. A-E: Seizure tracking comparing the effects of dosing with individual verses paired cannabinoids (error bars are SEM). "0 µM" treatment is the vehicle control. Significance is noted by data labels (one-way ANOVA with Tukey HSD, $p<0.05$); bars with a different letter data label are significantly different. A: n=68-72 per treatment B: n=66-72 per treatment, C: n=69-72 per treatment, D: n=68-71 per treatment, E: n=67-72 per treatment.

Discussion

Spontaneous epilepsy was modelled in zebrafish using the convulsant PTZ. Behavioural monitoring of seizures was completed with video tracking and used to measure effects of phytocannabinoid treatments. I created and optimized a method for the measurement of epileptic behaviour in zebrafish using a prototype tracking apparatus and the Noldus Ethovision XT software. The several experiments (Fig 3-9; Appendix B) required to determine the best tracking settings and algorithm lead me to the final answer of activity analysis, which is a sensitive and robust method for behaviour analysis. A challenge that was faced in this work, and that is often faced when attempting to replace human lead analysis with a software, is that software is developed based on healthy baseline observations. The Noldus Ethovision software is designed with tools to eliminate erratic movements, assuming these tracked movements were erroneous and the result of a camera or computer glitch. These tools would be useful in traditional behaviour analyses such as fear-learning, but in the case of epileptic behaviours which are erratic by definition, recognizing the difference between a true erratic movement and a glitch is very challenging. This of course was helped greatly by an upgrade in equipment, and the final method was reliable and high throughput.

When studying living organisms, it often an adage that “they don’t do what you want”. High variability is unavoidable, especially when processing behavioural data, and it is often necessary to reduce population variability in order to discern experimental results. It is common in fish studies to have high variation between holding tanks (personal communication), and so it was unsurprising that when experiments were

conducted on offspring from the same breeding pairs, variation was lower. What was unexpected was the great difference in response observed between strains of AB wildtype zebrafish (Fig 9), which all have the same origin but were reared in different populations in locations across the country. This is an important factor to consider for both conducting and interpreting future pharmacological studies using zebrafish.

Development of HPLC method

A novel HPLC method was developed and employed, allowing for direct quantitation of cannabinoids in larvae. The developed method is simple and highly reproducible, allowing for reliable use for the quantitation of cannabinoids in pharmacological studies. The method runtime of 12 minutes is suitable for medium-throughput analysis, with separation of 6 cannabinoids. CBG eluted at 4.0 min, followed by CBD at 4.3 min, CBN at 6.6 min, Δ^9-THC at 8.3 min, Δ^8-THC at 8.6 min, CBC at 10.3 min. Calibration curves for each cannabinoid were linear, with R^2 values ranging from 0.9994-1.0 (Fig 10). The lower limits of detection and quantification (LLOD and LLOQ, respectively) were calculated by multiplying the standard error of the y-intercept by 3 or 10, respectively for LLOD or LLOQ, and adding this to the intercept value. The obtained values are within the useful limits for dosing larval zebrafish with cannabinoids (Table 3). Upper limits of quantification are well above the practical dosing range for larval zebrafish. Inter-day variability of the method was determined through injection of a 1 $\mu g \cdot mL^{-1}$ mixed standard on ten different days (n=10), giving an average percent deviation of 5.3% with individual cannabinoids ranging from 1.3 to 8.6% (Table 4). In the vehicle control treatments (0 μM concentration of cannabinoid), noise in the UV signal gave a

small numerical value for detection of CBD, CBN, Δ^9-THC, and CBC. These values are negligible as they are lower than the LLOQ in all cases as well as based on their associated standard deviation (ex. 0 μM concentration of CBD gave a reading of 0.0 ± 0.1 ng/larva). This observation shows that the HPLC method is robust and reliable, as the observed noise in zebrafish tissue samples is lower than the LLOQ of cannabinoids.

To ensure complete extraction of cannabinoids from larvae, we conducted three sequential extractions on samples of treated larvae and found that a single extraction, on average for all compounds, recovered 95.7% while the second and third extractions yielded 2.4% and 1.8%, respectively. Individual recoveries from single extractions ranged from 92.0% to 98.5% (Fig 11). This high and reliable recovery from a single step extraction is superior to previously published methods.

Individual treatments of cannabinoids

Individual treatment of cannabinoids on wild-type larvae showed a relative lack of change in movement at 1 μM and 2 μM concentrations for most cannabinoids tested. The exceptions of which was the 1 μM CBN treatment, which caused a statistically significant decrease in movement, and the 2 μM CBG treatment, which caused a statistically significant increase in movement (Fig 12). What is quite interesting compared to the movement results after PTZ treatment, is that all cannabinoids tested caused an increase in movement at a 4 μM treatment concentration. Previously reports suggest that a decrease in activity was expected given the dark environment the individuals were subjected to[106,116]. It was found that concentrations of CBD and Δ^9-THC above 3 μM led to an increase in hyperactivity of 5 dpf *GABRA1*-/- larvae[106], however the larvae used in

this study were wild-type and therefore this result is unexpected. The parameters used to measure movement differ in this study compared to those referenced, and this may explain the difference in result. The measure of activity using pixel change is likely more sensitive to detecting small movements than using centre-point tracking and it is possible that this explains the discrepancy. In the following data, which used the same individuals but with added PTZ treatment to model epilepsy, the larvae with 4 μM cannabinoid treatment showed the lowest amount of movement.

Analysis of experimental samples with varying concentrations of cannabinoids showed an increasing amount of cannabinoid quantified relative to concentration given (Fig 13). Our seizure tracking data were consistent with a breadth of previous literature supporting the use of CBD as one of the most effective cannabinoids in the reduction of seizures. CBN and CBC also showed a potent reduction of seizures with significant measurable reduction at 1 μM dosage. Interestingly, CBC appeared to be the most potent anti-epileptic in our study, as significant effects were observed with 1.70 ng CBC measured per single larva, the lowest abundance quantified that was associated with a reduction in seizures. Additionally, there was no measurable sedative effects of CBC at both 1 and 2 μM doses before PTZ, and a more potent (per ng) anti-convulsant effect after PTZ with very little accumulation of the drug in larvae. This clinically relevant finding could provide next steps in alternative cannabinoids for the treatment of epilepsy. The structural isomers Δ^9-THC and Δ^8-THC, as well as CBG, showed significant reduction in seizures only at a 4 μM dosage. Interestingly, a 2 μM concentration of CBG repeatedly increased movement significantly to a level higher than

the vehicle control. CBG has a broad range of binding affinities for a unique range of receptors, which has been heavily reported to change based on concentration[70,73,81,84], which is likely the reason behind this unexpected concentration-response trend.

It is unclear why the movement behaviour and trends are so opposing in wild-type larvae verses larvae that model epilepsy. This is likely due to the molecular mechanisms of action of cannabinoids as well as the mechanisms associated with seizures and epilepsy. Further research into the mechanism of action and molecular targets of cannabinoids, specifically components of the ECS, could help explain the difference in observed behaviours.

GPR55 partially mediates CBD seizure relief

After establishing the effects of treatment with individual cannabinoids, I then sought to further investigate the mechanism of action of CBD mediated seizure relief. By treating larvae with CBD as well as antagonists of CB1R, GPR55, and GPR18, mechanism of action was determined by observing which conditions negatively affected seizure relief (Fig 14). The data shows that CBD acts through GPR55 as one modality to reduce seizures. When GPR55 is blocked, CBD induced seizure reduction is reduced but not eliminated, suggesting there is more than one mechanism of action, or that the blockade of GPR55 was incomplete. It was reported that CBD did not act upon GPR55 to cause an increase in intracellular calcium[32], so it is possible that CBD inactivates GPR55. Significance of the data was determined by one-way ANOVA with Tukey HSD (Fig 14), and it should be noted that when data were analyzed as two separate experiments to determine GPR55 vs GPR18 activity, a slightly different significance trend was observed.

That is, when the ANOVA was conducted on the treatment data from VC, CBD, AM-251 + CBD, ML-193 + CBD, and AM-251 + ML-193 + CBD, the last treatment had the same significance as VC and ML-193 + CBD. When both GPR55 and CB1R are blocked, the reduction in seizure relief is slightly more than when GPR55 alone is blocked. This suggests that CB1R may also mediate CBD's anti-epileptic effects, which is supported by reports of CBD having low affinity to CB1R, however further investigation is required. CB1R activation has been reported to suppress GABAergic transmission in the hypothalamic proopiomelanocortin, oxytocin-expressing neurons, and hippocampal slices[30]. Blocking GPR18 showed no effect on CBD induced seizure reduction, which is a novel report and supports the idea that GPR18 is more-so associated with CB2R[38] rather than being its own ECS receptor. Further work could be carried out using a GPR55 knockout zebrafish line to determine if the observed effects are dampened, suggesting the mechanism of action may be due to interaction of CBD with GPR55.

Despite treatment with ECS antagonists indicating a clear involvement of the ECS in CBD induced seizure relief through GPR55, treatment of larvae with 2-AG or AEA did not provide any seizure reduction in our model (Fig 15). More investigation on the mechanism of action of AEDs and anti-epileptic cannabinoids is required, as there are many interwoven pathways that may have an effect. The lack of seizure relief observed after treating with endocannabinoids in this model is likely due to the experimental design. Endocannabinoids are highly unstable and lipidic in nature[30], so the mechanism of dosing used in this study of adding treatments to the fish water to be ingested or absorbed is not the best for unstable and hydrophobic compounds. Beyond this, it is unlikely that sufficient concentrations of intact endocannabinoid travelled through the digestive system

and into the brain in order to actually affect a change. Foundational investigation on endocannabinoids providing seizure reduction would be better suited to a simpler model system such as neuronal cell culture where digestion and more complex compound transport and metabolism can be avoided, before proceeding with further fish model experiments.

Cannabinoid induced changes in expression

The mechanism of action of CBD, CBN, and Δ^9-THC was further investigated through gene expression studies (Fig 16-17). Using RT-qPCR change in expression of seven genes was measured in our epilepsy model after a concentration of 4 μM cannabinoid. The neuronal activity marker c-Fos (*fosab*) commonly serves as a seizure marker in epilepsy studies, however it is primarily a transcription factor in terms of function and is more appropriate for determining seizure progression than intensity of seizures[20]. We found that treatments of CBD, CBN, and Δ^9-THC dramatically increased *fosab* expression, while the vehicle control (treated with PTZ and methanol) which displayed the most epileptic behaviour, did not have a similarly dramatic increase expression (Fig 16A). This may be due to the experimental design as RNA was isolated from entire larvae, and it has been established that *fosab* expression is increased primarily in the brain during PTZ-induced seizures. Treatment with CBD or Δ^9-THC was reported to cause a concentration-dependent increase in *c-fos* expression in 96 hpf embryos[127], and a fear-learning study found that only specific brain structures increase c-Fos expression following Δ^9-THC treatment[111]. Future work could mitigate this by sampling only brain tissue for RNA isolation, or qualitative data could be collected through in-situ

hybridization using a *fosab* probe. It is also possible that the increased expression of *fosab* after cannabinoid treatment is completely unrelated to seizure mechanisms.

We showed that expression of the appetite suppressing signalling peptide *pyya* is increased during seizures as well as after CBD and CBN treatment (Figure 16B). Expression of *pyya* after Δ^9-THC treatment is the same as that in wild-type untreated embryos, suggesting a return to homeostasis counter-acting the effects of the convulsant PTZ, which is expected as it is Δ^9-THC that is often associated with an increase in appetite. To the best of my knowledge, there has not yet been a report of a change in *pyya* or peptide YY levels after CBD treatment. Due to the interlinked nature of the NPY system and the possible promiscuity of ligand-receptor interactions within the NPY system[118,120,122], the literature is divided on the involvement of *pyya* in seizures. More investigation is needed to determine if *pyya* may contribute to the mechanism of action of seizure relief by CBD and CBN and could be investigated using *pyya* knockout lines.

Expression of the enzyme responsible for the creation of the endocannabinoid anandamide (AEA), *napepld*, decreased after Δ^9-THC treatment (Fig 16C). Δ^9-THC and AEA have been reported to act on the same receptors[32,36,37,50,66] and this further supports literature on the putative mechanism of action of Δ^9-THC. The decrease in expression of *napepld* is likely due a negative feedback loop in the ECS. Similarly, expression of *gde1* was decreased after Δ^9-THC treatment but remained constant after all other treatments (Fig 16D). In patients treated with CBD, there was an observed increase in serum levels of AEA compared to the placebo-control patients[144], which is one hypothesis for the mechanism of action of CBD mediated seizure relief[50]. Though the expression of *napepld* and *gde1* did not change significantly after CBD treatment, there is a visual decrease in

napepld and *gde1* expression. The significance of *gde1* expression after CBD treatment was the same as the expression after Δ^9-THC treatment, which was significantly downregulated, however this is confounded by the CBD treatment also having the same significance as the wildtype and vehicle control expressions. These results indicate a feedback system designed to regulate AEA synthesis that can be triggered by phytocannabinoid treatment.

Expression of the zebrafish ortholog of *cox-2*, *ptgs2a*, was increased after cannabinoid treatment, with results from CBD and CBN treatment being statistically significant (Fig 16E). COX-2 is responsible for the oxidation of the endocannabinoid 2-AG[145], and it is likely increased in expression as CBD and CBN act on the same receptors as 2-AG[36,50], though this has not been fully established for CBN. This data supports the hypothesis that CBD and CBN share a similar mechanism of action, and that Δ^9-THC has a complementary mechanism of action to CBD. The zebrafish ortholog of *cox-1* is *ptgs1*, which did not undergo significant changes in expression after the treatments tested, however expression was decreased after CBD treatment when compared to an increased expression after Δ^9-THC treatment (Fig 16F). This supports the hypothesis that CBD and Δ^9-THC have different but complementary mechanisms of action.

Mixed treatments of cannabinoids

To determine if the effects of CBD could be enhanced through synergism with another cannabinoid, we evaluated seizure behaviours after treatments of CBD paired with each of the remaining 5 cannabinoids in this study (Fig 18). Strikingly, we observed synergistic effects between CBD and cannabinoids that when treated individually were

only effective at 4 μM, namely Δ^9-THC, Δ^8-THC, and CBG. This interaction suggests and supports a complementary mechanism of action that promotes the effects of CBD. This finding is quite exciting, as it suggests that an opportunity for future work exists in defining and determining the effects of many combinations and concentrations of mixed cannabinoid treatments. In contrast, CBN and CBC, which show antiepileptic effects when used individually, did not show synergism with CBD, suggesting they share the same mechanism of action. This data supports previously reported observations that CBD treatment can provide more effective seizure reduction when combined with other *Cannabis* compounds[62,116,117]. Most studies thus far utilize *Cannabis* plant extracts, with cannabinoids quantified using LC-MS methods, on either wild-type zebrafish[146] or severe epilepsy models[62]. This approach has the benefit of observing combined effects of cannabinoids and terpenes, however in order to understand mechanism of action and elucidate specific interactions, systematic dosing of standards is required. To the best of my knowledge, this is the first report of systematic paired dosing of CBD with five other cannabinoids in an epilepsy model. The data shown here has clinical relevance and can be rapidly built upon for clinical use.

Conclusions

The data reported in this thesis support the hypothesis that cannabinoids are promising anti-epileptics and that cannabinoids can be used in combination for a greater anti-epileptic effect. A robust and high-throughput behavioural analysis method was optimized for the measurement of overall seizure intensity. The behaviour tracking method yielded sensitive and accurate measurements of seizures and reductions of seizures resulting from cannabinoid treatment. A HPLC method was created and employed for the sensitive and reliable measurement of six therapeutically important cannabinoids in zebrafish larvae. When treated individually, CBC and CBN were observed to have anti-epileptic effects at lower concentrations than what was observed with CBD, and CBC appeared to have highest potency with a significant reduction in seizures observed corresponding to the lowest mass quantified (1.70 ng/larva). The direct and accurate quantitation of cannabinoids allows for further investigation of therapeutic use of cannabinoids using zebrafish models. CBD when paired with CBG, Δ^9-THC, or Δ^8-THC showed increased anti-epileptic activity. To the best of my knowledge, this is the first report of synergism observed between CBD + CBG and CBD + Δ^8-THC. The synergistic effect of CBD + CBG treatment is of particular clinical relevance and promise as CBG is non-psychoactive (unlike Δ^9-THC).

The use of ECS antagonists and RT-qPCR for expression analysis after cannabinoid treatment provides novel insights into the mechanism of action of some cannabinoids. CBD induced seizure relief is partially mediated by GPR55, as shown by a medial reduction in seizure relief when CBD was treated alongside a GPR55 antagonist.

Treatment with 2-AG or AEA did not provide any seizure reduction in our model, however further studies with more appropriate dosing methods are required to make a conclusion. Expression of *fosab* increases with phytocannabinoid treatment and in response to PTZ, expression of *pyya* increases after CBD and CBN treatment and in response to PTZ. Expression of *napepld* and *gde1* decreases after Δ^9-THC treatment, likely due to negative feedback regulation of AEA. Expression of *ptgs2a* increases after CBD and CBN treatment, and expression of *ptgs1* is slightly decreased after CBD treatment and slightly increased after Δ^9-THC treatment. These data supports the interaction of phytocannabinoids with the ECS, and the hypothesis that phytocannabinoids related seizure relief is mediated by the ECS. Further studies are required to fully elucidate the ECS pathways and how phytocannabinoids impact the ECS, in the context of both healthy function and epilepsy.

This thesis presents novel data related to the pharmacology, therapeutic potential, and potential mechanism of action of several less studied phytocannabinoids that could be further built upon to soon lead to clinical relevancy. The clinical use of cannabinoids is an interesting research field as the compounds are simultaneously at pre-clinical and clinical stages. Since Cannabis has been used by humans for millennia, and the slow legalization happening around the world, some cannabinoids are readily accessible to patients to wish to self-medicate. Recent legalization also makes it relatively easier to conduct pilot studies in a clinical setting. At the same time, in most countries *Cannabis* is still a heavily controlled substance. In situations where cannabinoids are still illegal, and in situations where potential patients are vulnerable populations such as children, pregnant people, and elderly people, preclinical work is of the utmost importance to establish potential side-

effects by understanding the mechanism of action. A fully elucidated mechanism of action and a fully elucidated ECS can help clinicians predict and avoid adverse effects. With over 100 phytocannabinoids in existence, using cannabinoids as treatments is an understudied realm with many future discoveries on the horizon.

Bibliography

1. Bergen, D. C. Do Seizures Harm the Brain? *Epilepsy Curr* **6**, 117–118 (2006).
2. Kotsopoulos, I. A. W., Van Merode, T., Kessels, F. G. H., De Krom, M. C. T. F. M. & Knottnerus, J. A. Systematic Review and Meta-analysis of Incidence Studies of Epilepsy and Unprovoked Seizures. *Epilepsia* **43**, 1402–1409 (2002).
3. Kwan, P. & Brodie, M. J. Early Identification of Refractory Epilepsy. *N Engl J Med* **342**, 314–319 (2000).
4. Perucca, P. & Gilliam, F. G. Adverse effects of antiepileptic drugs. *The Lancet Neurology* **11**, 792–802 (2012).
5. Scheffer, I. E. *et al.* ILAE classification of the epilepsies: Position paper of the ILAE Commission for Classification and Terminology. *Epilepsia* **58**, 512–521 (2017).
6. Perucca, E. Antiepileptic drugs: evolution of our knowledge and changes in drug trials. *Epileptic Disord* **21**, 11 (2019).
7. Coppola, A. & Moshé, S. L. Animal models. in *Handbook of Clinical Neurology* vol. 107 63–98 (Elsevier, 2012).
8. Grone, B. P. & Baraban, S. C. Animal models in epilepsy research: legacies and new directions. *Nat Neurosci* **18**, 339–343 (2015).
9. Pentetrazol. in *Meyler's Side Effects of Drugs* (ed. Aronson, J. K.) 623 (Elsevier, 2016). doi:10.1016/B978-0-444-53717-1.01243-9.
10. Hansen, S. L., Sperling, B. B. & Sánchez, C. Anticonvulsant and antiepileptogenic effects of $GABA_A$ receptor ligands in pentylenetetrazole-kindled mice. *Progress in Neuro-Psychopharmacology and Biological Psychiatry* **28**, 105–113 (2004).
11. Baraban, S. C., Taylor, M. R., Castro, P. A. & Baier, H. Pentylenetetrazole induced changes in zebrafish behavior, neural activity and c-fos expression. *Neuroscience* **131**, 759–768 (2005).

12. Mussulini, B. H. M. *et al.* Seizures Induced by Pentylenetetrazole in the Adult Zebrafish: A Detailed Behavioral Characterization. *PLoS ONE* **8**, e54515 (2013).

13. Copmans, D. *et al.* Zebrafish-Based Discovery of Antiseizure Compounds from the North Sea: Isoquinoline Alkaloids TMC-120A and TMC-120B. *Mar Drugs* **17**, E607 (2019).

14. Anderson, L. L., Low, I. K., McGregor, I. S. & Arnold, J. C. Interactions between cannabidiol and Δ^{9}-tetrahydrocannabinol in modulating seizure susceptibility and survival in a mouse model of Dravet syndrome. *Br J Pharmacol* **177**, 4261–4274 (2020).

15. Orellana-Paucar, A. M. *et al.* Anticonvulsant activity of bisabolene sesquiterpenoids of *Curcuma longa* in zebrafish and mouse seizure models. *Epilepsy & Behavior* **24**, 14–22 (2012).

16. Serikawa, T. *et al.* Advances on genetic rat models of epilepsy. *Exp Anim* **64**, 1–7 (2015).

17. Berghmans, S., Hunt, J., Roach, A. & Goldsmith, P. Zebrafish offer the potential for a primary screen to identify a wide variety of potential anticonvulsants. *Epilepsy Research* **75**, 18–28 (2007).

18. Baxendale, S. *et al.* Identification of compounds with anti-convulsant properties in a zebrafish model of epileptic seizures. *Dis Model Mech* **5**, 773–784 (2012).

19. Tanwar, G. *et al.* Target identification, screening and in vivo evaluation of pyrrolone-fused benzosuberene compounds against human epilepsy using Zebrafish model of pentylenetetrazol-induced seizures. *Sci Rep* **9**, 7904 (2019).

20. Dragunow, M. & Faull, R. The use of c-fos as a metabolic marker in neuronal pathway tracing. *Journal of Neuroscience Methods* **29**, 261–265 (1989).

21. Morgan, J., Cohen, D., Hempstead, J. & Curran, T. Mapping patterns of c-fos expression in the central nervous system after seizure. *Science* **237**, 192–197 (1987).

22. Snyder-Keller, A. M. & Pierson, M. G. Audiogenic seizures induce c-fos in a model of developmental epilepsy. *Neuroscience Letters* **135**, 108–112 (1992).

23. Velazquez, F. N., Caputto, B. L. & Boussin, F. D. c-Fos importance for brain development. *Aging (Albany NY)* **7**, 1028–1029 (2015).

24. Sharp, F. R., Gonzalez, M. F., Hisanaga, K., Mobley, W. C. & Sagar, S. M. Induction of the c-fos gene product in rat forebrain following cortical lesions and NGF injections. *Neuroscience Letters* **100**, 117–122 (1989).

25. Hunt, S. P., Pini, A. & Evan, G. Induction of c-fos-like protein in spinal cord neurons following sensory stimulation. *Nature* **328**, 632–634 (1987).

26. Ceccatelli, S., Villar, M. J., Goldstein, M. & Hökfelt, T. Expression of c-Fos immunoreactivity in transmitter-characterized neurons after stress. *Proc. Natl. Acad. Sci. U.S.A.* **86**, 9569–9573 (1989).

27. Halazonetis, T. D., Georgopoulos, K., Greenberg, M. E. & Leder, P. c-Jun dimerizes with itself and with c-Fos, forming complexes of different DNA binding affinities. *Cell* **55**, 917–924 (1988).

28. Freund, T. F., Katona, I. & Piomelli, D. Role of Endogenous Cannabinoids in Synaptic Signaling. *Physiological Reviews* **83**, 1017–1066 (2003).

29. Hussain, Z., Uyama, T., Tsuboi, K. & Ueda, N. Mammalian enzymes responsible for the biosynthesis of N -acylethanolamines. *Biochimica et Biophysica Acta (BBA) - Molecular and Cell Biology of Lipids* **1862**, 1546–1561 (2017).

30. Alger, B. E. & Kim, J. Supply and demand for endocannabinoids. *Trends in Neurosciences* **34**, 304–315 (2011).

31. Long, J. Z. *et al.* Selective blockade of 2-arachidonoylglycerol hydrolysis produces cannabinoid behavioral effects. *Nat Chem Biol* **5**, 37–44 (2009).

32. Lauckner, J. E. *et al.* GPR55 is a cannabinoid receptor that increases intracellular calcium and inhibits M current. *Proc. Natl. Acad. Sci. U.S.A.* **105**, 2699–2704 (2008).

33. Mackie, K. & Stella, N. Cannabinoid receptors and endocannabinoids: evidence for new players. *AAPS J* **8**, E298-306 (2006).

34. Neumann, S., Doubell, T. P., Leslie, T. & Woolf, C. J. Inflammatory pain hypersensitivity mediated by phenotypic switch in myelinated primary sensory neurons. *Nature* **384**, 360–364 (1996).

35. Callén, L. *et al.* Cannabinoid Receptors CB1 and CB2 Form Functional Heteromers in Brain. *Journal of Biological Chemistry* **287**, 20851–20865 (2012).

36. Zhang, S.-S. *et al.* The impact of phyto- and endo-cannabinoids on central nervous system diseases : A review. *Journal of Traditional and Complementary Medicine* S2225411022000761 (2022) doi:10.1016/j.jtcme.2022.10.004.

37. Zygmunt, P. M. *et al.* Vanilloid receptors on sensory nerves mediate the vasodilator action of anandamide. *Nature* **400**, 452–457 (1999).

38. Reyes-Resina, I. *et al.* Molecular and functional interaction between GPR18 and cannabinoid CB2 G-protein-coupled receptors. Relevance in neurodegenerative diseases. *Biochem Pharmacol* **157**, 169–179 (2018).

39. Gantz, I. *et al.* Cloning and Chromosomal Localization of a Gene (GPR18) Encoding a Novel Seven Transmembrane Receptor Highly Expressed in Spleen and Testis. *Genomics* **42**, 462–466 (1997).

40. Kohno, M. *et al.* Identification of N-arachidonylglycine as the endogenous ligand for orphan G-protein-coupled receptor GPR18. *Biochemical and Biophysical Research Communications* **347**, 827–832 (2006).

41. Okamoto, Y., Morishita, J., Tsuboi, K., Tonai, T. & Ueda, N. Molecular Characterization of a Phospholipase D Generating Anandamide and Its Congeners. *Journal of Biological Chemistry* **279**, 5298–5305 (2004).

42. Oltrabella, F., Melgoza, A., Nguyen, B. & Guo, S. Role of the endocannabinoid system in vertebrates: Emphasis on the zebrafish model. *Develop. Growth Differ.* **59**, 194–210 (2017).

43. Cravatt, B. F. *et al.* Molecular characterization of an enzyme that degrades neuromodulatory fatty-acid amides. *Nature* **384**, 83–87 (1996).

44. McKinney, M. K. & Cravatt, B. F. Structure and function of fatty acid amide hydrolase. *Annu. Rev. Biochem.* **74**, 411–432 (2005).

45. Cravatt, B. F. *et al.* Chemical Characterization of a Family of Brain Lipids That Induce Sleep. *Science* **268**, 1506–1509 (1995).

46. Ahn, K., Johnson, D. S. & Cravatt, B. F. Fatty acid amide hydrolase as a potential therapeutic target for the treatment of pain and CNS disorders. *Expert Opinion on Drug Discovery* **4**, 763–784 (2009).

47. Giang, D. K. & Cravatt, B. F. Molecular characterization of human and mouse fatty acid amide hydrolases. *Proc. Natl. Acad. Sci. U.S.A.* **94**, 2238–2242 (1997).

48. Krug, R. G. *et al.* The endocannabinoid gene faah2a modulates stress-associated behavior in zebrafish. *PLoS ONE* **13**, e0190897 (2018).

49. Elmes, M. W. *et al.* Fatty acid-binding proteins (FABPs) are intracellular carriers for Δ9-tetrahydrocannabinol (THC) and cannabidiol (CBD). *J Biol Chem* **290**, 8711–8721 (2015).

50. Kwan Cheung, K. A., Peiris, H., Wallace, G., Holland, O. J. & Mitchell, M. D. The interplay between the endocannabinoid system, epilepsy and cannabinoids. *IJMS* **20**, 6079 (2019).

51. De Petrocellis, L. *et al.* Effects of cannabinoids and cannabinoid-enriched *Cannabis* extracts on TRP channels and endocannabinoid metabolic enzymes: Novel pharmacology of minor plant cannabinoids. *British Journal of Pharmacology* **163**, 1479–1494 (2011).

52. Aguado, T. *et al.* The endocannabinoid system drives neural progenitor proliferation. *FASEB j.* **19**, 1704–1706 (2005).

53. Zheng, B., Berrie, C. P., Corda, D. & Farquhar, M. G. GDE1/MIR16 is a glycerophosphoinositol phosphodiesterase regulated by stimulation of G protein-coupled receptors. *Proc. Natl. Acad. Sci. U.S.A.* **100**, 1745–1750 (2003).

54. Yu, M., Ives, D. & Ramesha, C. S. Synthesis of Prostaglandin E2 Ethanolamide from Anandamide by Cyclooxygenase-2. *Journal of Biological Chemistry* **272**, 21181–21186 (1997).

55. Alhouayek, M. & Muccioli, G. G. COX-2-derived endocannabinoid metabolites as novel inflammatory mediators. *Trends in Pharmacological Sciences* **35**, 284–292 (2014).

56. Desjardins, P. *et al.* Induction of astrocytic cyclooxygenase-2 in epileptic patients with hippocampal sclerosis. *Neurochemistry International* **42**, 299–303 (2003).

57. Serrano, G. E. *et al.* Ablation of cyclooxygenase-2 in forebrain neurons is neuroprotective and dampens brain inflammation after status epilepticus. *Journal of Neuroscience* **31**, 14850–14860 (2011).

58. Russo, E. B. *et al.* Phytochemical and genetic analyses of ancient cannabis from Central Asia. *Journal of Experimental Botany* **59**, 4171–4182 (2008).

59. Porter, B. E. & Jacobson, C. Report of a parent survey of cannabidiol-enriched cannabis use in pediatric treatment-resistant epilepsy. *Epilepsy & Behavior* **29**, 574–577 (2013).

60. Śledziński, P., Nowak-Terpiłowska, A. & Zeyland, J. Cannabinoids in Medicine: Cancer, Immunity, and Microbial Diseases. *IJMS* **22**, 263 (2020).

61. Aran, A. & Cayam-Rand, D. Medical Cannabis in Children. *Rambam Maimonides Med J* **11**, e0003 (2020).

62. Berman, P. *et al.* A new ESI-LC/MS approach for comprehensive metabolic profiling of phytocannabinoids in *Cannabis*. *Sci Rep* **8**, 14280 (2018).

63. Micalizzi, G. *et al.* Cannabis Sativa L.: a comprehensive review on the analytical methodologies for cannabinoids and terpenes characterization. *Journal of Chromatography A* **1637**, 461864 (2021).

64. Thomas, A. *et al.* Cannabidiol displays unexpectedly high potency as an antagonist of CB1 and CB2 receptor agonists in vitro. *Br J Pharmacol* **150**, 613–623 (2007).

65. Amin, M. R., Ahmed, K. T. & Ali, D. W. Cannabinoid receptor 2 (Cb2r) mediates cannabinol (CBN) induced developmental defects in zebrafish. *Sci Rep* **12**, 20251 (2022).

66. Matsuda, L. A. & Young, A. C. Structure of a cannabinoid receptor and functional expression of the cloned eDNA. **346**, 4 (1990).

67. Hollister, L. E. & Gillespie, H. K. Delta-8- and delta-9-tetrahydrocannabinol; Comparison in man by oral and intravenous administration. *Clinical Pharmacology & Therapeutics* **14**, 353–357 (1973).

68. Razdan, R. K. Chemistry and structure-activity relationships of cannabinoids: An overview. in *The Cannabinoids: Chemical, Pharmacologic, and Therapeutic Aspects* (eds. Agurell, S., Dewey, W. L. & Willette, R. E.) 63–78 (Elsevier, 1984). doi:10.1016/B978-0-12-044620-9.X5001-5.

69. Tagen, M. & Klumpers, L. E. Review of delta-8-tetrahydrocannabinol (Δ^{8}-THC): Comparative pharmacology with Δ^{9}-THC. *British J Pharmacology* **179**, 3915–3933 (2022).

70. Cascio, M., Gauson, L., Stevenson, L., Ross, R. & Pertwee, R. Evidence that the plant cannabinoid cannabigerol is a highly potent α_2-adrenoceptor agonist and moderately potent 5HT1A receptor antagonist: Novel pharmacological actions of cannabigerol. *British Journal of Pharmacology* **159**, 129–141 (2010).

71. Rosenthaler, S. *et al.* Differences in receptor binding affinity of several phytocannabinoids do not explain their effects on neural cell cultures. *Neurotoxicology and Teratology* **46**, 49–56 (2014).

72. Zagzoog, A. *et al.* In vitro and in vivo pharmacological activity of minor cannabinoids isolated from Cannabis sativa. *Sci Rep* **10**, 20405 (2020).

73. Navarro, G. *et al.* Cannabigerol Action at Cannabinoid CB1 and CB2 Receptors and at CB1–CB2 Heteroreceptor Complexes. *Front. Pharmacol.* **9**, 632 (2018).

74. Udoh, M., Santiago, M., Devenish, S., McGregor, I. S. & Connor, M. Cannabichromene is a cannabinoid CB 2 receptor agonist. *Br J Pharmacol* **176**, 4537–4547 (2019).

75. Bouron, A. Phyto and endocannabinoids exert complex actions on calcium and zinc signaling in mouse cortical neurons. *Biochemical Pharmacology* **152**, 244–251 (2018).

76. Kaplan, J. S., Stella, N., Catterall, W. A. & Westenbroek, R. E. Cannabidiol attenuates seizures and social deficits in a mouse model of Dravet syndrome. *Proc. Natl. Acad. Sci. U.S.A.* **114**, 11229–11234 (2017).

77. Ryberg, E. *et al.* The orphan receptor GPR55 is a novel cannabinoid receptor: GPR55, a novel cannabinoid receptor. *British Journal of Pharmacology* **152**, 1092–1101 (2007).

78. Anavi-Goffer, S. *et al.* Modulation of l-α-Lysophosphatidylinositol/GPR55 Mitogen-activated Protein Kinase (MAPK) Signaling by Cannabinoids. *Journal of Biological Chemistry* **287**, 91–104 (2012).

79. Muller, C., Morales, P. & Reggio, P. H. Cannabinoid Ligands Targeting TRP Channels. *Front. Mol. Neurosci.* **11**, 487 (2019).

80. Hassan, S. *et al.* Cannabidiol enhances microglial phagocytosis via transient receptor potential (TRP) channel activation: Cannabidiol enhances microglial phagocytosis. *Br J Pharmacol* **171**, 2426–2439 (2014).

81. Nadal, X. *et al.* Tetrahydrocannabinolic acid is a potent PPARγ agonist with neuroprotective activity: Cannabinoid acids are PPARγ agonists. *British Journal of Pharmacology* **174**, 4263–4276 (2017).

82. Russo, E. B., Burnett, A., Hall, B. & Parker, K. K. Agonistic Properties of Cannabidiol at 5-HT1a Receptors. *Neurochem Res* **30**, 1037–1043 (2005).

83. Limebeer, C. L., Rock, E. M., Sharkey, K. A. & Parker, L. A. Nausea-Induced 5-HT Release in the Interoceptive Insular Cortex and Regulation by Monoacylglycerol Lipase (MAGL) Inhibition and Cannabidiol. *eNeuro* **5**, ENEURO.0256-18.2018 (2018).

84. De Petrocellis, L. *et al.* Plant-Derived Cannabinoids Modulate the Activity of Transient Receptor Potential Channels of Ankyrin Type-1 and Melastatin Type-8. *J Pharmacol Exp Ther* **325**, 1007–1015 (2008).

85. O'Sullivan, S. E., Kendall, D. A. & Randall, M. D. Time-Dependent Vascular Effects of Endocannabinoids Mediated by Peroxisome Proliferator-Activated Receptor Gamma (PPAR). *PPAR Research* **2009**, 1–9 (2009).

86. O'Sullivan, S. E. An update on PPAR activation by cannabinoids: Cannabinoids and PPARs. *British Journal of Pharmacology* **173**, 1899–1910 (2016).

87. Devinsky, O. *et al.* Cannabidiol in patients with treatment-resistant epilepsy: an open-label interventional trial. *The Lancet Neurology* **15**, 270–278 (2016).

88. Devinsky, O. *et al.* Trial of Cannabidiol for Drug-Resistant Seizures in the Dravet Syndrome. *N Engl J Med* **376**, 2011–2020 (2017).

89. Devinsky, O. *et al.* Effect of Cannabidiol on Drop Seizures in the Lennox–Gastaut Syndrome. *N Engl J Med* **378**, 1888–1897 (2018).

90. Thiele, E. A. *et al.* Cannabidiol in patients with seizures associated with Lennox-Gastaut syndrome (GWPCARE4): a randomised, double-blind, placebo-controlled phase 3 trial. *The Lancet* **391**, 1085–1096 (2018).

91. Abu-Sawwa, R. & Stehling, C. Epidiolex (Cannabidiol) Primer: Frequently Asked Questions for Patients and Caregivers. *The Journal of Pediatric Pharmacology and Therapeutics* **25**, 75–77 (2020).

92. European Medicines Agency. Epidyolex (cannabidiol): An overview of Epidyolex and why it is authorised in the EU. (2021).

93. da Costa, V. F. D. D. & de Carvalho, W. S. R. Use of Medicinal Cannabis for Palliative Care Patients: A Systematic Review. *JBM* **10**, 242–252 (2022).

94. Thornton, C., Dickson, K. E., Carty, D. R., Ashpole, N. M. & Willett, K. L. Cannabis constituents reduce seizure behavior in chemically-induced and scn1a-mutant zebrafish. *Epilepsy & Behavior* **110**, 107152 (2020).

95. Munson, A. E., Harris, L. S., Friedman, M. A., Dewey, W. L. & Carchman, R. A. Antineoplastic activity of cannabinoids. *JNCI: Journal of the National Cancer Institute* **55**, 597–602 (1975).

96. Alves, P., Amaral, C., Teixeira, N. & Correia-da-Silva, G. *Cannabis sativa*: Much more beyond Δ9-tetrahydrocannabinol. *Pharmacological Research* **157**, 104822 (2020).

97. Hill, A. J., Williams, C. M., Whalley, B. J. & Stephens, G. J. Phytocannabinoids as novel therapeutic agents in CNS disorders. *Pharmacology & Therapeutics* **133**, 79–97 (2012).

98. Maurya, N. & Velmurugan, B. K. Therapeutic applications of cannabinoids. *Chemico-Biological Interactions* **293**, 77–88 (2018).

99. Choi, S., Huang, B. C. & Gamaldo, C. E. Therapeutic Uses of Cannabis on Sleep Disorders and Related Conditions: *Journal of Clinical Neurophysiology* **37**, 39–49 (2020).

100. Szkudlarek, H. J. *et al.* THC and CBD produce divergent effects on perception and panic behaviours via distinct cortical molecular pathways. *Progress in Neuro-Psychopharmacology and Biological Psychiatry* **104**, 110029 (2021).

101. Shinjyo, N. & Di Marzo, V. The effect of cannabichromene on adult neural stem/progenitor cells. *Neurochemistry International* **63**, 432–437 (2013).

102. Prenderville, J. A., Kelly, Á. M. & Downer, E. J. The role of cannabinoids in adult neurogenesis: Cannabinoids and neurogenesis. *Br J Pharmacol* **172**, 3950–3963 (2015).

103. Grunfeld, Y. & Edery, H. Psychopharmacological activity of the active constituents of hashish and some related cannabinoids. *Psychopharmacologia* **14**, 200–210 (1969).

104. Mechoulam, R., Shani, A., Edery, H. & Grunfeld, Y. Chemical Basis of Hashish Activity. *Science* **169**, 611–612 (1970).

105. Borrelli, F. *et al.* Beneficial effect of the non-psychotropic plant cannabinoid cannabigerol on experimental inflammatory bowel disease. *Biochemical Pharmacology* **85**, 1306–1316 (2013).

106. Samarut, É., Nixon, J., Kundap, U. P., Drapeau, P. & Ellis, L. D. Single and Synergistic Effects of Cannabidiol and Δ-9-Tetrahydrocannabinol on Zebrafish Models of Neuro-Hyperactivity. *Frontiers in Pharmacology* **10**, (2019).

107. Avraham, Y., Latzer, Y., Hasid, D. & Berry, E. M. The Impact of Δ9-THC on the Psychological Symptoms of Anorexia Nervosa: A Pilot Study. *Isr J Psychiatry* **54**, 44–51 (2017).

108. Rock, E. M. & Parker, L. A. Cannabinoids As Potential Treatment for Chemotherapy-Induced Nausea and Vomiting. *Front. Pharmacol.* **7**, (2016).

109. Riggs, P. K. *et al.* A pilot study of the effects of cannabis on appetite hormones in HIV-infected adult men. *Brain Res* **1431**, 46–52 (2012).

110. Colasanti, B. K., Powell, S. R. & Craig, C. R. Intraocular pressure, ocular toxicity and neurotoxicity after administration of Δ9-Tetrahydrocannabinol or cannabichromene. *Experimental Eye Research* **38**, 63–71 (1984).

111. Ruhl, T., Zeymer, M. & von der Emde, G. Cannabinoid modulation of zebrafish fear learning and its functional analysis investigated by c-Fos expression. *Pharmacology Biochemistry and Behavior* **153**, 18–31 (2017).

112. Roitman, P., Mechoulam, R., Cooper-Kazaz, R. & Shalev, A. Preliminary, Open-Label, Pilot Study of Add-On Oral Δ9-Tetrahydrocannabinol in Chronic Post-Traumatic Stress Disorder. *Clin Drug Investig* **34**, 587–591 (2014).

113. Kruger, J. S. & Kruger, D. J. Delta-8-THC: Delta-9-THC's nicer younger sibling? *J Cannabis Res* **4**, 4 (2022).

114. Vandrey, R. Comparative Pharmacokinetic and Pharmacodynamic Effects of Delta-8 and Delta-9 THC. *ClinicalTrials.gov* https://clinicaltrials.gov/ct2/show/NCT05287256 (2022).

115. Cherny, N. Comparison of Delta-8-THC to Ondansetron in the Prevention of Acute Nausea From Moderately Emetogenic Chemotherapy. *ClinicalTrials.gov* https://clinicaltrials.gov/ct2/show/NCT00285051 (2006).

116. Achenbach, J. C. *et al.* Analysis of the uptake, metabolism, and behavioral effects of cannabinoids on zebrafish larvae. *Zebrafish* **15**, 349–360 (2018).

117. Koppel, B. S. *et al.* Systematic review: Efficacy and safety of medical marijuana in selected neurologic disorders: Report of the Guideline Development Subcommittee of the American Academy of Neurology. *Neurology* **82**, 1556–1563 (2014).

118. Sundström, G., Larsson, T. A., Xu, B., Heldin, J. & Larhammar, D. Interactions of zebrafish peptide YYb with the neuropeptide Y-family receptors Y4, Y7, Y8a, and Y8b. *Front. Neurosci.* **7**, (2013).

119. Nahvi, R. J. & Sabban, E. L. Sex Differences in the Neuropeptide Y System and Implications for Stress Related Disorders. *Biomolecules* **10**, 1248 (2020).

120. Holzer, P., Reichmann, F. & Farzi, A. Neuropeptide Y, peptide YY and pancreatic polypeptide in the gut–brain axis. *Neuropeptides* **46**, 261–274 (2012).

121. McGowan, B. M. C. & Bloom, S. R. Peptide YY and appetite control. *Curr Opin Pharmacol* **4**, 583–588 (2004).

122. Morimoto, R. *et al.* Expression of peptide YY in human brain and pituitary tissues. *Nutrition* **24**, 878–884 (2008).

123. Colmers, W. F. & El Bahh, B. Neuropeptide Y and Epilepsy. *Epilepsy Currents* **3**, 53–58 (2003).

124. Hortopan, G. A., Dinday, M. T. & Baraban, S. C. Spontaneous Seizures and Altered Gene Expression in GABA Signaling Pathways in a mind bomb Mutant Zebrafish. *Journal of Neuroscience* **30**, 13718–13728 (2010).

125. Lessman, C. A. The developing zebrafish (Danio rerio): A vertebrate model for high-throughput screening of chemical libraries. *Birth Defects Research Part C: Embryo Today: Reviews* **93**, 268–280 (2011).

126. Berghmans, S., Hunt, J., Roach, A. & Goldsmith, P. Zebrafish offer the potential for a primary screen to identify a wide variety of potential anticonvulsants. *Epilepsy Research* **75**, 18–28 (2007).

127. Carty, D. R., Thornton, C., Gledhill, J. H. & Willett, K. L. Developmental Effects of Cannabidiol and Δ9-Tetrahydrocannabinol in Zebrafish. *Toxicological Sciences* **162**, 137–145 (2018).

128. Carty, D. R. *et al.* Multigenerational consequences of early-life cannabinoid exposure in zebrafish. *Toxicology and Applied Pharmacology* **364**, 133–143 (2019).

129. Kimmel, C. B., Ballard, W. W., Kimmel, S. R., Ullmann, B. & Schilling, T. F. Stages of embryonic development of the zebrafish. *Developmental Dynamics* **203**, 253–310 (1995).

130. Baraban, S. C., Dinday, M. T. & Hortopan, G. A. Drug screening in *Scn1a* zebrafish mutant identifies clemizole as a potential Dravet syndrome treatment. *Nat Commun* **4**, 2410 (2013).

131. Griffin, A. *et al.* Clemizole and modulators of serotonin signalling suppress seizures in Dravet syndrome. *Brain* aww342 (2017) doi:10.1093/brain/aww342.

132. Griffin, A. *et al.* Preclinical Animal Models for Dravet Syndrome: Seizure Phenotypes, Comorbidities and Drug Screening. *Front. Pharmacol.* **9**, 573 (2018).

133. Kumar, M. G. *et al.* Altered Glycolysis and Mitochondrial Respiration in a Zebrafish Model of Dravet Syndrome. *eNeuro* **3**, ENEURO.0008-16.2016 (2016).

134. Griffin, A., Anvar, M., Hamling, K. & Baraban, S. C. Phenotype-Based Screening of Synthetic Cannabinoids in a Dravet Syndrome Zebrafish Model. *Frontiers in Pharmacology* **11**, (2020).

135. Griffin, A. *et al.* Phenotypic analysis of catastrophic childhood epilepsy genes. *Commun Biol* **4**, 680 (2021).

136. Acevedo-Canabal, A. *et al.* Altered swimming behaviors in zebrafish larvae lacking cannabinoid receptor 2. *Cannabis and Cannabinoid Research* **4**, 88–101 (2019).

137. Cassar, S. *et al.* Use of Zebrafish in Drug Discovery Toxicology. *Chemical Research in Toxicology* **33**, 95–118 (2020).

138. Ahmed, K. T., Amin, M. R., Shah, P. & Ali, D. W. Motor neuron development in zebrafish is altered by brief (5-hr) exposures to THC (Δ9-tetrahydrocannabinol) or CBD (cannabidiol) during gastrulation. *Scientific Reports* **8**, (2018).

139. Campos-Rodriguez, C., Fredrick, E., Ramirez-San Juan, E. & Olsson, R. Enantiomeric N-substituted phthalimides with excitatory amino acids protect zebrafish larvae against PTZ-induced seizures. *European Journal of Pharmacology* **888**, 173489 (2020).

140. Jaiswal, Y. *et al.* Evaluation of Anti-Convulsive Properties of Aqueous Kava Extract on Zebrafish Using the PTZ-Induced Seizure Model. *Brain Sciences* **10**, 541 (2020).

141. Liao, M. *et al.* Targeted knockout of GABA-A receptor gamma 2 subunit provokes transient light-induced reflex seizures in zebrafish larvae. *Disease Models & Mechanisms* **12**, dmm040782 (2019).

142. Kotsikorou, E. *et al.* Identification of the GPR55 Antagonist Binding Site Using a Novel Set of High-Potency GPR55 Selective Ligands. *Biochemistry* **52**, 9456–9469 (2013).

143. Rempel, V. *et al.* Bicyclic imidazole-4-one derivatives: a new class of antagonists for the orphan G protein-coupled receptors GPR18 and GPR55. *Med. Chem. Commun.* **5**, 632–649 (2014).

144. Leweke, F. M. *et al.* Cannabidiol enhances anandamide signaling and alleviates psychotic symptoms of schizophrenia. *Transl Psychiatry* **2**, e94 (2012).

145. Sang, N., Zhang, J. & Chen, C. COX-2 oxidative metabolite of endocannabinoid 2-AG enhances excitatory glutamatergic synaptic transmission and induces neurotoxicity: PGE_2-G in synaptic signaling and neurotoxicity. *Journal of Neurochemistry* **102**, 1966–1977 (2007).

146. Nixon, J. *et al.* Assessing the bioactivity of cannabis extracts in larval zebrafish. *J Cannabis Res* **3**, 44 (2021).

Appendices

Appendix A: Ethics approval required for all projects in this thesis

Project Info.

File No: 20222627
Project Title: (22-01-CF) Use of Zebrafish to model human disease.
Principal Investigator: Dr. Curtis French (Faculty of Medicine\Discipline of Genetics)
Start Date: 2022/05/25
End Date: 2025/05/25
Keywords: Biological Sciences

1. Project Description

#	Question	Answer
1.1	Is this a new protocol?	Renewal of a Previously Approved Protocol (3-year full renewal)
1.2	If a renewal, please provide the previous protocol number.	19-01-CF
1.3	If renewing or resubmitting, provide a summary of changes made to the application.	Additional zebrafish mutant strains and procedures will be used. Changes made for this re-submission include removing some procedural details from the lay summary, and the addition of details concerning compounds used in this study (added in section 7.22).
1.4	The purpose of this animal protocol is to conduct:	Research|Contract Work
1.5	Lay Summary: Describe the objectives and rationale of your study in terms the general public would understand.	In my laboratory, we make mutations in the zebrafish genome to study the function of genes that are associated with human disease. By causing the gene to not function, we can gain understanding as to why people with the defective gene get the specific disease. We use zebrafish because of their sequenced genome, the ability to use transgenic lines already made by other laboratories, and the ease in which we can induce our own mutations. They are also much cheaper to house than other lab animals such as mice and rats. In my laboratory, we study complex diseases such as stroke and osteoporosis. Creating mutations (that have been found in humans) in our zebrafish allow us to figure out how the genes in question are important for preventing such diseases. Lastly, we can apply compounds to zebafish adults and larvae, such as cannabinoids and terpenes, to asses their toxicity and medicinal benefits.

13. Declaration

#	Question	Answer
13.1	I will ensure that all procedures performed under the protocol will be conducted in accordance with the policies of the Canadian Council for Animal Care and the Institutional Animal Care Committee of Memorial University and all relevant university, provincial, national, and international policies and regulations that govern the use of animal in research and teaching.	Agree
13.2	I understand that if I misrepresent and/or fail to accurately and fully disclose any aspects of the research, my Animal Care Committee Protocol approval clearance may be suspended.	Agree
13.3	I understand that I am required to submit an amendment request to the IACC before enacting any changes to my approved protocol. I understand that changes implemented without approval constitute a violation of policy.	Agree
13.4	I understand that I am required to keep record of all animals used and that I am required to submit an annual report for each year my protocol is active.	Agree
13.5	I understand that as the primary applicant, I am responsible to ensure personnel listed on the protocol have completed all required training prior to interacting with live animals. Failure to complete training could result in removal of personnel from a protocol or suspension of that protocol.	Agree
13.6	I understand that personnel added to the Project Team Info tab are granted full editing rights to my Animal Use Protocol and the ability to submit Events relating to Amendments, Reports, and Animal Orders for this protocol. I understand that as the primary applicant I retain full responsibility and accountability for all Amendments, Reports, or Orders submitted by authorized team members.	Agree
13.7	Annual site visits by the IACC, or designates, are required for all locations where animals are housed or used for testing and/or procedures. I understand that a site visit is required as part of the annual report if live animal work is taking place in my laboratory.	Agree
13.8	If there is any occurrence of an adverse event(s), I will notify the applicable facility manager and will report the incident through the Researcher Portal Event: Incident Report.	Agree

Appendix B: Optimization of tracking protocol before camera upgrade

To evaluate the most impactful behavioural movement measurements, 6 days post fertilization (dpf) larvae were exposed to various concentrations of PTZ and tracked in a 96-well plate (Fig A2).

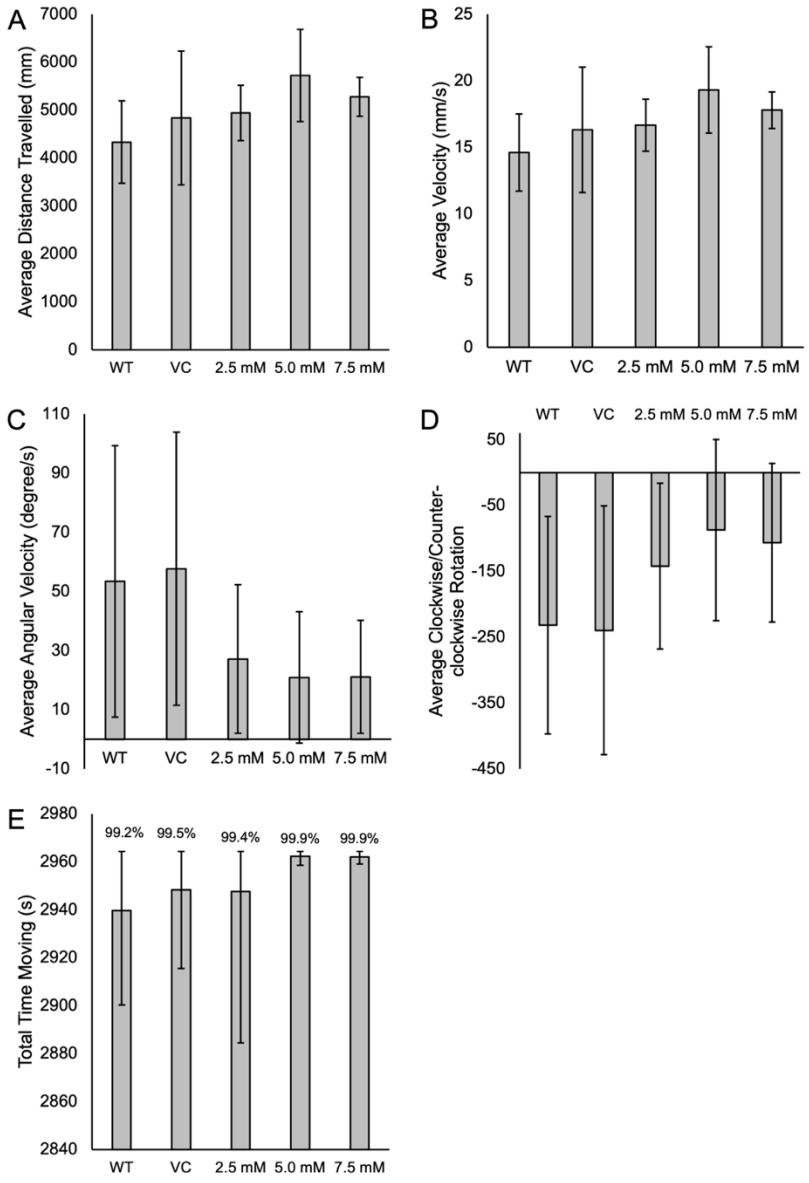

Figure A2. Measured change in movement of zebrafish larvae (6 dpf) after exposure to various concentrations of PTZ. A: Average distance travelled by larvae. B: Measurement

of velocity of larvae. C: Measurement of angular velocity of larvae. D: Change in center-point rotation of larvae. Error bars are ±SD for A-D. E: Total time spent moving by larvae, Negative error bars are SD, positive error bars signify total time of assay as calculated SD exceeded assay time in each instance. Data labels are percent of assay time spent moving. WT: true wild-type larvae in embryo media with no additives (n=12); VC: vehicle control embryo media 1% methanol (n=24); concentrations represent concentration of PTZ, n=24, 24, 12 for 2.5 mM, 5.0 mM, and 7.5 mM, respectively.

Parameters were compared to observe the best measure of the expected concentration-response relationship established in the PTZ model of epilepsy. Average distance travelled (Fig A2A) and average velocity (Fig A2B) are the two most common parameters reported in the literature. Average angular velocity (Fig A2C) and average clockwise/counter clockwise rotation (Fig A2D) measure curved and cyclic movements of the larva and seem to indicate that seizure behaviours have less curved movements. The standard deviation of the data also indicates that movement between individuals becomes more consistent with a higher rate and intensity of convulsions. Time spent moving was very similar between treatments, and the graph in Fig A2E has a truncated y-axis in order to be able to visualize any differences in the treatment groups. Similar to angular velocity and clockwise/counter clockwise rotation, it seemed the variation between individuals for time spent moving became more consistent with more intense seizures. The most useful measures of movement were determined to be average distance moved and average velocity, which were used to determine the optimal developmental stage (Fig A3 and A4).

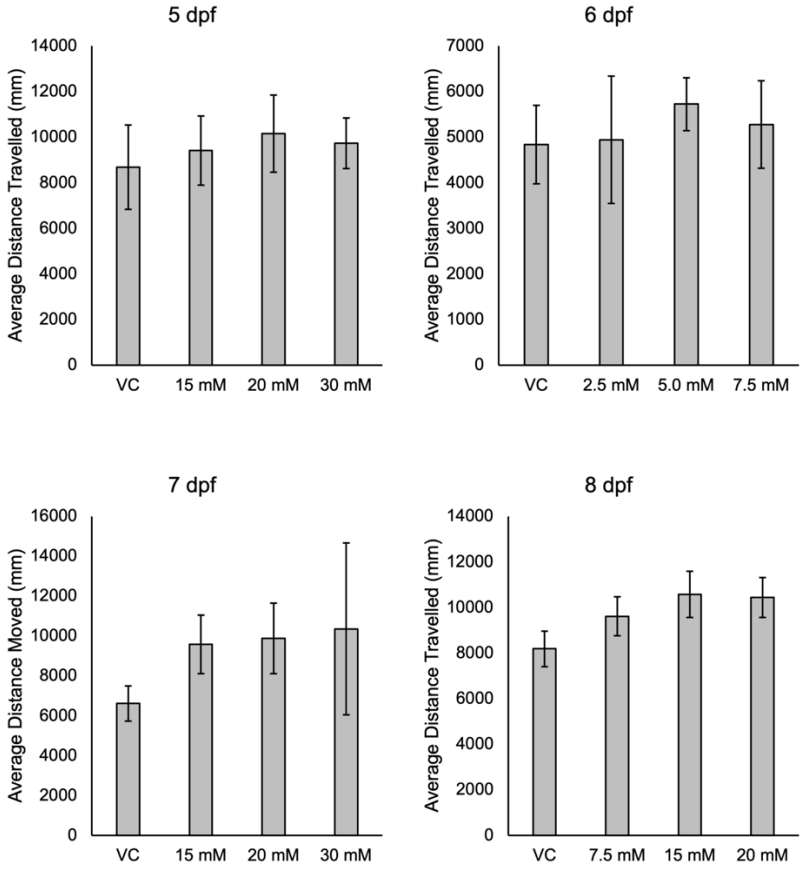

Figure A3. Comparison of average distance travelled of zebrafish larvae at different ages (days post fertilization). VC: vehicle control, embryo media 1% methanol. Concentrations are concentrations of PTZ in VC. Error bars are ±SD. 5 dpf (n= 24 per treatment); 6 dpf (n= 12, 24, 24, 12); 7 dpf (n= 24, 12, 12, 12); 8 dpf (n = 12, 12, 24, 24).

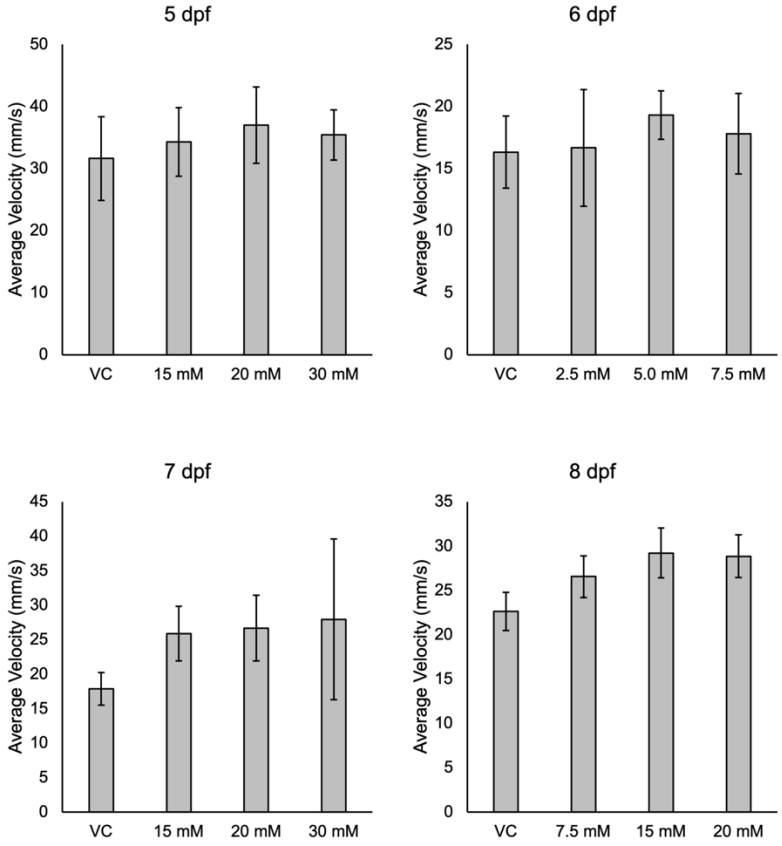

Figure A4. Comparison of average velocity of swimming movement of zebrafish larvae at different ages (days post fertilization). VC: vehicle control, embryo media 1% methanol. Concentrations are concentrations of PTZ in VC. Error bars are ±SD. 5 dpf (n= 24 per treatment); 6 dpf (n= 12, 24, 24, 12); 7 dpf (n= 24, 12, 12, 12); 8 dpf (n = 12, 12, 24, 24).

Observed changes in distance travelled and velocity appeared to be greater between wild-type movement and seizures at later larval stages (Fig A3 and A4, 7 and 8 dpf). Survivability of 8 dpf larvae in stagnant water (changed daily) is lower as at this stage as the yolk sac is completely depleted and external food is required. Survival of larvae to 7 dpf is much higher without external supplementation. The trends observed in

changes in distance moved were similar to changes in velocity, so average distance travelled was the parameter used to evaluate seizure intensity henceforth.

The difference in measurement between wild-type movement and seizures was still not what was expected based on literature values. Upon further inspection of the tracking data, there were some values of distance travelled and velocity that were close to impossible for a larva to achieve, indicating that the tracking algorithm "lost" the larva and was tracking noise or water reflections instead. This error is more common to occur on the outside-most wells of a well plate due to parallax error. Parallax error is observed when the viewing point is perpendicular to an object, and the object appears to be in an accurate position. In this situation, it is possible that the outside-most wells of a plate are distorted in the video recording, thereby causing erroneous tracking. To assess the error of the tracking apparatus, 96 wild-type larvae were tracked, and the data plotted based on location on the 96-well plate (Fig A5).

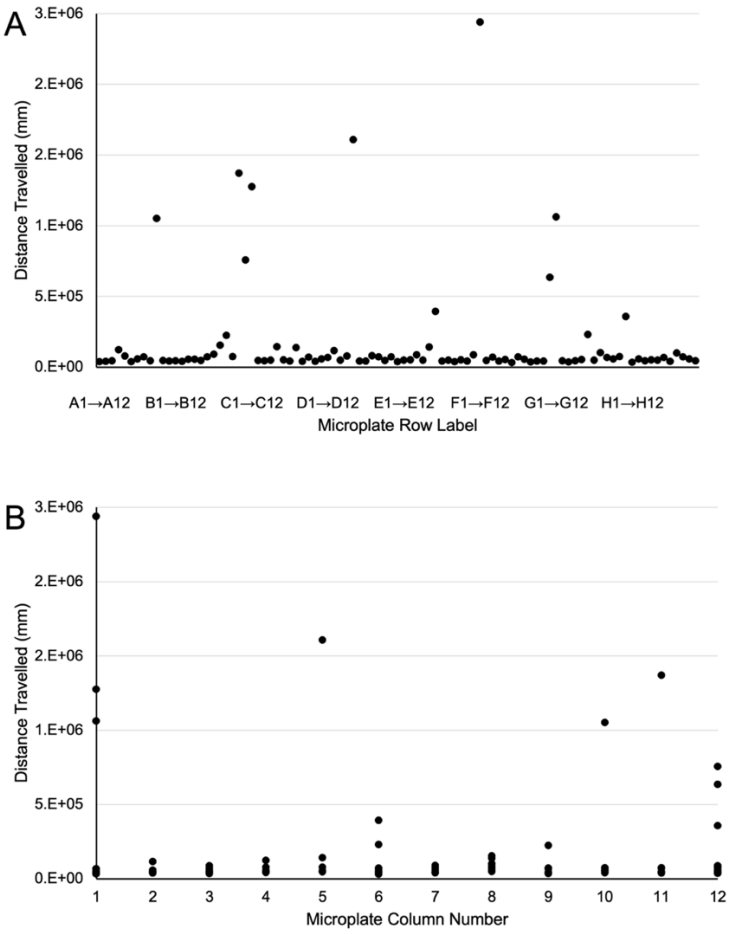

Figure A5. Acquisition error in distance travelled of zebrafish larvae (5 dpf) in embryo media with no treatments. A: Scatter of individual distances organized by plate column (A-H). B: Scatter of individual distances organized by plate row (1-12).

Most of the data clustered together around an expected baseline of movement, however several outliers can be seen. It appears that the row location did not influence prevalence of outliers (Fig A5A), however the column location likely contributed to errors in tracking (Fig A5B). Most outliers can be seen in the first and last columns, with a few in the center. To determine whether it was in fact a loss of tracking that caused the observed outlier, the tracking video was manually scored based on a visual loss of

tracking. A tally was taken for each time the tracking point moved off a larva for each well, and the instances were plotted based on plate location (Fig A6).

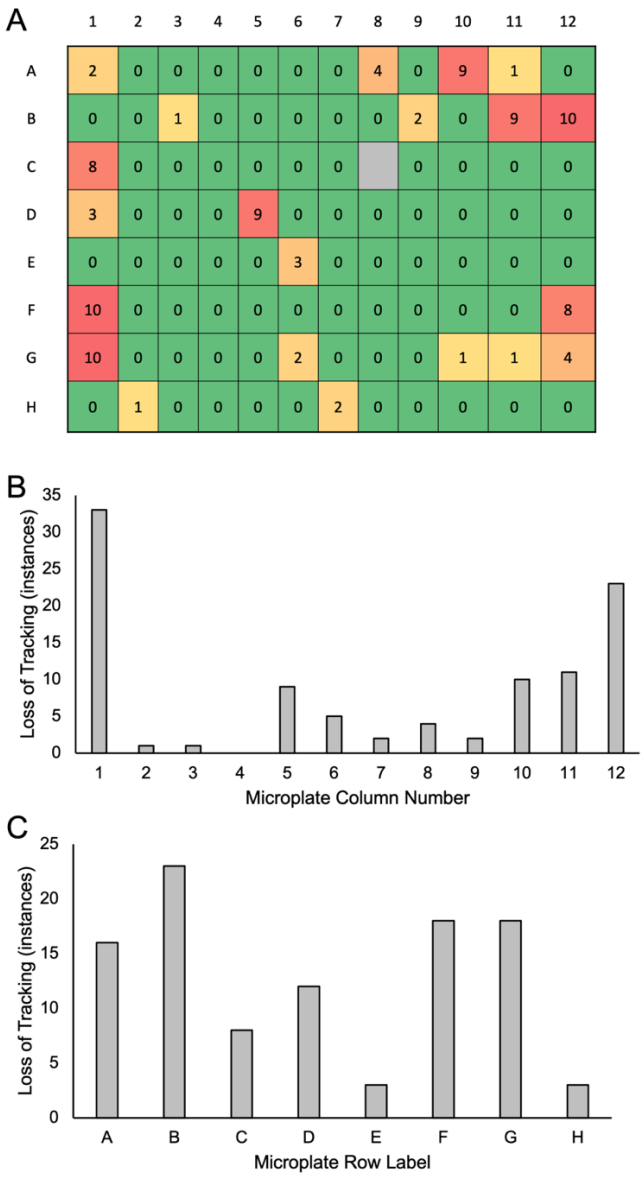

Figure A6. Manual scoring of loss of tracking individual larvae during acquisition. A: Heatmap of instances of loss of tracking per well of 96-well plate. B: Summed instances of loss of tracking organized by column number (1-12). C: Summed instances of loss of tracking organized by microplate row (A-H).

The instances of tracking loss were localized to the edges of the plate (Fig A6), with some loss observed in the center of the plate. When a loss of tracking occurred more than once in a well, it was increasingly difficult for the software to relocate and stay on the larva and resulted in unreliable data. The angle, tilt, and height of the camera was adjusted in the tracking apparatus. When the experiment was repeated, no loss of tracking was observed.

Another experimental variable that was inconsistent in the literature was trial time. A 1-hour trial was conducted, and the distances travelled separated into bins of 15 min increments (Fig A7). The distances travelled in each 15 min bin were insignificant from each other, and so a 30 min trial time was chosen for more timely processing of the experiments.

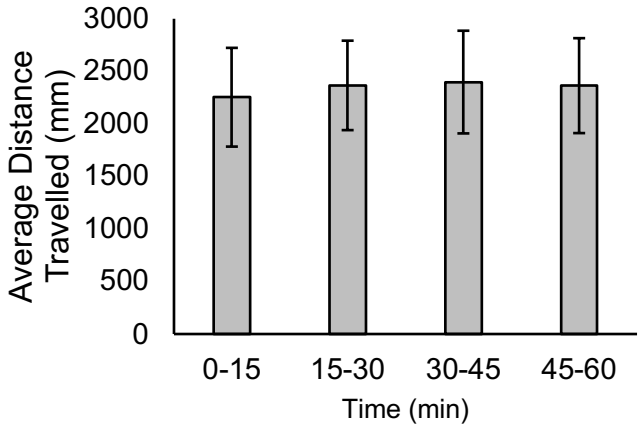

Figure A7. Time binning of distance travelled by wildtype larvae during a 1-hour assay length. Error bars are ±SD, n=33 per bar.

To determine the optimal carrier solvent and the optimal concentration of carrier solvent, a study was conducted to understand the effect of carrier on PTZ dosing and behaviour (Fig A8). Firstly, toxic effects of DMSO and methanol were compared (Fig

A8A) without addition of PTZ. The difference in treatments was insignificant but DMSO chosen as the interindividual variable appeared lower.

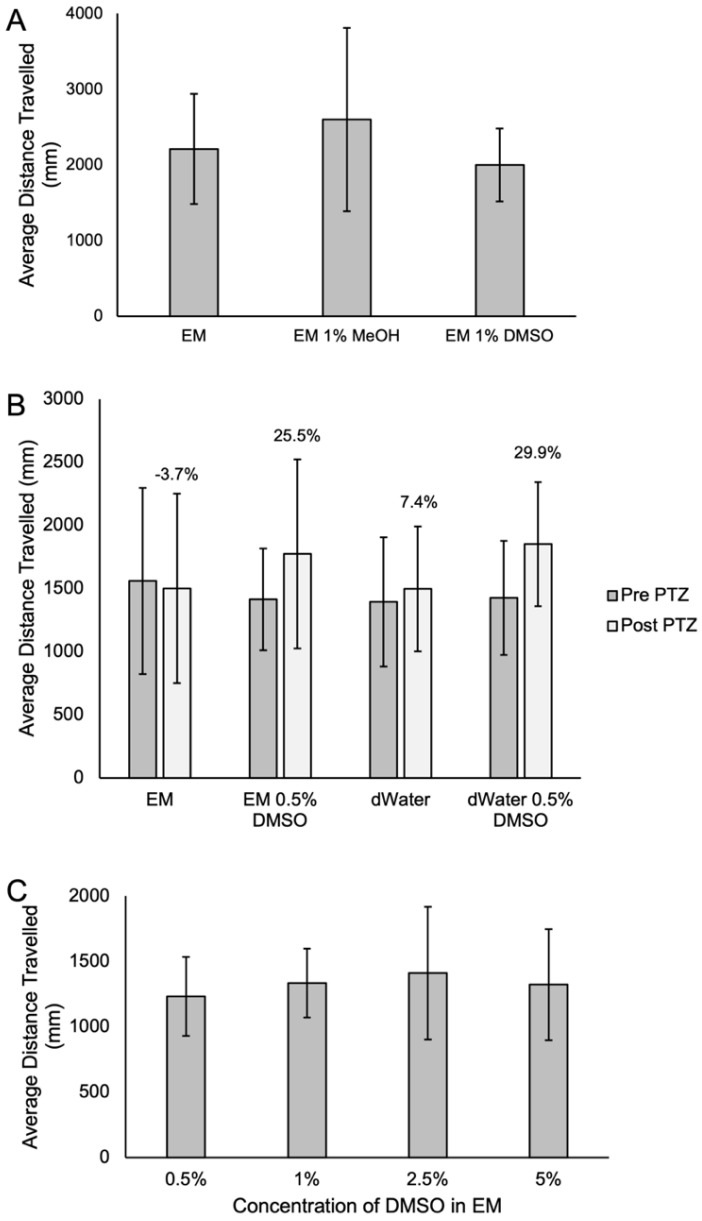

Figure A8. The effect of carrier on PTZ dosing and behaviour. A: Comparison of movement of wildtype larvae with methanol (MeOH) or DMSO as the vehicle carrier. EM: embryo media. Error bars are ±SD, n=16 per bar. B: Comparison of solution used to

prepare PTZ stock with respect to average distance travelled. Data labels are percent difference in distance after treatment with 10 mM PTZ. Error bars are ±SD, n=12 per bar. C: Comparison of increasing concentration of DMSO on distance travelled after treatment with 10 mM PTZ. Error bars are ±SD, n=12 per bar.

The difference in movement observed between treatment in EM or distilled water was studied next (Fig A8B). PTZ is a basic compound, and the buffering capacity of EM was hypothesized to be impacting absorption into the larval body. Based on the observed response to the same concentration of PTZ, it appears that the buffered capacity of EM does not influence absorption, but DMSO likely does. A greater increase in distance travelled was observed in both PTZ treatments with DMSO as a carrier. To determine the optimal concentration of DMSO, larvae were treated with PTZ with various final concentrations of the carrier (Fig A8C). There appeared to be toxic affects at DMSO concentrations higher than 2% v/v, observed visually after the assay, and so 1% DMSO was used in further work. Though the changes in movement were optimized to what seemed to be the highest possible in this model with this equipment, it was still not as large as the changes reported in literature. Further analysis was conducted, where PTZ concentration-response was evaluated over time (Fig A9).

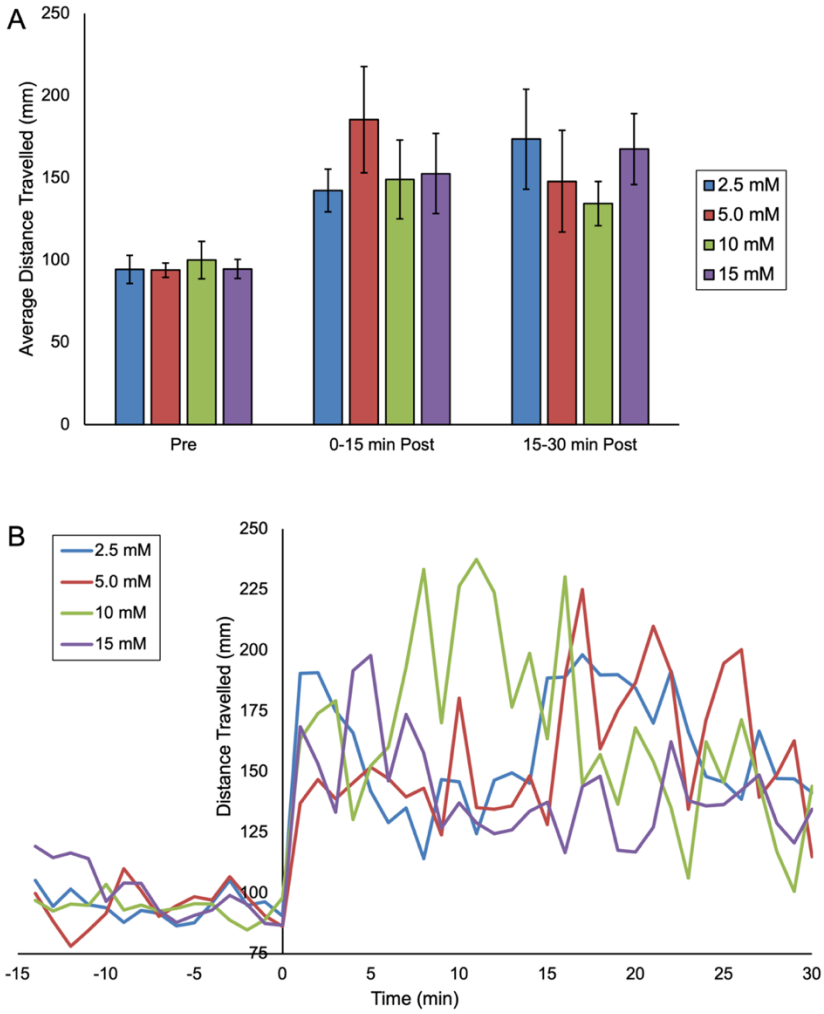

Figure A9. Comparison of distance travelled in time bins over 30 min exposure to various concentrations of PTZ. A: Distance travelled in 15 min bins before exposure to PTZ (Pre), and after exposure to PTZ (Post). Error bars are ±SD, n=24 per bar. B: Distance travelled (non-cumulative) in 1 min time bins before and after exposure to PTZ (negative times indicate pre-exposure tracking). Legends indicate concentration of PTZ concentration.

Analysis of binned distance travelled showed surprisingly that a concentration of 5 mM PTZ had the biggest increase in the first 15 min of the trial and a concentration of

2.5 mM PTZ had the biggest increase in the second 15 min of the trial, both much lower concentrations of PTZ than what has been used (Fig A9A). The trends of the changes in distance travelled deviated from the expected increase over time, and so data was plotted by minute of trial time (Fig A9B). Based on this rough data, it appeared that the first 5 min after addition of PTZ was required as an acclimation period after disturbing the larvae's water by addition of solution. The highest concentration of PTZ tested, 15 mM, showed less movement overall than the lower concentrations of PTZ. This likely due to reaching Stage III convulsions. The concentration of PTZ that had been used in the optimization studied thus far, 10 mM, did cause the earliest increase in movement however after about 15 min movement decreased to Stage III convulsions. The two lowest concentrations of PTZ, 2.5 and 5.0 mM, appeared to follow as more reliable pattern of gradual increase in movement, likely not achieving Stage III convulsions much before the trial end. These observations indicated that a lower concentration of PTZ was most optimal, however further experiments were needed to ensure optimal data processing.

In addition to the optimization required of seizure induction and measurement, the treatment of larvae with cannabinoids was equally inconsistent in literature and needed optimization. Larvae were treated with CBD at various concentrations, for various treatment times, and then exposure to PTZ and their movements tracked (Fig A10).

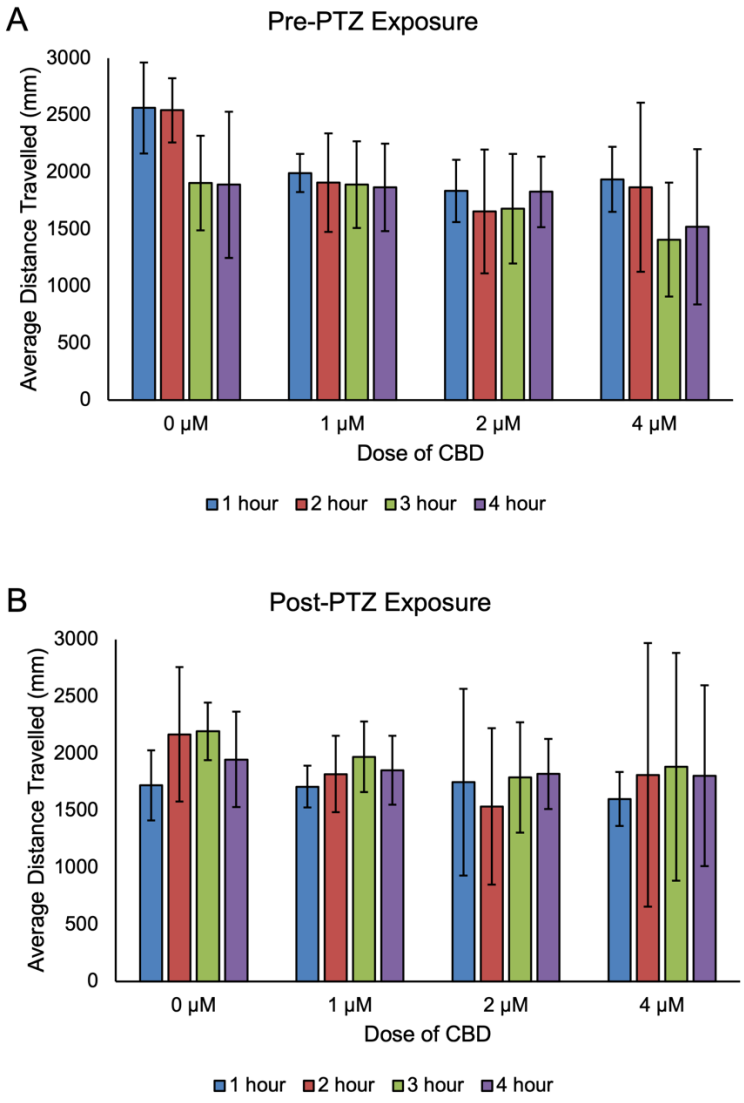

Figure A10. Comparison of treatment times for CBD dosage, before (A) and after (B) exposure to 2.5 mM PTZ, as average distance travelled. Legend indicates treatment times prior to addition of PTZ. Error bars are ±SD, n=12 per bar.

The pre-exposure movement data suggests that incubation time in addition to CBD concentration reduces activity (Fig A10A). The distance travelled by all larvae with CBD treatments is quite similar, but within treatments the distance is lower in larvae that were incubated for longer than 2 hours. In contrast the post-exposure movement data

suggests that incubation time does not have an effect on CBD efficacy as all incubation times were similar within a treatment concentration (Fig A10B).

The Noldus Ethovision software has several data filtering options aimed at separating noise from valuable movement data. The first data filtering option I tried was minimum distance moved (MDM) which sets a minimum threshold of movement (Fig A11). This is aimed at counteracting animal vibrations or system noise.

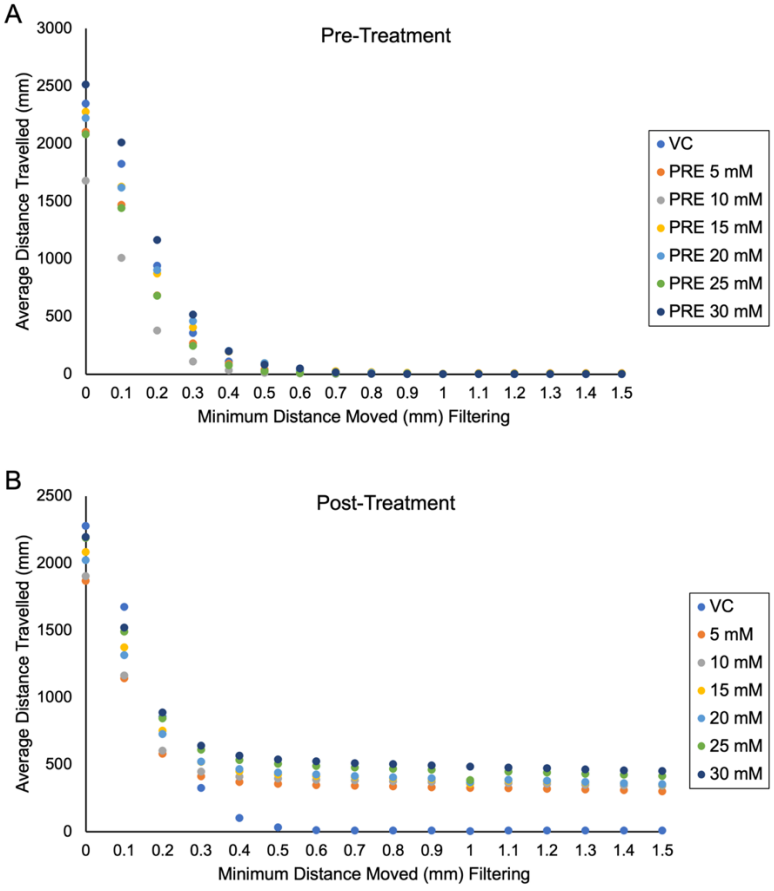

Figure A11. Comparison of minimum distance moved (MDM) filtering, calibrated in mm, before and after treatment with concentrations of PTZ. A: Distance moved prior to PTZ treatment. B: Distance moved after PTZ treatment. Legends indicate concentrations of PTZ treatments.

Larvae were treated with varying concentrations of PTZ and were tracked for 30 min before (Fig A11A) and after PTZ exposure (Fig A11B). MDM filtering between 0.1- and 1.5-mm thresholds was analyzed and all treatments plotted. The data before PTZ exposure shows interindividual variation lessening with an increasing filter threshold, eventually plateauing at no distance moved at all. This trend was repeated in the vehicle control treatment post-exposure data, but all PTZ treatments showed a clear increase in distance moved at MDM filtering thresholds of 0.4 mm and higher.

Locally weighted scatterplot smoothing (LOWESS) is a filtering technique in which a data point is averaged with X number of points before and after it, in order to eliminate noise. This data filtering technique was evaluated next, with X = 2, 5, 10, and 14 (Fig A12).

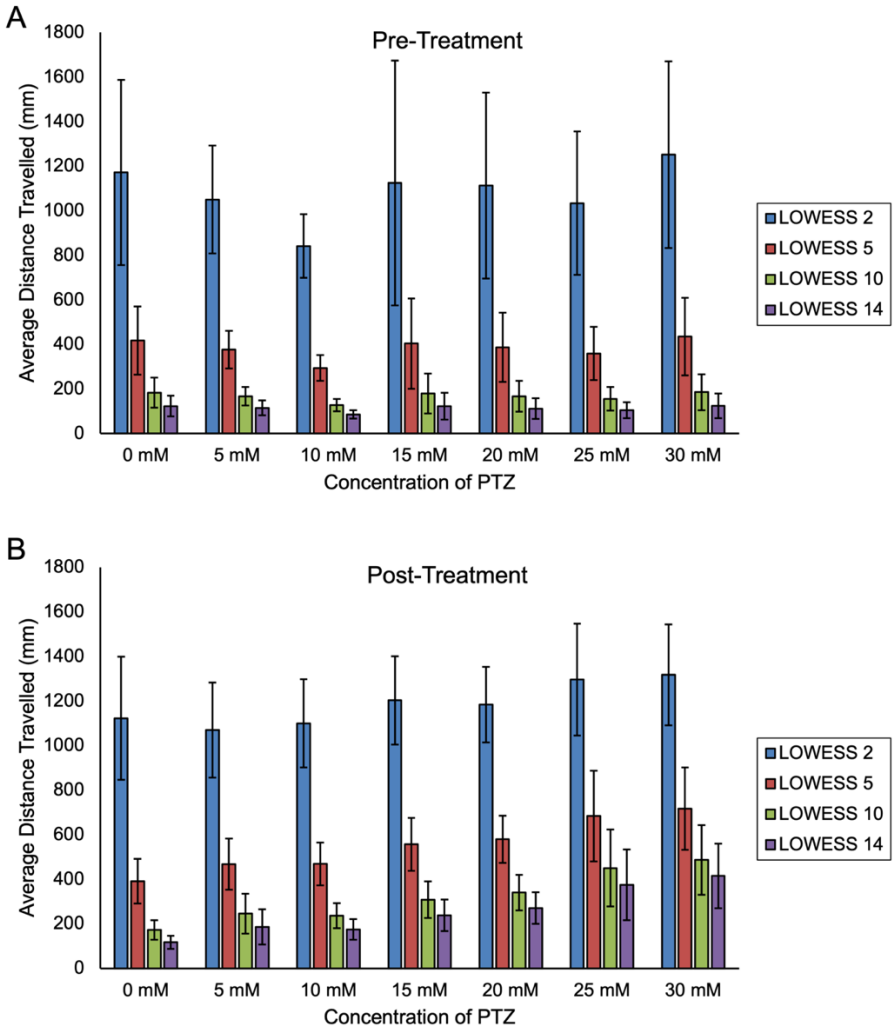

Figure A12. Comparison of LOWESS smoothing bin averaging sizes on distance travelled after PTZ treatment. A: Distance moved prior to PTZ treatment. B: Distance moved after PTZ treatment. Legends indicate LOWESS smoothing bin averaging sizes. Error bars are ±SD, n=12 per bar.

Similar to MDM filtering, the observed differences between the vehicle control and the PTZ treatments were exemplified in the strong filtering conditions (Fig A12), however it was not as dramatic an increase as what was observed in Figure A11. The interindividual variability also appeared to decrease with stronger data filtering settings.

The strong filtering settings needed to observe a great difference in baseline movement and seizures often reduced baseline movement to zero. To avoid processing the data to this extent, a combination of MDM and LOWESS filtering was used to determine if it was possible to filter data sufficiently without reducing values to zero (Fig A13).

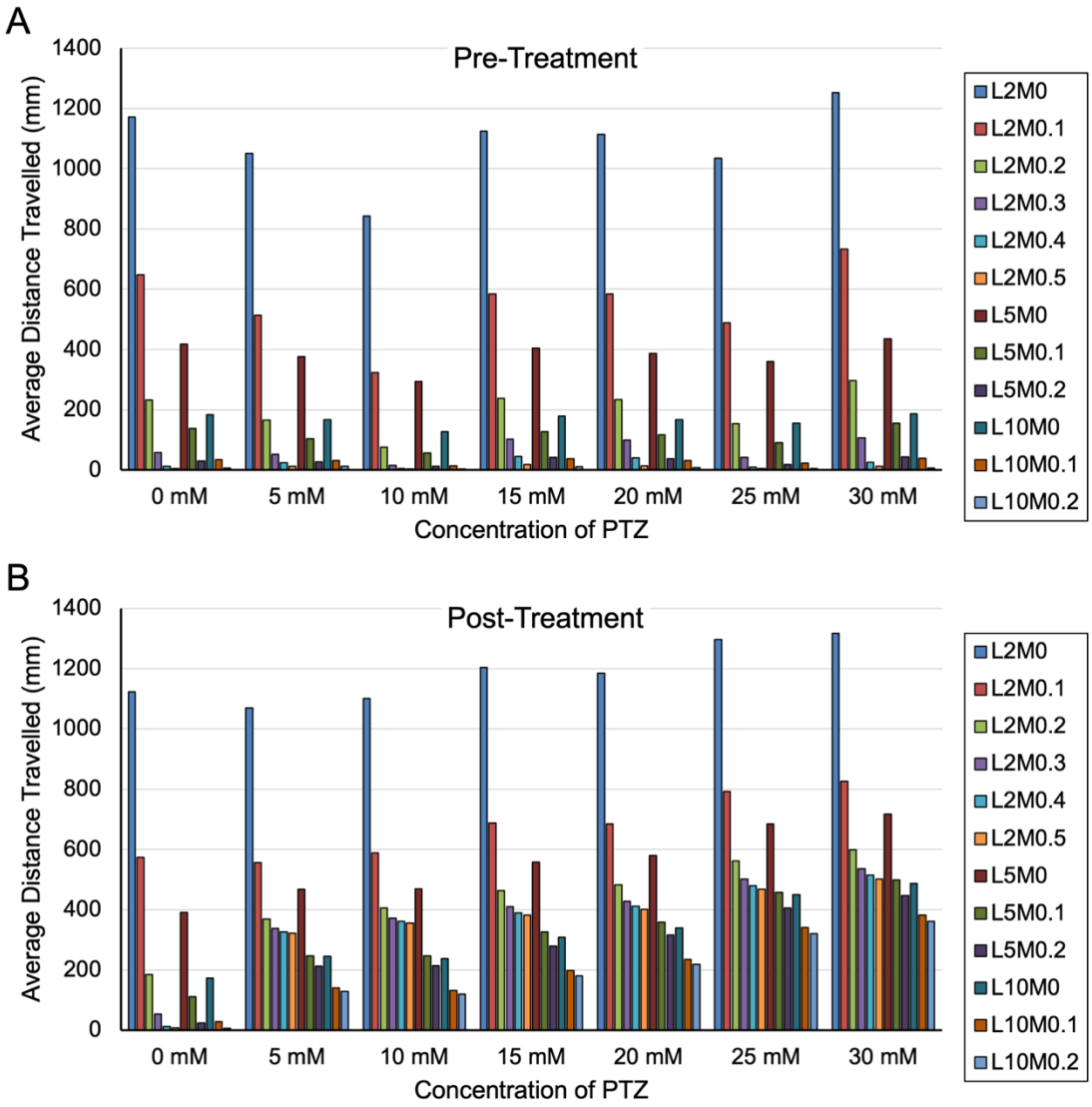

Figure A13. Comparison of LOWESS smoothing bin averaging sizes combined with MDM filtering on distance travelled after PTZ treatment. A: Distance moved prior to PTZ

treatment. B: Distance moved after PTZ treatment. Legends indicate LOWESS smoothing (L) and MDM filtering (M) parameters.

As observed previously, MDM filtering appeared to have the greatest effect on data reduction (Fig A13A). The combined filtering techniques of LOWESS 2/ MDM 0.1, LOWESS 2/ MDM 0.2, and the sole technique of LOWESS 5 appeared to be the most reasonable data filtering (Fig A13B).

Appendix C: Mutation of foxl1 Results in Reduced Cartilage Markers in a Zebrafish Model of Otosclerosis

Co-authorship statement: Appendix B is a published paper in which I am co-author for the contribution of cartilage and bone staining experiments. This paper is published in Genes and features as a main chapter in PhD candidate Alexia Hawkey-Noble's thesis. I optimized, performed and imaged the alcian blue/alizarin red double staining of all mutant and wildtype larvae ages 4-10 dpf. I interpreted the results with the assistance of Alexia Hawkey-Noble and Dr. French. All other data in the paper were collected and analysed by the respective co-authors.

Alexia Hawkey-Noble[1], Justin A. Pater[1], **Roshni Kollipara**[1], Meriel Fitzgerald[1], Alexandre Maekawa[1], Christopher S. Kovacs[1], Terry-Lynn Young[1], Curtis R. French[1]*

[1]Division of Biomedical Sciences, Faculty of Medicine, Memorial University of Newfoundland

* Correspondence: curtis.french@med.mun.ca (1 709 864-6503)

Abstract

Bone diseases such as otosclerosis (conductive hearing loss) and osteoporosis (low bone mineral density) can result from the abnormal expression of genes that regulate cartilage and bone development. The Forkhead Box Transcription Factor *FOXL1*, has been identified as the causative gene in a family with autosomal dominant otosclerosis

and has been reported as a candidate gene in GWAS-meta-analyses for osteoporosis. This potentially indicates a novel role for *foxl1* in chondrogenesis, osteogenesis, and bone remodelling. We created a foxl1 mutant zebrafish strain as a model for otosclerosis and osteoporosis and examined jaw bones that are homologous to the mammalian middle ear bones, and mineralization of the axial skeleton. We demonstrate that *foxl1* regulates the expression of collagen genes such as *collagen type 1 alpha 1a,* and *collagen type 11 alpha 2*, and results in a delay of jawbone mineralization, while the axial skeleton remains unchanged. *foxl1* may also act with other forkhead genes such as *foxc1a*, as loss of *foxl1* in a *foxc1a* mutant background increases the severity of jaw calcification phenotypes when compared to each mutant alone. Our zebrafish model demonstrates atypical cartilage formation and mineralization in the zebrafish craniofacial skeleton in *foxl1* mutants and demonstrates that aberrant collagen expression may underlie the development of otosclerosis.

Keywords: *FOXL1, FOXC1*, Zebrafish, Otosclerosis, Collagen, Osteoporosis, Iron Binding, Bone Mineral Density

Introduction

Vertebrate skeletal development requires extracellular signalling cues and transcription factor expression to direct the development of cartilage, bone and other connective tissues [147–150]. In vertebrates, cranial neural crest cells (NCCs) derived from a specialized population within the first, second, and third pharyngeal arches, are responsible for developing into the progenitor cells of the craniofacial skeleton, while the

paraxial mesoderm condenses into epithelial somites that give rise to the sclerotome from which the axial skeleton develops [149,151]. This cellular commitment is induced by external paracrine factors leading to *pax1* and *scleraxis* expression [147,152], followed by subsequent expression of transcription factors (TFs), like those of the *SOX* gene family in skeletal progenitors that aid in chondrogenesis and osteogenesis [153,154]. Many other well-known signaling cascades such as Hedgehog (Hh), [155–161], Fibroblast growth factor (Fgf), [162,163], Jagged-Notch, and Bone Morphogenic Protein (Bmp) signalling [162,164–166] are also required to direct progenitor cells into their specialized skeletal fates. Mutation of genes in these pathways can result in developmental defects in cartilage and bone formation/remodelling and can result in bone diseases like otosclerosis (conductive hearing loss from abnormal middle ear bone growth) or osteoporosis (low bone density).

Forkhead Box transcription factors (FOX), have been previously shown to be crucial in craniofacial patterning as well as the differentiation of chondrocytes and osteoblasts in humans, mice and zebrafish [163,167–172]. FOX TFs contain highly conserved DNA-binding domains consisting of 110 amino acids, and may enhance or repress downstream gene expression by binding to forkhead consensus sequences in regulatory regions of the DNA [173,174]. Several FOX genes like those in classes C and F [171], have been studied regarding craniofacial and axial skeletal development. This prior work suggests an inherent FOX expression map resulting from the partial overlap of FOX genes to create distinct boundaries that position bone and cartilage fields in the head during development. Genes such as *Foxc1* [mouse, (*foxc1a* in zebrafish)] and *Foxc2* [mouse (*foxc1b* in zebrafish)] are required for chondrocyte and osteoblast differentiation, contributing to much of the expression map necessary for dermal bone formation (derived

from intramembranous and endochondral ossification) in the upper and lower facial cartilages[169,171,175–177]. As such they are associated with diseases such as Axenfeld-Rieger Syndrome which often presents with craniofacial abnormalities and hearing loss[167,178–180].

Recently, a mutation in the forkhead gene (*FOXL1*) was identified as the causative gene of autosomal dominant otosclerosis in a large Newfoundland family[181] and previous studies have associated this gene with osteoporosis[182–185]. In animal models, *Foxl1* is expressed in the paraxial mesoderm, NCCs of the pharyngeal arches, and is a downstream target of both BMP and Hh signalling[186,187], yet few studies have examined *foxl1*'s role in bone development and remodelling of the craniofacial and axial skeleton. Given its association with two bone remodelling disorders, further study into its role in regulating skeletal development and remodelling in conjunction with other forkhead transcription factors is warranted.

Herein, we utilize a zebrafish model to determine the role of *foxl1* in cartilage and bone development in the embryonic head and axial skeleton to further understand its role in disease pathogenesis. We also utilize two previously studied zebrafish forkhead mutants (*foxc1a* and *foxc1b*)[188,189] in conjunction with a new *foxl1* mutant line to examine the importance of foxl1 in the FOX map. As key cartilage/bone developmental and remodelling pathways are conserved between teleosts and mammals[150,156,162,177,190–196], as well as aspects of the zebrafish jaw being homologous to the middle ear bones of mammals[195,197–199], zebrafish make an excellent model for the study of otosclerosis and osteoporosis[200–204]. We find that while *foxl1* regulates the expression of known markers of chondro/osteogenesis, CRISPR induced mutation of *foxl1* in zebrafish only results in a delay in the formation of craniofacial cartilages and subsequent calcification, with no

apparent effects on axial skeletal development. As loss of *foxl1* is insufficient to overtly alter skeletal development, we assessed skeletal patterning in *foxl1* mutants crossed onto *foxc1a* or *foxc1b* mutant backgrounds, which overlap in expression domains with *foxl1*. We find that *foxl1/foxc1a* double mutants exhibit an exacerbated phenotype with a more severe calcification defects in the craniofacial skeleton when compared to either mutant alone, and that *foxc1a* and *foxl1* share gene targets involved in skeletal development. Thus, we propose that *foxl1* is dispensable for overall craniofacial and axial skeleton development but may act as a modifier locus for *foxc1a*.

Materials and Methods

Zebrafish Husbandry

As per Kimmel et al.[129], both wild-type (strain AB) and mutant zebrafish were reared under standard conditions and staged in terms of hours (hpf) or days (dpf) post fertilization as described. All experiments were preformed following the regulations and procedures outlined by Memorial University of Newfoundland's Animal Care Committee and the Canadian Council on Animal Care. To prevent pigmentation and ensure optic clarity all embryos 24 hpf and older were subject to 0.003% 1-phenyl 2-thiourea (PTU; Sigma-Aldrich, St. Louis, MO). 0.168 mg/mL Tricaine was used to anesthetize embryos 48 hpf and older during experiments or prior to fixation with 4% paraformaldehyde (PFA; Sigma-Aldrich, St. Louis, MO).

Zebrafish strains used in this study

CRISPR-Cas9 sgRNAs were designed to target zebrafish foxl1 zebrafish. sgRNAs were designed to target bind before the forkhead DNA binding domain, inducing a 52 bp deletion and shift in the open reading frame before this critical region. We have designated this allele *foxl1*^{n1001}. Heterozygous fish were in-crossed to produced homozygous embryos and wildtype (WT) sibling controls. *foxc1*^{aua101} and *foxc1b*^{ua1018} [188] alleles previously generated were utilized for single and double mutant analysis.

Alcian Blue and Alizarin Red Staining

Larvae were stained at 6- and 10-dpf using an acid-free alcian blue and alizarin red double stain, based on methods previously reported [205]. Up to 50 larvae were collected in a 1.5 mL microcentrifuge tube and fixed for 2 hours in 4% w/v paraformaldehyde in phosphate buffered saline pH 7.4 with gentle shaking at room temperature. After washing with 1 mL 50% v/v ethanol, larvae were gently shaken in 1 mL 50 % ethanol for 10 minutes. The ethanol solution was removed and replaced with 1 mL of alcian blue (0.01% w/v alcian blue 8 GX, 100 mmol·L^{-1} $MgCl_2$, 70% v/v ethanol) and 25 µL of alizarin red (5 mg·mL^{-1} alizarin red in ultrapure water). Larvae were incubated in the staining solution for 1 hour at room temperature with gentle rocking. The stain solution was removed, and larvae were washed with 1 mL ultrapure water, followed by addition of 1 mL bleaching solution (1.5% v/v H_2O_2, 1% w/v KOH in ultrapure water). Larvae were incubated in bleaching solution for 20 minutes at room temperature with the microcentrifuge tubes uncapped. After removing the bleaching solution, a solution of

20% w/v glycerol and 0.25% w/v KOH was added. Larvae were gently rocked at room temperature for 30 min, before the solution was replaced with 50% w/v glycerol and 0.25% w/v KOH. Larvae were incubated overnight at 4°C before being imaged and transferred to storage solution (50% w/v glycerol and 0.1% w/v KOH), before being genotyped. For genotyping, individual larvae were washed twice with 100 µL PBSTw (phosphate buffered saline 0.1% w/v Tween 20) and once with 100 µL PCR-clean water. Larvae were then boiled in 50 µL 50 mmol·L^{-1} NaOH for 20 minutes at 95°C and cooled to room temperature before addition of 5 µL 1 mol·L^{-1} Tris-HCl pH 8. The resulting solution was used as the template for PCR.

Whole Mount in Situ Hybridizations

In accordance with Thisse and Thisse[206], an *in situ* hybridization probe (*foxl1*) was synthesized from a pooling of whole-body RNA. PCR amplicons for probe synthesis were generated using the One Step Superscript IV RT-PCR Kit (Invitrogen). Antisense probes labelled with DIG (Roche) were constructed using an incorporated T7 RNA polymerase promoter (added at the 5' end of the antisense primer). Proteinase K was used to permeabilize older embryos before incubation with probe: 3 min for 24 hpf, 18 min (48 hpf). DIG labelled probes were detected using alkaline phosphatase coupled anti-DIG FAB fragments, with subsequent coloration via Nitro-blue tetrazolium (NBT; Roche) and 5-bromo-4-chloro-3-indolyl phosphate (BICP; Roche).

Calcein Staining

Live embryos previously growing in 0.003% PTU embryo media at ages 6- and 10- dpf, were incubated in a 0.2% (w/v) calcein solution, pH 7.5 (Sigma-Aldrich, St. Louis, MO), for 12 minutes followed by three, 5-minute washes in 0.003% PTU embryo media. Embryos were subsequently anesthetized in Tricaine (see Zebrafish Husbandry) and mounted in 6% methylcellulose for imaging. Images were collected in the dark using a Nikon SMZ18 microscope equipped with long pass green filter (excitation 480 ± 40 nm; emission 510 nm). Significance testing for delayed craniofacial cartilage and bone at 6 dpf was calculated using the Fisher's Exact test. Delay of cartilage development and bone calcification was characterized by decreased staining intensity, shape, and size of area (in the case of primary ossification centres), and presence/lack-thereof in comparison to their WT siblings in their respective experimental groups.

Taqman Real-Time Quantitative PCR

Total RNA was isolated using Trizol (Invitrogen) at 6 dpf from WT sibling controls and foxl1-/- mutants as per Peterson and Freeman [207]. cDNA was then generated using the High-Capacity cDNA Reverse-Transcription Kit (Applied Biosystems). 50 ng of cDNA was used in each reaction. Two biological replicates (containing a pool of 20 embryos) with three technical replicates were used with each probe and normalized to expression levels of the TATA-box binding protein (*tbp*) housekeeping gene. RT-qPCR runs were completed on an Applied Biosystems 7500 Real-Time PCR System or a ViiA 7 system. Data was analyzed using the ΔΔCT method [208,209]. Data bars are given as means ±

standard error of the mean (SEM) with significance testing (p-values) calculated using a two-tailed t-test. Previously validated TaqMan assays were purchased from Thermo Fisher as follows: *matn1* (Dr_03092841), *col1a1a* (Dr_03150834), *col1a1b* (Dr03074863), *col11a2* (Dr03085627), *hbae3* (Dr03125483), *hpx* (Dr03430535), *sp7* (Dr03133254).

DXA Scanning

Whole body BMD assessment was performed using DXA scanning and was completed as per Green et al[210]. using a PIXImus Scanner (GE/Lunar; WI, USA) which was calibrated daily with a standard phantom. Data bars are given as means ± standard error of the mean (SEM) with significance testing (p-values) calculated using a one-way ANOVA to compare WT, *foxl1* heterozygotes, and homozygotes, and a two-tailed t-test to compare WT to *foxl1*+/-;*foxc1b*+/- mutants.

Results

foxl1 mutant generation

A CRISPR-Cas9 induced mutant zebrafish strain was generated for *foxl1*, creating a 52 base-pair deletion in the lone foxl1 exon. Although not degraded through the nonsense mediated decay pathway due to the gene containing a single exon, the predicted protein is expected to have a shift in the reading frame that disrupts the forkhead DNA binding domain with a premature termination codon (PTC) after amino acid 148, removing over half the protein sequence (Supplemental Figure 1). Homozygous mutants are viable and fertile, with heterozygotes and homozygotes produced at expected Mendelian frequencies.

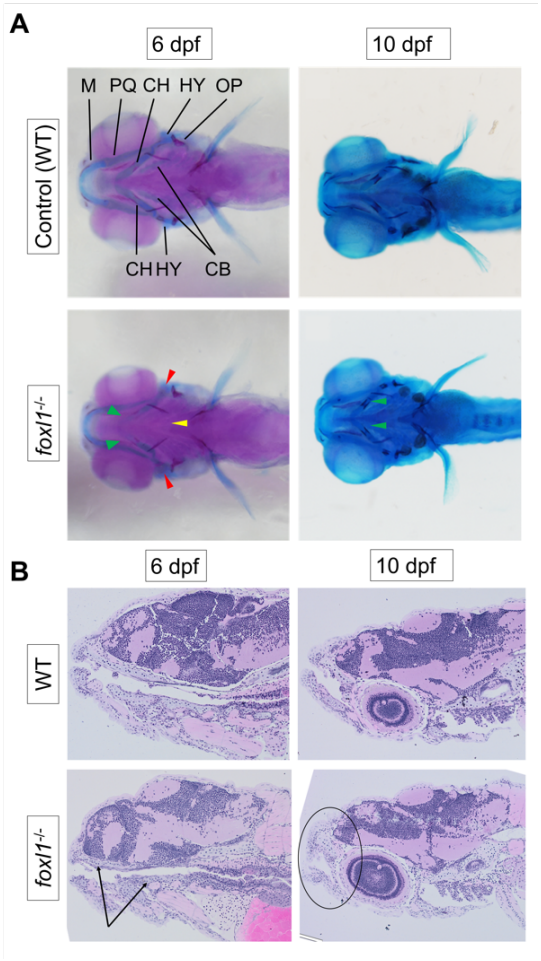

Figure 1: Reduction of cartilage in *foxl1* mutants. (A) Alcian blue (staining cartilage) indicates a delay in ceratohyal cartilages at 6 dpf (green arrowhead) but begins to recover by 10 dpf. Alizarin red indicates a delay in the ossification of the hyomandibula (red arrowhead), in *foxl1* mutants at 6 dpf, which also begins to normalize by 10 dpf. (B) Longitudinal sections through jaw demonstrating a reduced presence of cartilage formation in the upper and lower jaw as indicated by the arrows at 6 dpf, along with a shortened and round jaw structure that progresses by 10 dpf (circle). PQ, palatoquadrate; M, Meckel; HY, hyomandibula (hyosympletic) ; CH, ceratohyal; CB, ceratobranchials and OP, operculum.

Craniofacial cartilage formation and calcification in foxl1 mutants

Given the association of otosclerosis with aberrant cartilage formation [211–215], we assessed the underlying cartilage formation of the zebrafish jaw by using alcian blue staining combined with alizarin red at 6- and 10- dpf. Homozygous *foxl1* mutants exhibit a visible reduction in cartilage (alcian blue) staining of the ceratohyal (Figure 1A, green arrowheads), ceratobranchials (Figure 1A, yellow arrowhead), and hyomandibular cartilages at 6 dpf (Figure 1A, red arrowheads), which have mostly recovered by 10- dpf. At 10 dpf, all skeletal elements are well stained indicating a recovery in chondrogenesis (Figure 1A, 10pf).

Similarly, at 6 dpf, alizarin red staining for calcified bone demonstrates a reduction in calcification in *foxl1* mutants. Normal calcification of the operculum is evident while the calcification of the hyomandibula (Figure 1A, red arrowheads) and ceratohyal cartilages (Figure 1A, 6 dpf green arrowheads) are reduced at their respective primary centres of ossification as shown by the reduced alizarin red staining. By 10 dpf *foxl1* mutants appear to recover with no major morphological differences observed at this developmental stage, but still have less calcification at the primary centres of ossification in the ceratohyals than their WT counterparts as indicated by the lesser staining (alizarin red, Figure 1A, 10 dpf green arrowheads).

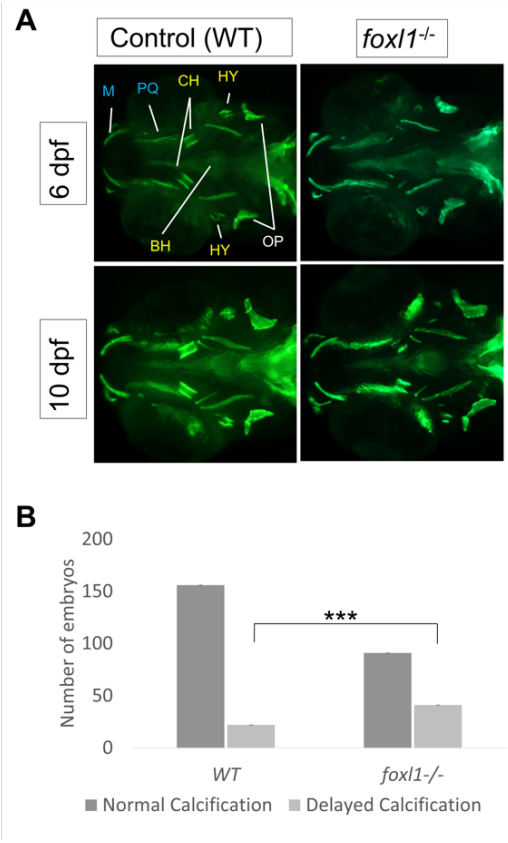

Figure 2: Calcein staining illustrating the impact of *foxl1* loss on craniofacial development and calcification. (A) 6- and 10- dpf old embryos of WT (n=173 and 99, respectively), *foxl1*$^{-/-}$(n=116 and 65, respectively). WT embryos at both 6- and 10- dpf exhibit normal craniofacial development and calcification of all jaw structures. *foxl1*$^{-/-}$ embryos show a delayed calcification in the ceratohyal and hyomandibula at 6 dpf yet appear mostly recovered by 10 dpf. (B) The proportion of embryos with delayed calcification in *foxl1* mutants is statistically significant (Fisher's p= 0.0001) when compared to wildtype siblings. PQ, palatoquadrate; M, Meckel; HY, hyomandibula (hyosympletic); BH, basihyal; and OP, opercula.

As we observed a reduction in cartilage formation of the jaw in *foxl1* mutants via alcian blue staining, further analysis in the form of histology with an H&E stain was used

to compare jaw morphology of between WT and *foxl1-/-* embryos at 6 and 10 dpf (Figure 1B). It was evident that the *foxl1-/-* mutants have reduced cartilage elements (arrows Figure 1B) and a shortened and rounded jawline that became more prominent as the embryos aged from 6 to 10 dpf (circle, Figure 1B).

To further visualize the effect that the *foxl1* mutation has on bone formation and calcification, calcein staining was performed on live embryos at both 6- and 10 dpf. The hyomandibula and ceratohyal were examined closely as they are the homologous structures of the stapes middle ear bone in mammals that is often the afflicted structure in otosclerosis and was delayed in its calcification according with alizarin red staining. At 6 dpf, fewer *foxl1* homozygous mutant embryos had complete calcification of the hyomandibula and ceratohyal bones when compared to wildtype siblings ($p= 0.0001$) (Figure 2A and B), which had mostly recovered by 10 dpf (Figure 2A) as indicated by the reduced staining/presence of calcium. This agrees with the alizarin red staining and indicates a delay in calcification specifically at primary centers of ossification in the developing jaw.

Overlapping expression of foxl1, foxc1a and foxc1b in zebrafish

Given that phenotypes in jaw development recover in *foxl1* mutants as development proceeds, we asked whether genetic redundancy may allow for overtly normal jaw development in *foxl1* mutants. We assessed the expression of other forkhead genes that can cause craniofacial and axial skeletal defects in defects in zebrafish and humans when mutated, mainly *foxc1a* and *foxc1b* (*FOXC2*) [170,170,171]. All three fox genes are expressed in the head in a pattern consistent with NCC development at 24 hpf (Figure

3A, C, E) and in the pharyngeal arches (Figure 3B, D, F) that are predominantly responsible for giving rise to Meckel's, palatoquadrate, ceratohyal, and hyomandibular cartilages by 48 hpf. Expression in the ventral somite domains is observed for both *foxl1* and *foxc1a* at 24 hpf.

foxl1 mutation in foxc1a and foxc1b mutant backgrounds

To assess the effect that *foxl1* mutation has in combination with other forkhead mutants, calcein staining was performed on live embryos at 6 dpf. In agreement with other studies [170,171], *foxc1b* mutants did not exhibit any morphological changes in comparison to WT embryos, however loss of *foxc1a* in zebrafish embryos clearly resulted in the lack of development of most major craniofacial structures such as the hyomandibula, palatoquadrate, and Meckel's composing the developing jaw (Figure 4A). *foxc1a* mutants also display hydrocephalous and cardiac/abdominal edema compared to wildtype siblings. *foxc1a* homozygous mutants die around 7 dpf.

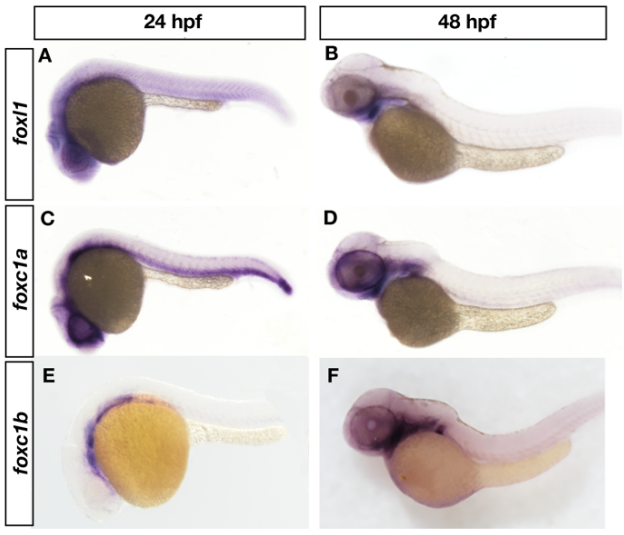

Figure 3: Expression of *foxl1*, *foxc1a* and *foxc1b* in wildtype zebrafish at 24 and 48 hpf. At 24hpf, *foxl1* is expressed at in the brain and trunk (A), similar to *foxc1a* (C), while *foxc1b* is observed in the ventral head/brain regions (E). At 48 hpf, all three forkhead genes are expressed in the pharyngeal arches.

Double *foxc1a-/-; foxl1-/-* mutants (Figure 4B, Figure 6B) exhibited reduced bone formation, including a lack of calcification of the operculum, when compared to foxc1a mutants alone which exhibit normal operculum calcification. Unlike *foxc1a-/-; foxl1-/-* double mutants, *foxl1-/-; foxc1b-/-* embryos did not exhibit an abnormal phenotype in comparison to the wild-type controls (Figure 4B, Figure 6B). *foxc1a-/-; foxc1b-/-* double mutant embryos had similar phenotypes as the *foxc1a-/-; foxl1-/-* embryos at 6 dpf, which included further loss of bone calcification in the face (Figure 4B, Figure 6B).

Axial skeletal calcification in forkhead mutants

In humans, variants in *FOXL1* and *FOXC2* are associated with reduced bone mineral density (BMD) and osteoporosis risk [182,185,211]. Furthermore, the co-occurrence of otosclerosis and osteoporosis has been noted [211], suggesting similar aetiologies for both bone remodelling diseases. We thus tested *foxl1, foxc1a*, and *foxc1b*, for defects in the calcification of the zebrafish spine to determine if either gene affects calcification o the axial skeleton. Mutation of *foxl1* has little effect on the patterning and formation of the vertebrae of the skeleton at 6- and 10- dpf when compared with WT controls (Figure 5), as vertebral calcification appeared to be variable within experimental groups (Figure 5B and C). This could possibly be due to environmental changes or natural variability in

bone formation. This led to an overall decrease in the number of calcified vertebrae at 6 dpf, but an increased trend in rate of vertebrae calcification on average in our foxl1 mutants in comparison WT siblings (Figure 5B and C). The average number of vertebrate calcified (based on primary center of ossification) for WT and *foxl1-/-* was 5 and 4 approximately by 6 dpf and 8 and 10 approximately by 10 dpf (Figure 5B and C).

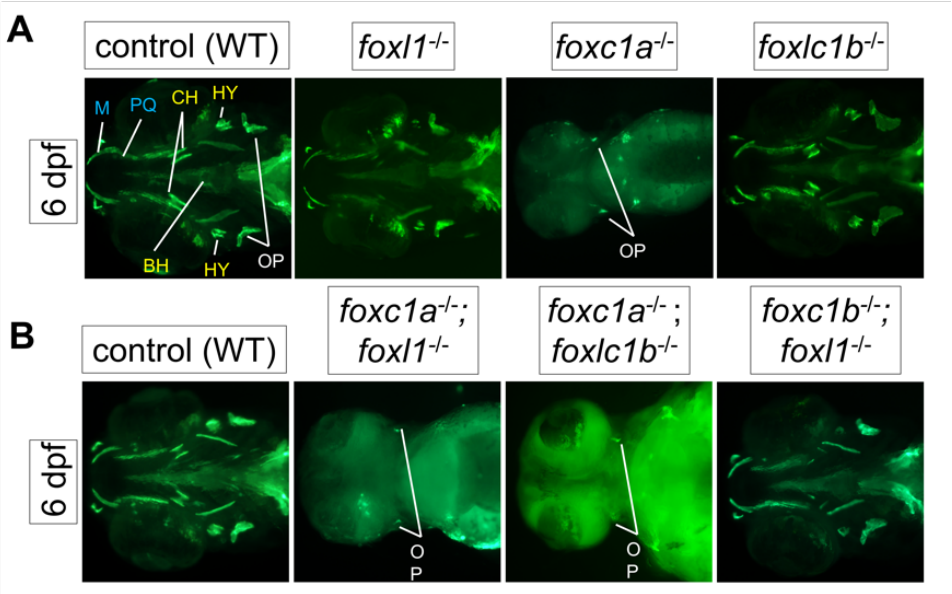

Figure 4: Calcein staining illustrating the impact of *foxl1, foxc1a,* and *foxc1b* lone and combined loss on craniofacial development and calcification. (A) f*oxc1a*$^{-/-}$ embryos have a lack of bone development in all craniofacial bones resulting from the first (blue) and second (yellow) pharyngeal arches and diminished formation of the opercula bones at 6 dpf. *foxc1b*$^{-/-}$ embryos exhibit no change at either developmental stage (B) WT (n=173), *foxc1a*$^{-/-}$; *foxl1*$^{-/-}$(n=6), *foxc1b*$^{-/-}$; *foxl1*$^{-/-}$(n=2), and *foxc1a*$^{-/-}$; *foxc1b*$^{-/-}$ (n=4) embryos at 6 dpf. *foxc1a*$^{-/-}$; *foxl1*$^{-/-}$ embryos exhibit a further loss of craniofacial bone formation and calcification with increased size in the cardiac edema present. While *foxc1b*$^{-/-}$; *foxl1*$^{-/-}$ embryos exhibit no change from their respective individual knockout models. *foxc1a*$^{-/-}$;

foxc1b$^{-/-}$ double mutants show a similar phenotype as *foxc1a*$^{-/-}$ and *foxc1a*$^{-/-}$; *foxl1*$^{-/-}$ embryos.

foxc1a mutants lack any axial skeleton formation at 6 dpf while presenting with edemas around the heart and body cavity that grew over the course of time (Figure 6A), thus preventing the analysis of spine calcification in *foxl1-/-;foxc1a-/-* mutants entirely (Figure 6B). It should be noted however that lateral views presented in Figure 6A reiterate the increased severity of craniofacial phenotypes observed in *foxl1-/-;foxc1a-/-* mutants previously shown in in Figure 4A and 6B. *foxc1b* mutant embryos did not exhibit any abnormal phenotypes regarding axial skeletal development at 6 dpf (Figure 6A), nor did double *foxl1-/-;foxc1b-/-* mutants (Figure 6B).

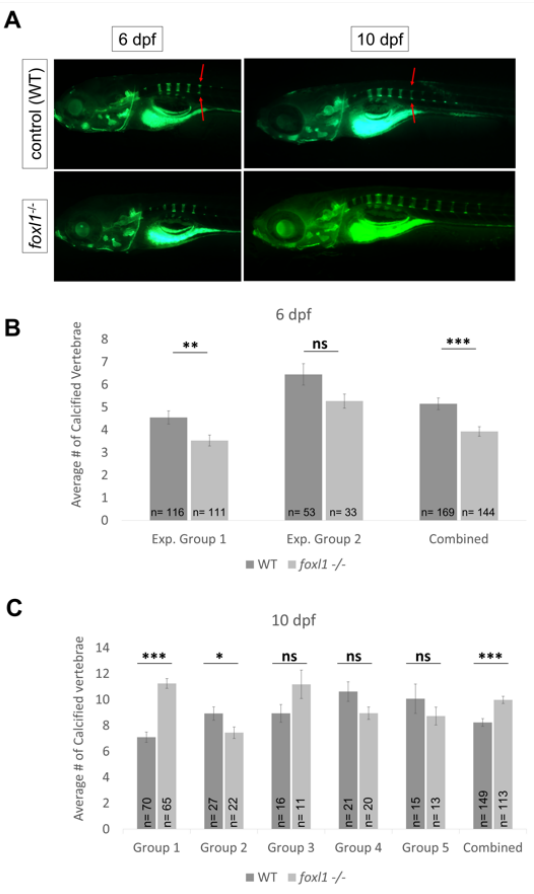

Figure 5: Calcein staining illustrating the impact of *foxl1* loss on axial skeletal development and calcification. (A) WT and *foxl1*$^{-/-}$ embryos at 6- and 10- dpf showing normal formation of the vertebrae in *foxl1*. (B) and (C) experimental groups of calcein staining illustrating the variability in calcification of the zebrafish vertebrate between WT and *foxl1* homozygotes at 6 and 10 dpf, respectively (*p< 0.05, **p< 0.01, ***p< 0.001), showing an increased trend in number of calcified vertebrae in *foxl1* mutants by 10 dpf.

To further investigate the calcification of the zebrafish skeleton, dual-energy X-ray absorptiometry (DXA) was performed on *foxl1* mutants to measure bone mineral density as per Green et al. (Supplemental Figure 2) [216]. No significant difference was found between WT siblings and heterozygous or homozygous *foxl1* mutants alone at 5.5 months old (Supplemental Figure 2A). As both *foxl1* and *foxc1b* have been associated with osteoporosis we also assessed *foxl1+/-; foxc1b+/-* double heterozygous mutants and WT controls at 1 year of age and similarly, no difference in their BMD was observed (Supplemental Figure 2B).

Expression of genes required for bone formation in forkhead mutants

To further demonstrate the role of *foxl1* on skeletal development, we assessed the expression of genes with known roles in cartilage and bone formation in zebrafish *foxl1, foxc1a* and *foxc1b* mutants. To determine candidate target genes of *foxl1* an RNA-Seq screen was completed on WT and *foxl1-/-* embryos at 6 dpf. Prominent genes with differential expression were then validated using TaqMan Real-Time quantitative PCR (RT-qPCR). At 6 dpf, we identified markers of cartilage and heme-binding proteins as differentially expressed (Figure 7). Chondrocyte markers such as *matrilin 1* (*matn1*, 36%

reduction), *collagen type 1 alpha 1a* (*col1a1a*, 40% reduction), *collagen type 1 alpha 1b* (*col1a1b*, 46% reduction), *collagen type 11 alpha 2* (*col11a2*, 38% reduction) saw statistically significant ($p < 0.05$) reductions in gene expression based on total-whole embryo RNA (Figure 7A). *hemoglobin alpha embryonic-3* (*hbae3*, 64% reduction) and *hemopexin* (*hpx*, 92% reduction) both important factors in heme-binding and transport were even more so reduced in our mutants. *osterix* (*sp7*) a marker of osteoblast differentiation was downregulated in foxl1 mutants but did not reach statistical significance (Figure 7A). These data demonstrate the reduction of genes required for collagen and bone formation at 6 dpf, consistent with the delay in chondrogenesis and subsequent calcification of aspects of the craniofacial skeleton at this developmental timepoint. To further illustrate the genetic redundancy that may allow overtly normal jaw development in the absence of *foxl1*, we tested the expression of the same genes in *foxc1a* and *foxc1b* mutants. Much like *foxl1* mutants, *foxc1a-/-* embryos saw significant reduction in *matrilin 1, collagen type 1 alpha 1a, collagen type 11 alpha 2,* and *hemopexin* indicating target gene overlap (Figure 7B). Intriguingly foxc1b-/- embryos saw an increase in *collagen type 11 alpha 2* (Figure 7C), suggesting it acts as a repressive regulator in comparison to the enhancing mechanism of *foxl1* and *foxc1a.*

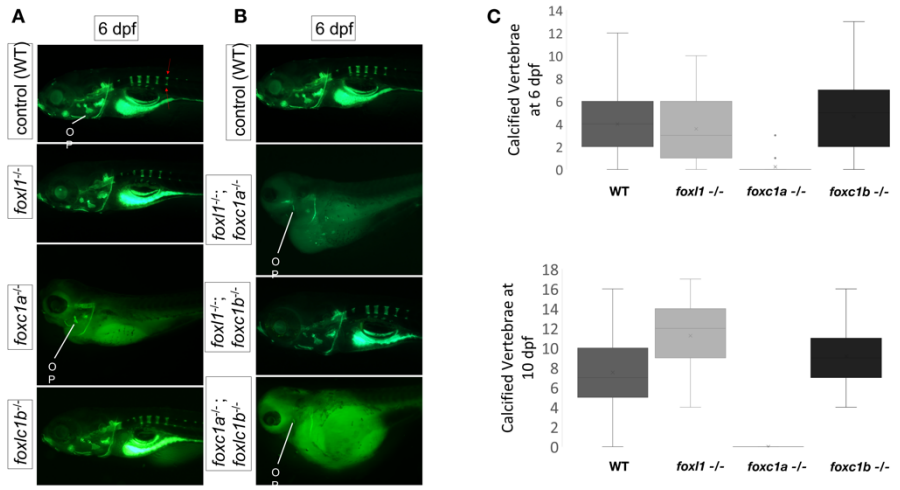

Figure 6: Calcein staining illustrating the impact of *foxl1, foxc1a*, and *foxc1b* lone and combined loss on axial skeleton development and calcification. (A) WT, *foxl1*$^{-/-}$, *foxc1a*$^{-/-}$, and *foxc1b*$^{-/-}$ embryos at 6 dpf showing normal formation of the vertebrae in *foxl1* and *foxc1b* mutants. *foxc1a*$^{-/-}$ embryos did not develop or calcify vertebrae and had large abdomen cavity edemas that grew over time. (B) WT, *foxc1a*$^{-/-}$*; foxl1*$^{-/-}$*, foxc1b*$^{-/-}$*; foxl1*$^{-/-}$*,* and *foxc1a*$^{-/-}$*; foxc1b*$^{-/-}$ embryos at 6 dpf. Double *foxc1a*$^{-/-}$*; foxl1*$^{-/-}$ embryos exhibit larger edemas and the lack of most calcified structures at 6 dpf, including the operculum (OP). *foxc1b*$^{-/-}$*; foxl1*$^{-/-}$ embryos had no significant change. *foxc1a*$^{-/-}$*; foxc1b*$^{-/-}$ mutants elicited similar results as *foxc1a*$^{-/-}$*; foxl1*$^{-/-}$ embryos that include edemas and lack of craniofacial calcification. (C) Boxplots illustrating the variability of the number of vertebrae calcified in *foxl1*$^{-/-}$*, foxc1a*$^{-/-}$, *foxc1b*$^{-/-}$, and *foxl1*$^{-/-}$*;foxc1b*$^{-/-}$ mutants in comparison with WT embryos at 6 dpf. Red arrows indicate primary centres of ossification within the vertebrae.

Discussion

Here, we report on a foxl1 mutant strain in zebrafish as a potential model of otosclerosis and osteoporosis. Structures in the mammalian middle ear are homologous

with the ceratohyal, palatoquadrate, and hyomandibular jaw bones in zebrafish [194,197–199,217] and as such the malformation of these bones leads to the loss of sound conduction in mammals and jaw formation in zebrafish. Despite abundant *foxl1* expression in the pharyngeal arches and a delay in cartilage formation and calcification in the jaw, loss of *foxl1* does not significantly affect the overall structure and function of the craniofacial skeleton, consistent with recent reports using strain harboring a *foxl1* nonsense mutation [171]. In agreement with a delay in cartilage formation and calcification at 6 dpf, we do observe a reduction in the expression of cartilage markers such as *matrillin1* and *col1a1a/b* in *foxl1* homozygous mutants at this developmental time point. Conversely, previous *foxl1* morpholino studies have shown much more pronounced phenotypes including abnormalities in craniofacial skeleton, midbrain, eye and pectoral fin, [218]. While these discrepancies may be due to morpholino off-target effects, genetic compensation in CRISPR generated INDEL mutants [219–221] may also play a role.

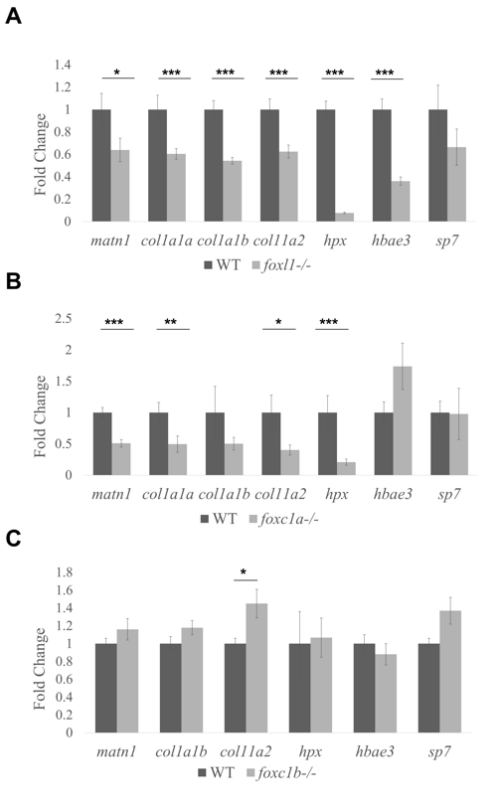

Figure 7: Fold-change of downstream *foxl1* targets from WT, *foxl1*$^{-/-}$, *foxc1a*$^{-/-}$, and *foxc1b*$^{-/-}$ embryos at 6 dpf using TaqMan RT-qPCR to confirm genes of interest from RNA-Seq screen. Fold change between WT and *foxl1*$^{-/-}$ plotted with WT values set to 1 (*p< 0.05, **p< 0.01, ***p< 0.001). Fold change values plotted with expression is WT set to 1.

While *FOXL1* (and *FOXC2*) have been associated with osteoporosis in humans, and the co-occurrence of otosclerosis and osteoporosis has been reported [211,212,222], we did not find any defects in development of the larval zebrafish axial skeleton in *foxl1* or *foxc1b* (*FOXC2* homolog) mutants. The axial skeleton in *foxnln1001 -/-* mutants showed an increased trend of vertebrae calcified by 10 dpf but remained largely unaffected by the loss of *foxl1*. It is also possible that foxl1 may play a specific role in endochondral

ossification, which includes the jaw, but may not regulate intramembranous bone development that occurs in the zebrafish spine. No differences in BMD are observed in adult *foxl1* mutant zebrafish using DXA scanning, however detection of BMD in fish using this method may not be sensitive enough to determine small changes in BMD, and only relatively young fish (5.5 months of age) were tested in this study. Additional studies assessing BMD in varying ages of adult fish through more sensitive μCT imaging could determine whether *foxl1* mutants have defects in maintaining BMD as they age.

Since *foxl1* has been shown to be expressed in cartilage and bone-specific tissues, and is associated with bone remodelling diseases such as otosclerosis and osteoporosis[181,182,203] it is interesting that the loss of *foxl1* does not cause such profound bone phenotypes in the head or axial skeleton in the developing zebrafish. This indicates that, like many other FOX genes, *foxl1* may only act as minor genetic modifier in development[174,223,224]. Our data indicates that when mutated alone the development of bone and cartilage is predominantly normal in zebrafish larvae which only exhibit minor delays by 10 dpf. However, when mutated in conjunction with *foxc1a*, another FOX gene known to be central in upper craniofacial cartilage formation and somite patterning, further loss of bone is observed than in *foxc1a* mutants alone. In zebrafish, bones in the craniofacial skeleton of *foxc1a-/-; foxl1-/-* double mutants that had formed and began to calcify, albeit abnormally, in *foxc1a-/-* embryos, did not form or were even more malformed. Taken together with qPCR data indicating that *foxl1* shares similar targets as *foxc1a*, this supports a model whereby *foxl1* may act as a modifier locus for *foxc1a*. Alternatively, the increased severity of phenotypes through the combined loss of *foxl1*

and *foxc1a* may represent reduced growth and failure to thrive when compared to *foxc1a* mutants alone, as opposed to a specific effect on bone development. This possibility should be explored further. Heterozygous loss of *FOXC1* in humans results in Axenfeld Rieger syndrome (ARS), which results in increased risk for glaucoma and variable systemic anomalies including defects in craniofacial bone development[225]. Recently, an atypical FOXC1-attributable ARS patient was described with clinical otosclerosis[179], again highlighting the potential overlapping function *foxl1* and *foxc1a*.

Another novel hypothesis indicating *foxl1*'s possible involvement of bone development and maintenance is its regulation of hemopexin, which is responsible for high-affinity heme-binding and transport to the liver for degradation, preventing oxidative stress and iron loss[226,227] as well as hemoglobin alpha embryonic-3 that is involved up-stream of the oxygen transport chain as an early marker of erythrocyte development[228]. Both genes were significantly downregulated in *foxl1-/-* mutants and there is a known association between heme-transport/blood diseases such as anemia and low BMD leading to fracture over time[229–231]. This could suggest that a loss of *foxl1* may cause an increase in oxidative stress which in turn may exacerbate the mild cartilage and bone phenotypes observed during growth and remodelling. This hypothesis warrants further investigation.

Conclusions

In zebrafish, *foxl1* is required for the expression of key collagen genes but plays only a minor role in the formation and maintenance of zebrafish jaw cartilages and bones. Given the homology of zebrafish jawbones and mammalian middle ear bones, *foxl1*

mutant zebrafish serve as a useful model to gain understanding of the mechanistic insights regarding the pathophysiology of otosclerosis. Additional analyses will be needed to determine if BMD defects occur in *foxl1* mutant zebrafish and whether they may serve as a useful model of osteoporosis. Our study supports the hypothesis that *foxl1* and *foxc1a* function together to regulate bone development, however, the manner in which *foxl1* and *foxc1a* function together to achieve optimal expression of cartilage and bone markers has yet to be determined and needs further exploration. This study highlights a new *foxl1* mutant zebrafish line, finding novel gene target genes of *foxl1* that could be utilized for new therapies to treat otosclerosis.

References

129. Kimmel, C. B., Ballard, W. W., Kimmel, S. R., Ullmann, B. & Schilling, T. F. Stages of embryonic development of the zebrafish. *Developmental Dynamics* **203**, 253–310 (1995).

147. Berendsen, A. D. & Olsen, B. R. Bone development. *Bone* **80**, 14–18 (2015).

148. Fleming, A., Kishida, M. G., Kimmel, C. B. & Keynes, R. J. Building the backbone: the development and evolution of vertebral patterning. *Development* **142**, 1733–1744 (2015).

149. Javidan, Y. & Schilling, T. F. Development of Cartilage and Bone. in *Methods in Cell Biology* vol. 76 415–436 (Elsevier, 2004).

150. Kozhemyakina, E., Lassar, A. B. & Zelzer, E. A pathway to bone: signaling molecules and transcription factors involved in chondrocyte development and maturation. *Development* **142**, 817–831 (2015).

151. Dash, S. & Trainor, P. A. The development, patterning and evolution of neural crest cell differentiation into cartilage and bone. *Bone* **137**, 115409 (2020).

152. Winnier, G. E., Hargett, L. & Hogan, B. L. The winged helix transcription factor MFH1 is required for proliferation and patterning of paraxial mesoderm in the mouse embryo. *Genes Dev.* **11**, 926–940 (1997).

153. Lefebvre, V. Roles and regulation of SOX transcription factors in skeletogenesis. *Curr Top Dev Biol* **133**, 171–193 (2019).

154. Long, F. & Ornitz, D. M. Development of the Endochondral Skeleton. *Cold Spring Harb Perspect Biol* **5**, a008334 (2013).

155. Abe, Y., Tanaka, N., Abe, Y. & Tanaka, N. Roles of the Hedgehog Signaling Pathway in Epidermal and Hair Follicle Development, Homeostasis, and Cancer. *Journal of Developmental Biology* **5**, 12 (2017).

156. Ahlgren, S. C. & Bronner-Fraser, M. Inhibition of Sonic hedgehog signaling in vivo results in craniofacial neural crest cell death. *Current Biology* **9**, 1304–1314 (1999).

157. Armstrong, B. E., Henner, A., Stewart, S. & Stankunas, K. Shh promotes direct interactions between epidermal cells and osteoblast progenitors to shape regenerated zebrafish bone. *Development* **144**, 1165–1176 (2017).

158. Avaron, F., Smith, A. & Akimenko, M.-A. *Sonic Hedgehog Signaling in the Developing and Regenerating Fins of Zebrafish*. *Madame Curie Bioscience Database [Internet]* (Landes Bioscience, 2013).

159. Carballo, G. B., Honorato, J. R., de Lopes, G. P. F. & Spohr, T. C. L. de S. e. A highlight on Sonic hedgehog pathway. *Cell Communication and Signaling* **16**, 11 (2018).

160. Chung, U., Schipani, E., McMahon, A. P. & Kronenberg, H. M. *Indian hedgehog* couples chondrogenesis to osteogenesis in endochondral bone development. *J Clin Invest* **107**, 295–304 (2001).

161. Eberhart, J. K., Swartz, M. E., Crump, J. G. & Kimmel, C. B. Early Hedgehog signaling from neural to oral epithelium organizes anterior craniofacial development. *Development* **133**, 1069–1077 (2006).

162. Katoh, M. Networking of WNT, FGF, Notch, BMP, and Hedgehog Signaling Pathways during Carcinogenesis. *Stem Cell Reviews; Totowa* **3**, 30–8 (2007).

163. Rice, R., Rice, D. P. C. & Thesleff, I. Foxc1 integrates Fgf and Bmp signalling independently of twist or noggin during calvarial bone development. *Developmental Dynamics* **233**, 847–852 (2005).

164. Asharani, P. V. *et al.* Attenuated BMP1 Function Compromises Osteogenesis, Leading to Bone Fragility in Humans and Zebrafish. *The American Journal of Human Genetics* **90**, 661–674 (2012).

165. Katoh, M. & Katoh, M. Transcriptional regulation of WNT2B based on the balance of Hedgehog, Notch, BMP and WNT signals. *International Journal of Oncology* **34**, 1411–1415 (2009).

166. Wan, M. & Cao, X. BMP signaling in skeletal development. *Biochemical and Biophysical Research Communications* **328**, 651–657 (2005).

167. Chrystal, P. W. *et al.* The Axenfeld-Rieger Syndrome Gene FOXC1 Contributes to Left-Right Patterning. *Genes (Basel)* **12**, (2021).

168. Kim, S. H. *et al.* The forkhead transcription factor Foxc2 stimulates osteoblast differentiation. *Biochemical and Biophysical Research Communications* **386**, 532–536 (2009).

169. Kume, T., Jiang, H., Topczewska, J. M. & Hogan, B. L. M. The murine winged helix transcription factors, Foxc1 and Foxc2, are both required for cardiovascular development and somitogenesis. *Genes Dev.* **15**, 2470–2482 (2001).

170. Xu, P. *et al.* Foxc1 establishes enhancer accessibility for craniofacial cartilage differentiation. *eLife* **10**, e63595 (2021).

171. Xu, P. *et al.* Fox proteins are modular competency factors for facial cartilage and tooth specification. *Development* dev.165498 (2018) doi:10.1242/dev.165498.

172. You, W. *et al.* Foxc2 regulates osteogenesis and angiogenesis of bone marrow mesenchymal stem cells. *BMC Musculoskeletal Disorders* **14**, 199 (2013).

173. Dai, S., Qu, L., Li, J. & Chen, Y. Toward a mechanistic understanding of DNA binding by forkhead transcription factors and its perturbation by pathogenic mutations. *Nucleic Acids Research* **49**, 10235–10249 (2021).

174. Hannenhalli, S. & Kaestner, K. H. The evolution of Fox genes and their role in development and disease. *Nature Reviews Genetics* **10**, 233–240 (2009).

175. Nifuji, A., Miura, N., Kato, N., Kellermann, O. & Noda, M. Bone morphogenetic protein regulation of forkhead/winged helix transcription factor Foxc2 (Mfh1) in a murine mesodermal cell line C1 and in skeletal precursor cells. *J. Bone Miner. Res.* **16**, 1765–1771 (2001).

176. Sun, J., Ishii, M., Ting, M.-C. & Maxson, R. Foxc1 controls the growth of the murine frontal bone rudiment by direct regulation of a Bmp response threshold of Msx2. *Development* **140**, 1034–1044 (2013).

177. Mariotti, M., Carnovali, M. & Banfi, G. Danio rerio: the Janus of the bone from embryo to scale. *Clin Cases Miner Bone Metab* **12**, 188–194 (2015).

178. Tümer, Z. & Bach-Holm, D. Axenfeld–Rieger syndrome and spectrum of PITX2 and FOXC1 mutations. *Eur J Hum Genet* **17**, 1527–1539 (2009).

179. Wang, R. *et al.* A novel variant in FOXC1 associated with atypical Axenfeld-Rieger syndrome. *BMC Medical Genomics* **14**, 277 (2021).

180. French, C. R. Mechanistic Insights into Axenfeld-Rieger Syndrome from Zebrafish foxc1 and pitx2 Mutants. *Int J Mol Sci* **22**, 10001 (2021).

181. Abdelfatah, N. *et al.* A pathogenic deletion in Forkhead Box L1 (FOXL1) identifies the first otosclerosis (OTSC) gene. *Hum Genet* (2021) doi:10.1007/s00439-021-02381-1.

182. Kim, B.-J. *et al.* Replication of Caucasian Loci Associated with Osteoporosis-related Traits in East Asians. *J Bone Metab* **23**, 233–242 (2016).

183. Kung, A. W. C. Novel genetic loci associated with osteoporosis. *Bone* **47**, S376 (2010).

184. Liu, Y.-J., Zhang, L., Papasian, C. J. & Deng, H.-W. Genome-wide Association Studies for Osteoporosis: A 2013 Update. *J Bone Metab* **21**, 99–116 (2014).

185. the Genetic Factors for Osteoporosis (GEFOS) Consortium *et al.* Twenty bone-mineral-density loci identified by large-scale meta-analysis of genome-wide association studies. *Nature Genetics* **41**, 1199–1206 (2009).

186. Aoki, R. *et al.* Foxl1-Expressing Mesenchymal Cells Constitute the Intestinal Stem Cell Niche. *Cellular and Molecular Gastroenterology and Hepatology* **2**, 175–188 (2016).

187. Madison, B. B., McKenna, L. B., Dolson, D., Epstein, D. J. & Kaestner, K. H. FoxF1 and FoxL1 Link Hedgehog Signaling and the Control of Epithelial Proliferation in the Developing Stomach and Intestine. *J. Biol. Chem.* **284**, 5936–5944 (2009).

188. Umali, J., Hawkey-Noble, A. & French, C. R. Loss of foxc1 in zebrafish reduces optic nerve size and cell number in the retinal ganglion cell layer. *Vision Research* **156**, 66–72 (2019).

189. Whitesell, T. R. *et al.* foxc1 is required for embryonic head vascular smooth muscle differentiation in zebrafish. *Developmental Biology* **453**, 34–47 (2019).

190. Mackay, E. W., Apschner, A. & Schulte-Merker, S. A bone to pick with zebrafish. *BoneKEy Rep* **2**, 445 (2013).

191. Witten, P. E., Harris, M. P., Huysseune, A. & Winkler, C. Chapter 13 - Small teleost fish provide new insights into human skeletal diseases. in *Methods in Cell Biology* (eds. Detrich, H. W., Westerfield, M. & Zon, L. I.) vol. 138 321–346 (Academic Press, 2017).

192. Nikaido, M., Tada, M., Saji, T. & Ueno, N. Conservation of BMP signaling in zebrafish mesoderm patterning. *Mechanisms of Development* **61**, 75–88 (1997).

193. Wada, N. *et al.* Hedgehog signaling is required for cranial neural crest morphogenesis and chondrogenesis at the midline in the zebrafish skull. *Development* **132**, 3977–3988 (2005).

194. Raterman, S. T., Metz, J. R., Wagener, F. A. D. T. G. & Von den Hoff, J. W. Zebrafish Models of Craniofacial Malformations: Interactions of Environmental Factors. *Frontiers in Cell and Developmental Biology* **8**, 1346 (2020).

195. Mork, L. & Crump, G. Zebrafish Craniofacial Development: A Window into Early Patterning. *Curr Top Dev Biol* **115**, 235–269 (2015).

196. Bergen, D. J. M., Kague, E. & Hammond, C. L. Zebrafish as an Emerging Model for Osteoporosis: A Primary Testing Platform for Screening New Osteo-Active Compounds. *Front. Endocrinol.* **10**, (2019).

197. Anthwal, N., Joshi, L. & Tucker, A. S. Evolution of the mammalian middle ear and jaw: adaptations and novel structures. *Journal of Anatomy* **222**, 147–160 (2013).

198. Takechi, M. & Kuratani, S. History of studies on mammalian middle ear evolution: A comparative morphological and developmental biology perspective. *Journal of Experimental Zoology Part B: Molecular and Developmental Evolution* **314B**, 417–433 (2010).

199. Ankamreddy, H., Bok, J. & Groves, A. K. Uncovering the Secreted Signals and Transcription Factors Regulating the Development of Mammalian Middle Ear Ossicles. *Dev Dyn* **249**, 1410–1424 (2020).

200. Apschner, A., Schulte-Merker, S. & Witten, P. E. Chapter 10 - Not All Bones are Created Equal – Using Zebrafish and Other Teleost Species in Osteogenesis Research. in *Methods in Cell Biology* (eds. Detrich, H. W., Westerfield, M. & Zon, L. I.) vol. 105 239–255 (Academic Press, 2011).

201. Chang, Z., Chen, P.-Y., Chuang, Y.-J. & Akhtar, R. Zebrafish as a model to study bone maturation: Nanoscale structural and mechanical characterization of age-related changes in

the zebrafish vertebral column. *Journal of the Mechanical Behavior of Biomedical Materials* **84**, 54–63 (2018).

202. Du, S. J., Frenkel, V., Kindschi, G. & Zohar, Y. Visualizing Normal and Defective Bone Development in Zebrafish Embryos Using the Fluorescent Chromophore Calcein. *Developmental Biology* **238**, 239–246 (2001).
203. Huang, H. *et al.* Application of bone transgenic zebrafish in anti-osteoporosis chemical screening. *Animal Models and Experimental Medicine* **1**, 53–61 (2018).
204. Kwon, R. Y., Watson, C. J. & Karasik, D. Using zebrafish to study skeletal genomics. *Bone* **126**, 37–50 (2019).
205. Walker, D. M. & Kimmel, C. A two-color acid-free cartilage and bone stain for zebrafish larvae. *Biotechnic & Histochemistry* **82**, 23–28 (2007).
206. Thisse, C. & Thisse, B. High-resolution in situ hybridization to whole-mount zebrafish embryos. *Nature Protocols* **3**, 59–69 (2008).
207. Peterson, S. M. & Freeman, J. L. RNA Isolation from Embryonic Zebrafish and cDNA Synthesis for Gene Expression Analysis. *J Vis Exp* 1470 (2009) doi:10.3791/1470.
208. Livak, K. J. & Schmittgen, T. D. Analysis of Relative Gene Expression Data Using Real-Time Quantitative PCR and the 2−ΔΔCT Method. *Methods* **25**, 402–408 (2001).
209. Rao, X., Huang, X., Zhou, Z. & Lin, X. An improvement of the 2ˆ(–delta delta CT) method for quantitative real-time polymerase chain reaction data analysis. *Biostat Bioinforma Biomath* **3**, 71–85 (2013).
210. Green, J., Taylor, J. J., Hindes, A., Johnson, S. L. & Goldsmith, M. I. A gain of function mutation causing skeletal overgrowth in the rapunzel mutant. *Developmental Biology* **334**, 224–234 (2009).
211. Atan, D., Atan, T., Özcan, K. M., Ensari, S. & Dere, H. Relation of otosclerosis and osteoporosis: A bone mineral density study. *Auris Nasus Larynx* **43**, 400–403 (2016).

212. Markou, K. & Goudakos, J. An overview of the etiology of otosclerosis. *Eur Arch Otorhinolaryngol* **266**, 25 (2008).

213. Niedermeyer, H. P. & Arnold, W. Etiopathogenesis of Otosclerosis. *ORL : Journal for Oto - Rhino - Laryngology and Its Related Specialties* **64**, 114–9 (2002).

214. Schrauwen, I. *et al.* COL1A1 association and otosclerosis: A meta-analysis. *American Journal of Medical Genetics Part A* **158A**, 1066–1070 (2012).

215. Niedermeyer, H. P., Becker, E. T. & Arnold, W. Expression of collagens in the otosclerotic bone. *Adv Otorhinolaryngol* **65**, 45–49 (2007).

216. Green, J., Taylor, J. J., Hindes, A., Johnson, S. L. & Goldsmith, M. I. A gain of function mutation causing skeletal overgrowth in the rapunzel mutant. *Dev Biol* **334**, 224–234 (2009).

217. Kitazawa, T. *et al.* Distinct effects of Hoxa2 overexpression in cranial neural crest populations reveal that the mammalian hyomandibular-ceratohyal boundary maps within the styloid process. *Developmental Biology* **402**, 162–174 (2015).

218. Nakada, C., Satoh, S., Tabata, Y., Arai, K. & Watanabe, S. Transcriptional Repressor foxl1 Regulates Central Nervous System Development by Suppressing shh Expression in Zebra Fish. *Mol Cell Biol* **26**, 7246–7257 (2006).

219. El-Brolosy, M. A. *et al*. Genetic compensation triggered by mutant mRNA degradation. *Nature* **568**, 193–197 (2019).

220. El-Brolosy, M. A. & Stainier, D. Y. R. Genetic compensation: A phenomenon in search of mechanisms. *PLOS Genetics* **13**, e1006780 (2017).

221. Salanga, C. M. & Salanga, M. C. Genotype to Phenotype: CRISPR Gene Editing Reveals Genetic Compensation as a Mechanism for Phenotypic Disjunction of Morphants and Mutants. *Int J Mol Sci* **22**, 3472 (2021).

222. Clayton, A. E., Mikulec, A. A., Mikulec, K. H., Merchant, S. N. & McKenna, M. J. Association between osteoporosis and otosclerosis in women. *The Journal of Laryngology & Otology* **118**, 617–621 (2004).

223. Cuesta, I., Zaret, K. S. & Santisteban, P. The Forkhead Factor FoxE1 Binds to the Thyroperoxidase Promoter during Thyroid Cell Differentiation and Modifies Compacted Chromatin Structure. *Molecular and Cellular Biology* (2007) doi:10.1128/MCB.00758-07.

224. Sekiya, T., Muthurajan, U. M., Luger, K., Tulin, A. V. & Zaret, K. S. Nucleosome-binding affinity as a primary determinant of the nuclear mobility of the pioneer transcription factor FoxA. *Genes Dev.* **23**, 804–809 (2009).

225. Seifi, M. & Walter, M. a. Axenfeld-Rieger syndrome. *Clinical Genetics* **93**, 1123–1130 (2018).

226. Delanghe, J. R. & Langlois, M. R. Hemopexin: a review of biological aspects and the role in laboratory medicine. *Clinica Chimica Acta* **312**, 13–23 (2001).

227. Tolosano, E. & Altruda, F. Hemopexin: Structure, Function, and Regulation. *DNA and Cell Biology* **21**, 297–306 (2002).

228. Kobayashi, I. *et al.* Dual role of Jam3b in early hematopoietic and vascular development. *Development* **147**, dev181040 (2020).

229. Cesari, M. *et al.* Bone density and hemoglobin levels in older persons: results from the InCHIANTI study. *Osteoporos Int* **16**, 691–699 (2005).

230. Chuang, M.-H., Chuang, T.-L., Koo, M. & Wang, Y.-F. Low Hemoglobin Is Associated With Low Bone Mineral Density and High Risk of Bone Fracture in Male Adults: A Retrospective Medical Record Review Study. *Am J Mens Health* **13**, 1557988319850378 (2019).

231. Steer, K., Stavnichuk, M., Morris, M. & Komarova, S. V. Bone Health in Patients With Hematopoietic Disorders of Bone Marrow Origin: Systematic Review and Meta- Analysis. *Journal of Bone and Mineral Research* **32**, 731–742 (2017).

49 Spadina Ave. Suite 200
Toronto ON M5V 2J1 Canada
www.biorender.com

Confirmation of Publication and Licensing Rights

January 3rd, 2023
Science Suite Inc.

Subscription:	*Student Plan*
Agreement number:	*PO24UHU3RL*
Journal name:	*Memorial University of Newfoundland Thesis*

To whom this may concern,

This document is to confirm that Evan Langille has been granted a license to use the BioRender content, including icons, templates and other original artwork, appearing in the attached completed graphic pursuant to BioRender's Academic License Terms. This license permits BioRender content to be sublicensed for use in journal publications.

All rights and ownership of BioRender content are reserved by BioRender. All completed graphics must be accompanied by the following citation: "Created with BioRender.com".

BioRender content included in the completed graphic is not licensed for any commercial uses beyond publication in a journal. For any commercial use of this figure, users may, if allowed, recreate it in BioRender under an Industry BioRender Plan.

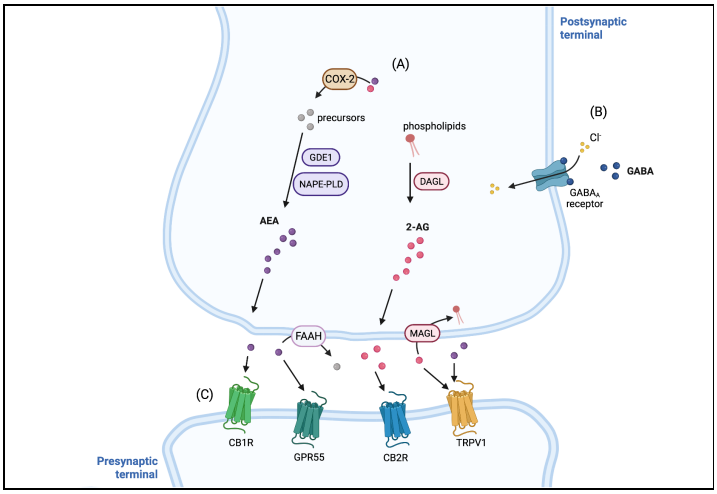

For any questions regarding this document, or other questions about publishing with BioRender refer to our BioRender Publication Guide, or contact BioRender Support at support@biorender.com.

49 Spadina Ave. Suite 200
Toronto ON M5V 2J1 Canada
www.biorender.com

Confirmation of Publication and Licensing Rights

November 29th, 2022
Science Suite Inc.

Subscription:	*Student Plan*
Agreement number:	*ZF24PFEGNY*
Journal name:	*Memorial University of Newfoundland Thesis*

To whom this may concern,

This document is to confirm that Evan Langille has been granted a license to use the BioRender content, including icons, templates and other original artwork, appearing in the attached completed graphic pursuant to BioRender's Academic License Terms. This license permits BioRender content to be sublicensed for use in journal publications.

All rights and ownership of BioRender content are reserved by BioRender. All completed graphics must be accompanied by the following citation: "Created with BioRender.com".

BioRender content included in the completed graphic is not licensed for any commercial uses beyond publication in a journal. For any commercial use of this figure, users may, if allowed, recreate it in BioRender under an Industry BioRender Plan.

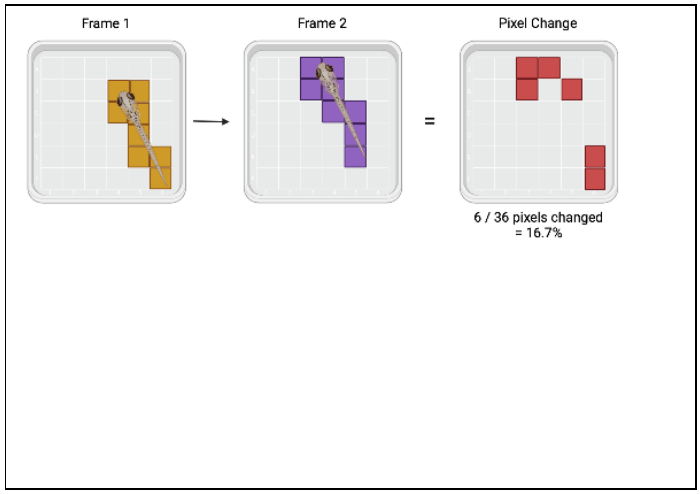

For any questions regarding this document, or other questions about publishing with BioRender refer to our BioRender Publication Guide, or contact BioRender Support at support@biorender.com.

49 Spadina Ave. Suite 200
Toronto ON M5V 2J1 Canada
www.biorender.com

Confirmation of Publication and Licensing Rights

November 29th, 2022
Science Suite Inc.

Subscription:	*Student Plan*
Agreement number:	*HO24PFEKA8*
Journal name:	*Memorial University of Newfoundland Thesis*

To whom this may concern,

This document is to confirm that Evan Langille has been granted a license to use the BioRender content, including icons, templates and other original artwork, appearing in the attached completed graphic pursuant to BioRender's Academic License Terms. This license permits BioRender content to be sublicensed for use in journal publications.

All rights and ownership of BioRender content are reserved by BioRender. All completed graphics must be accompanied by the following citation: "Created with BioRender.com".

BioRender content included in the completed graphic is not licensed for any commercial uses beyond publication in a journal. For any commercial use of this figure, users may, if allowed, recreate it in BioRender under an Industry BioRender Plan.

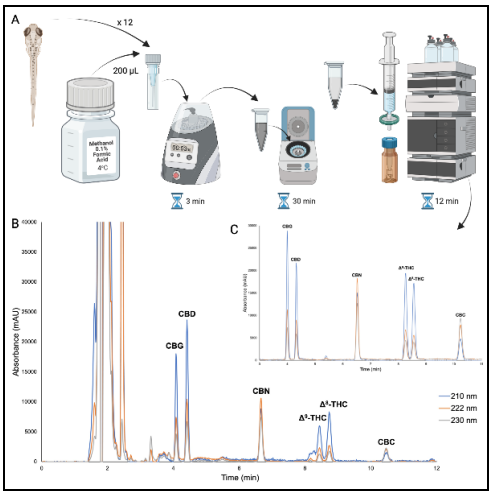

For any questions regarding this document, or other questions about publishing with BioRender refer to our BioRender Publication Guide, or contact BioRender Support at support@biorender.com.